A VARIABLE FREQUENCY PWM RECTIFIER FOR WIND DRIVEN INDUCTION GENERATORS

by

Kristian E. Medri, B. A. Sc. (University of Toronto, 2003)

A thesis
presented to Ryerson University
in partial fulfillment of the
requirements for the degree of
Master of Applied Science
in the Program of
Electrical and Computer Engineering

Toronto, Ontario, Canada, 2006

Author's Declaration

I hereby declare that I am the sole author of this thesis.

I authorize Ryerson University to lend this thesis to other institutions or individuals for the purpose of scholarly research.

I further authorize Ryerson University to reproduce this thesis by photocopying or by other means, in total or in part, at the request of other institutions or individuals for the purpose of scholarly research.

A VARIABLE FREQUENCY PWM RECTIFIER FOR WIND DRIVEN INDUCTION GENERATORS

Kristian E. Medri,
Master of Applied Science, 2006,
Electrical and Computer Engineering,
Ryerson University

Abstract

This thesis presents a strategy to minimize the front-end converter rating for wind-driven Self-Excited Induction Generators (SEIG). Conventionally front-end converters need to handle complex power while the converter used in this strategy is able to function with rated real power. This converter is a variable frequency Pulse Width Modulated (PWM) rectifier. This strategy is made possible by the discovery of a formula for selecting the optimal static capacitor value, which along with the rectifier, provides the SEIG excitation current. In addition, a practical control scheme was developed which, combined with the excitation capacitance formula, works for isolated wind energy conversion systems. The presented research includes the analysis, simulation, and experimental verification of this novel strategy.

Acknowledgements

Most importantly I would like to thank Professor Bin Wu for serving as my supervisor at Ryerson University's Laboratory for Electric Drive Research and Applications (LEDAR). I also thank my examination committee.

I am grateful to Dr. Congwei Liu for the opportunity to discuss engineering theory and to the others in the lab for intellectual discussion from time to time. Thank-you also to Jim Koch for allowing the use of components from his interface board for my application. Many thanks to my family and friends for their support.

Table of Contents

List of Tables

List of Figures

Chapter 1 – Introduction

Wind energy is the fastest growing source of electricity in the world. This growth fosters excitement and motivation to conduct research related to this subject. Wind power generation facilities are being installed at an increasing rate in Ontario, in Canada, and internationally year to year. Consequently, it is the time to focus on improving wind power generation facility technology. This body of work describes a novel contribution to this field. A summary of thesis components and an overview of the field is provided.

The main contribution of this thesis is a formula that calculates excitation capacitance. It provides the ability to meet a primary design objective of wind turbine systems by enabling the formation of a low cost wind turbine system for present-day use. With an optimal capacitance value, it is possible to construct the system with a less costly rectifier. This novel strategy can be implemented to reduce per unit cost of building wind turbine systems, and in fact to minimize the required rating of front-end power converters in modern installations. The identified strategy is intended for wind driven 690V Self-Excited Induction Generators (SEIGs) in the power range of 1MW. A derivative of this development has been the clarification of Pulse Width Modulated (PWM) rectifier control strategies.

This thesis elaborates on the research undertaken in the derivation and discovery of the capacitance optimization formula and subsequent corollaries. To better understand these developments this introduction presents the field of wind turbines. The theoretical work is presented in the second chapter while the third and fourth respectively present the simulation and the experimental verification of the work. The final chapter is a conclusion where the future of this research is considered.

Chapter one is intended to introduce the basics of the field and the important technical considerations. In order to introduce the field of wind turbines, we first consider wind energy in general which sheds light on the relevancy of this research. Next, the specific operation of wind turbines is considered finding that they need to operate at variable speed to most effectively capture the energy in the wind. Then rotating electrical machines, the next stage of the conversion of wind energy to electricity, are considered. The interdependent power converters

are considered in the next section. The aforementioned sections are then tied together in the design specifications section that describes the goals of the technical work focusing on the PWM rectifier and how to apply it in the particular converter strategy undergoing development. This is followed by the thesis outline providing the method taken to achieve these goals as the final section in the introductory chapter.

1.1 Wind energy background

The history, current developments, and the promises wind energy holds, provide the background of why this research is relevant. This background was amassed when investigating how to make a valued and useful contribution to the sustainable energy field. It provides insight into how the current level of development was reached and thus how it can be advanced. International and local developments are touched upon after briefly covering the historical background and roots of wind energy. The current status in the world is narrowed down to specifically consider Canada.

1.1.1 Historical roots of the technology

Here is a timeline that provides the dates that specific technological developments took place or when they were combined to improve the ability to manipulate wind energy:

- Approximately 10 000 B.C. – Aerodynamic throwing sticks were used in Europe, with the most familiar nomenclature for this class of tool being the Australian "boomerang" [1].
- 3500-2000 B.C. – Sumerians in Mesopotamia (in the Middle East) developed the first sailboat.
- 500-900 A.D. – First windmills used to pump water in Persia and China [2].
- 1200 – First use of windmills in Holland for corn then water [3].
- 1596 – First known wind-driven sawmill in the Netherlands [2].
- 1888 – American builds first wind powered electrical generator with automatic controls [2].
- 1897 – Dane reduces number of blades and increases speed leading to the birth of modern wind turbines [4]. N.B. The difference between a "windmill" and a "wind turbine" is that the former uses air drag to move while the latter uses blades designed similarly to boomerangs and airplane wings to make use of aerodynamic lift.

- 1973 – OPEC Embargo leads to a surge of interest in alternatives to oil.
- 1980 – Computational control becomes prevalent allowing more processing throughout all of technology.

The technology currently employed will be covered later in this chapter. Research developing wind energy technology for the future is the subject of this thesis.

1.1.2 International development

A survey of world wind energy development provides insight into successful endeavours in the field. In the six years prior to 1999 the average annual growth in sales of wind turbines was 40% [5]. Denmark has led the way in wind power. Denmark's 588.1 installed watts per capita more than doubles that of any other nation [6]. Germany, on the other hand is a larger country and its 16 629 MW of installed wind power is double that of the next largest user of wind power [6]. These two countries are home to a great deal of the wind industry. Nonetheless, In Spain 2 065 MW of wind power (52.4 W/capita) were installed in 2004. Respectively Spain has a sizeable industry as does the United States through the American company General Electric (GE) Wind [6]. GE Wind brings with it its parent company's military involvement which is a reputation not cared for by awareness groups. A frequently referenced American location is Altamont Pass in California where 4 000 turbines were installed as a result of tax incentives in the 1980's [7]. Much of the world's wind resources are close to the shorelines. Offshore wind energy capture technology has been developed and installed in locations shallow enough and close enough to load centres to warrant it. Currently there are relatively few such installations and this is expected to change.

1.1.3 Development in Canada

When this project was started in 2004, 124 MW had been installed in Canada [8]. As of April 2006, 943 MW had been installed [9]. The Canadian Wind Power Production Incentive (WPPI) is more dependable than the American program however the amount of support is less significant. Other more complicated emissions credit trading programs also exist. Governmental support is possible in other ways as well, for instance "to aid in the development and demonstration of an advanced power electronics and control system for wind turbines" Xantrex Technology Inc. received $5 million from Sustainable Development Technology Canada [10].

1.2 Wind turbine characteristics

It has been established that wind turbines are the preferred method of capturing wind energy. Capturing the most energy possible with the lowest expenditure is the goal. The next section specifically considers the conversion of wind energy into electricity. This section covers key factors that influence what a turbine provides as rotational energy. As mentioned in the previous section storage, reserve capacity, or demand control is required no matter how wind power is used for periods of no wind. Any method that can lessen this requirement or make it easier to facilitate is also important.

1.2.1 Aerodynamics

Let us first consider the source itself. The energy, initially in the form of wind, is to be captured using a 1MW wind turbine with a radius of 27.1m to capture it from a swept area of 2300m^2. The goal in wind turbine aerodynamic design is to efficiently extract the maximum possible energy from the wind provided a specific swept area. The limit of efficiency is defined by the fact that the air that has had energy removed still has to flow. According to Betz' law, it is only possible to use a wind turbine to convert less than 16/27 (or 59%) of the wind's kinetic energy in the wind to mechanical energy [11]. The ecological effects of disturbed airflow have yet to become relevant. Noise however, is a reported issue that is also indicative of lowered efficiency since some of the energy is producing sound. It must be limited and incorporated into the aerodynamic design even though the yawing noise (resulting from turning the turbine into the wind) can be more disturbing.

We are interested in knowing what the lowest wind speed that can provide the rated power is. This lowest wind speed corresponding to rated operation can be calculated by using the following relation describing power, P, in terms of conversion efficiency C_P, swept area A, air density d (1.2 kg/m^3), and wind speed x:

$$P = C_P \frac{1}{2} A d x^3 \qquad (1\text{-}1)$$

For a realistic turbine it is reasonable to expect efficiency of less than 50% of the Betz limit [12]. Solving for the wind speed for rated operation provides 13.5m/s and for half rated operation provides 10.7m/s.

The rotational speed of the turbine must keep the tips of the blades from reaching the speed of sound c (which depends on temperature, etc. but is generally >300m/s) at which point they are no longer effective, thus:

$$\omega_{tmax} < \frac{c}{r} \qquad (1\text{-}2)$$

Meaning ω_t should be at most 11Hz. It is interesting to note that the tips of onshore turbines are sometimes simply truncated to create the higher speed offshore variants.

The electrical frequency is directly proportional to the mechanical rotational speed. Various combinations of machines with numerous poles along with step up gearing allow the intended rated electrical frequency operation of 60Hz to be reached for the point of rated power operation. Gearboxes can, though in the case of trouble-free electronics performance they are the component demanding the most maintenance, provide a higher speed to the generating machine. This allows power transfer at a lower torque and thus a smaller machine may be used. This weighs against the direct drive technology trend especially for large machines. For direct grid connection, the requirement of a 200 pole direct drive generator to arrive at a reasonable rotational speed of 30 rpm provides some perspective [4]. It is added that the gear ratio is typically about 1 to 50 for a 600 to 750 kW generator. The fact that magnets are mentioned means synchronous machines are under consideration. Induction machines will likewise have to have many poles in a direct drive application.

The power coefficient $C_P(\beta,\lambda)$ is a function of the blade pitch angle β and the tip speed ratio λ of blade tip velocity $r\omega_t$ to wind velocity x [13]:

$$\lambda = \frac{r\omega_t}{x} \qquad (1\text{-}3)$$

Calculations involving β are turbine specific and will be left for the aerodynamic specialists [13]. Optimizing C_P by keeping λ constant by operating at an electrical frequency proportional to the wind speed provides an acceptable representation of peak power point tracking especially for those turbines with constant pitch. Thus the frequency for half rated operation is 47.6Hz.

1.2.2 Efficiency

Energy efficiency is critical for efficient use of the wind resources and capital expenditure. Generally the system can be broken up into blocks in the power path. Then the product of each

block's individual efficiency can be used to determine system efficiency. These blocks can be the method of capture i.e., the blades along with pitch and rotational speed control on the mechanical side, the gearbox (if one is used), the machine used, and the link to the grid. Various control methods in the link to the grid can be implemented to control the machine to extract the maximum mechanical power in varying wind conditions.

Economies of scale can be realized however it must also be realized that as the radius of a wind turbine increases its speed is limited since the blade's tip speed will approach the speed of sound. Offshore wind turbines that have be designed to operate at higher speeds than their onshore twins have sometimes identical blades that simply have the outboard ends of their blades truncated.

Peak power tracking and the respective variable speed operation that makes it possible have such a significant impact on efficiency that each is discussed in their own sub-sections below.

1.2.3 Peak power tracking

Wind can be approximated by a sum of sinusoids to create a simulated wind profile [14]. Wind data for an actual windy site can also been obtained. The power coefficient, which models how much of this available kinetic energy is captured, depends on the tip speed ratio. Figure 1-1 shows how the desired operating points line up with the simple cubic curve representing a constant tip speed ratio superimposed on the turbine characteristic power curves.

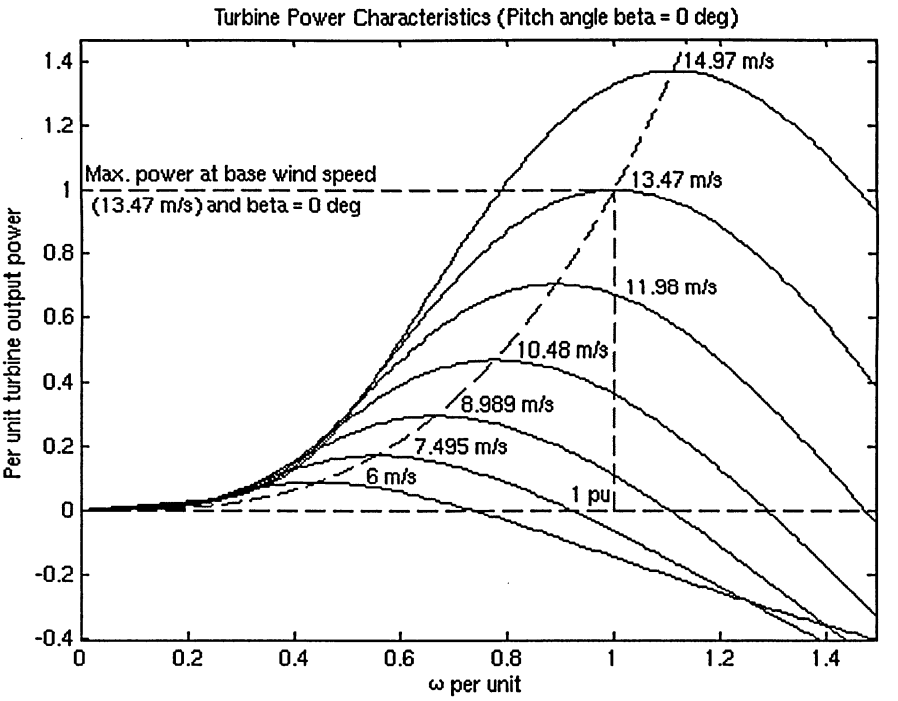

Figure 1-1: Power curve

Ensuring operation at these points is called peak power tracking and relatively complex control can be employed as turbines have interactive characteristics and wind patterns are widely ranging. The general idea is that as wind speed increases, it is desired to extract all available power which is maximized by allowing some of the power to be used to also increase the rotational speed of the wind turbine. Once the rated operation point is reached, structural loads are to be limited while continuing to extract power [15]. The captured power can be limited at the upper end by changing the pitch of the blades to a less than optimum value. This project follows the cubic curve while also limiting dynamic acceleration to avoid, for instance, a situation where all of the incident energy is used to accelerate the turbine and none is converted into electricity. Other methods for tracking operating points tend to be based on fuzzy logic, an accurate term for the technique [16, 17]. In addition to fuzzy logic control, hill climbing control is used for peak power tracking [18]. These types of iterative techniques are sufficient to maximize the output of a solar panel array encountering cloud cover but since a wind turbine has inertia the dynamics of a wind energy system in a gust are different.

1.2.4 Variable-Speed

It was shown above that in order to maintain $\lambda = \lambda_{optimal}$ variable speed operation is necessary. In

other words, a variable speed topology allows the turbine to rotate at a speed proportional to the wind to allow effective energy capture [19]. Although an asynchronous machine has some allowable speed variation any topology aiming to track peak power output requires a power electronic converter to be able to allow the machine to operate at speeds independent from the constant frequency of the grid.

Although clearly advantageous, the dominance of variable speed technology over constant speed turbines has been hindered by political reasons allowing proprietary rights to variable speed technology in the United States of America. An early "single" speed principle allowing some variability was to use a large generator for strong winds and a second, smaller, generator driven by the same turbine for periods of low winds [4]. A newer, more common, design is to use pole changing generators that connect the stator windings in different configurations to modify the number of poles such that they can run at different rotational speeds for the same electrical frequency output [4]. The now common doubly-fed induction generator is also able to operate to some extent as a variable speed machine [16, 17].

The ability of the turbine to follow the wind speed is limited by the inertia of the mechanical system. The maximum rate of angular acceleration is in the ballpark of 1Hz/second for the 27 100 kg rotational mass that is along with 42 000 kg of static mass in the nacelle on top of the turbine's 36 400 kg tower. The distribution of the rotational mass is important but actual data is difficult to obtain. Compared to the 5Hz sampled actual wind data, a rough estimation is in the same ball park meaning the turbine will be able to track it. The turbine specific optimal tip speed ratio ($\lambda_{optimal}$) is typically not provided by manufacturers but can be garnered from the rated operation point.

The theoretical time constant of the mechanical part of the wind turbine corresponding to the above is known to be much slower than the control systems. A ball park figure quantifying this would be helpful. Thus an approximate maximum angular acceleration for the mechanical system considered will be calculated for a 1 MW (1 MJ/s) power input. The angular kinetic energy can be calculated as follows:

$$E = \frac{1}{2} I \omega^2 \qquad (1\text{-}4)$$

For this calculation we will use the 1.5 MW Zephyros Z72 parameters of 18.5 rpm rated speed and rotor inertia of 35 000 kgm^2 which is a lower bound as rotating components affixed to the rotor, the blades most significantly, add to the inertia [20]. Thus:

$$E = \frac{1}{2}(35000)(18.5\frac{2\pi}{60})^2 \cong 65680J \qquad (1\text{-}5)$$

Which is an amount of energy that a 1MW input could provide in 65.7ms. However, the rated torque is 862 kN meaning a maximum angular acceleration of:

$$\alpha = \frac{T}{I} = \frac{862000}{35000} \cong 24.6 rad/s^2 \qquad (1\text{-}6)$$

Which means the time constant $t = \frac{\omega}{\alpha}$=18.5/24.6 which is about 752ms, which is much longer than the response time of most any type of power converter.

Variable speed operation is also useful for allowing the turbine to speed up during periods of high wind (gusts) and slow down in lulls. This can smooth out the power flow by acting as an energy storage device and at the same time reduce structural and torque loading.

1.3 Electric generators

When an electric machine converts electrical energy to rotational energy it is considered a motor while when it converts rotational energy to electrical energy it is considered a generator. Electric machines fall into two categories: synchronous and asynchronous. The output of synchronous generators is directly proportional to the shaft speed while asynchronous generators rely on a small variance for energy transfer. Rotors in generators may require brushes and may be squirrel cages, permanent magnet rotors, or wound rotors. Regardless of the machine, various techniques can be used to improve efficiency. The following notes directed towards motors also apply to generators [21]:

> Designers can minimize losses by improving the design of features that give rise to the main losses in the motor. The greatest losses are the iron losses that occur in the rotor and stator, accounting for 50 percent of the total loss. This can be improved by using low loss steel and thinner laminations. Copper losses account for 20 percent. Using an optimum slot fill design and larger conductors can reduce these. Bearing friction and windage losses total 23 percent and can be reduced by using a smaller cooling fan. Stray losses,

which account for 7 percent of the total, can be reduced by improving the slot geometry.

Brushes are not only a maintenance issue but also contribute to losses. The efficiency is also reduced when not operating at nominal output, although we are trying to make use of the most common machine available to reduce costs it would be interesting to consider the efficiency of various machines when operating at partial power. Let us now consider synchronous machines and then asynchronous machines.

1.3.1 Synchronous Machines

Synchronous machines use two sets of windings, one of which can be replaced by permanent magnets. As the magnetic field moves in relation to the second set of windings translational energy (which is tangential in the case of rotation) is converted into electrical power in the second set of windings. It is possible to use multiple secondary windings to provide flexibility in operational speed if say 60Hz is desired at all times. Here are the more specific forms of these machines:

1.3.1.1 Mechanically commutated

Brush commutated machines are often named dc machines as carbon brushes running over copper segments affixed to the turning shaft rectify the impinging current into direct current. The maintenance and reliability of this mechanical switching mechanism is considered its downfall whether operating as a motor or a generator. The mechanical losses of a mechanically commutated machine are 80% due to the brushes, 20% due to the bearings (other components such as the air resistance, windage, of the rotor play some part as well) [22]. They have been installed in small applications where the electricity can be used locally as dc. However as power electronics, or in the case of a generator simply diodes, are widely available at low cost, even this application is no longer common.

1.3.1.2 Electrically commutated

Simply using diodes to generate dc in an isolated system is probably the most numerous wind turbine installation type. For example, a 400W generator system based on the AIR-X 12 V_{dc} Marine, suited for battery charging, is available for around $1000. These small independent generators do not account for an appreciable amount of electricity used by society. The Kortright Centre has displays with examples of both auxiliary (sub kW) and homestead sized (multi kW)

generators of this type.

1.3.1.3 Permanent magnet synchronous machines

Certainly the most elegant solution is to have a 3-phase machine with a permanent magnet rotor. No brushes are required and the control and conversion from mechanical to electrical energy can have an entirely smooth transfer of torque from the rotational reference frame into electrical current generated with smooth waveforms. However these waveforms must still be matched to the end use of the power, typically via power electronics. The wind turbine installed at the Canadian National Exhibition Place is of this type. Permanent magnet machines may have demagnetization issues as well as magnetic losses [23, 24]. Another reason permanent magnet synchronous generators are not used very much in practice is that, even though prices have become reduced, the strong magnets used (made of rare earth metals such as Neodynium) are quite expensive [4].

1.3.1.4 Wound rotor synchronous machines

Instead of using permanent magnets it is possible to create an equivalent magnetic field emanating from the rotor by feeding electricity to a wound rotor. Wound rotor synchronous machines require brushes running on slip rings. Alternative connection schemes do exist such as those provided by manufacturers of alternative technologies such as fluid conductor rotating electrical connectors. It would be interesting to review a report on the comparison of how slip rings with electrical commutation compare to mechanical commutators. In the direct drive case, high torque is required for high power transfer across a slow moving interface. Thus, the machines become quite large, on the order of ten times bigger for a given power rating.

Enercon has made headway in large direct drive variable speed systems using this type of machine. They currently offer the largest wind turbine at 4.5 MW. The locations of the power handling and conversion equipment in such a turbine system can easily placed into the nacelle and the tower. Enercon's North American market is possibly limited to Canada as there is an interesting variable-speed American patent (that should from some perspectives only cover doubly-fed machines) which has ended up in the hands of GE Wind after passing through limbo and other companies when the original organization that held it went bankrupt. In Canada there is a court case regarding an Enercon turbine installed in Alberta which can be followed to see the outcome.

1.3.2 Asynchronous Machines

The rotor frequency and the electrical frequency in asynchronous machines are not absolutely tied to one another. The construction is similar to a wound rotor synchronous machine. The difference is that the rotor winding current is developed by induction from the stator windings. This means that three-phase currents in the rotor windings create the rotor field. The rotor windings can be connected to a resistance or simply shorted to create a loop for the induced current. These machines typically do not to have any power transfer at synchronous speed. When overdriven it becomes a generator as the rotor will rotate faster than synchronous speed with a (negative) slip factor and convert rotational energy into electrical energy.

1.3.2.1 Doubly-fed Induction Machines

These machines are actually operationally similar to a synchronous machine. They are asynchronous in that the rotor field orientation is decoupled from the rotor itself allowing a certain extent of variable speed operation. This induction machine topology requires a wound rotor, however only 25-30% of the power is required to flow through the power converter [25]. It also has the benefit of having control over compensation and thus has the ability to provide reactive power. These wound rotor machines offer reactive power control that is an order of magnitude faster than synchronous generators [26].

The concept of independent control for the rotor flux raises the interesting possibility of increasing the apparent speed of the machine electrically. This idea, however, does not solve the issue of high torque required across a slow moving interface for large power transfer. Energy storage can be added into the dc link of the converter that is used [16, 17]. These electronics, in the case of GE's doubly-fed offshore turbines, are housed in a lowerable shipping container that is raised and lowered with a built in crane.

1.3.2.2 Wound rotor brushless induction machines

The issues with brushes such as commutator wear and more relevantly slip ring wear cause serious consideration of brushless generators [27-31]. Induction machines and permanent magnet machines provide alternatives [32-34]. Due to the issues with permanent magnet machines let us consider induction machines. They have simpler construction but are more difficult to control. Control can be achieved by connecting a wound rotor to a variable load, this can be incorporated

into the actual rotor as opposed to via brushes. Control information can be transferred through a contactless magnetic technique or through optical methods. It is also possible to essentially integrate two separate machines together where one generates the output power and an auxiliary one (called the exciter) generates the current for the rotor winding. The rotor windings can be directly connected to one another or even use the same winding that makes use of two stator windings. It is also possible to use an asynchronous exciter along with a diode rectifier to create a synchronous generator as described by [35]. It will be interesting to monitor new development of these types of machines where more complex converters could be integrated on either the stator or the rotor side of the exciter.

Vestas uses the variable load method for variable slip. The Danish induction generator technology named Opti Slip® uses optical methods to signal across to the rotor electronics each time it passes a stationary optical fibre [4]. It is used to control the slip of the generator [4]. For operation near the rated power, the slip is kept at half of the maximum slip [4]. The slip is increased to allow the rotor to turn a bit faster to give the pitch mechanism a chance to react in the case of a gust [4]. Once the blades have been pitched somewhat out of the wind, the slip is decreased [4]. For lulls, the process is reversed [4].

Since induction machines require a large number of poles and large diameters, which lead to high magnetizing currents, they are not considered in a comparison of various direct-drive configurations [36]. Additional notes include that induction machine magnetizing currents cause a low power factor, that they have a low efficiency, and that their axial length must be increased substantially in order to give acceptable performance.

1.3.2.3 Self excited induction machines

To simplify the induction machine, a static rotor winding load can be connected. As any current running through this load would result in reduced efficiency the windings are shorted together with no impedance. The easiest way to construct such a shorted winding rotor is by making a simple squirrel cage rotor. This is the simplest, most reliable, and least expensive machine design. Induction machines are generally used as motors and as such are the most common machine sold. The IEEE equivalent circuit is shown in Figure 1-2. R_1 represents the stator resistance and X_1 represents the stator inductance while R_2' and X_2' respectively refer to the rotor

resistance and inductance referred to the stator side. X_m represents the magnetizing inductance and s is the rotor slip.

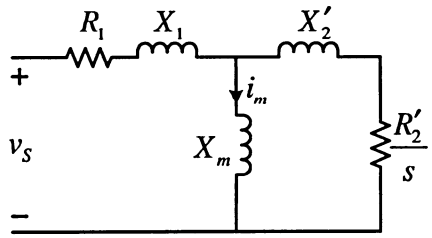

Figure 1-2: IEEE equivalent circuit of the induction machine

When such a machine is directly connected to the grid without additional system components, a strong grid is necessary. Grid support is necessary since the process of inducing the rotor current draws a reactive magnetizing current (i_m) whether operating as a motor or a generator. In order to avoid over-saturation the terminal voltage is to be kept proportional to the rotational speed of the machine. To establish the ratio of terminal voltage to rotational speed, the rated operational point is considered. This can simply be read from the name plate as rated voltage and idle amps. It can also be found by finding the knee point on the magnetization curve obtained measuring the machine's no load current for various terminal voltages. No load operation is considered in order to have minimum slip and thus the measured current is approximately equal to the magnetization current. Figure 1-3 shows a typical magnetization curve where the rated operation point has been indicated.

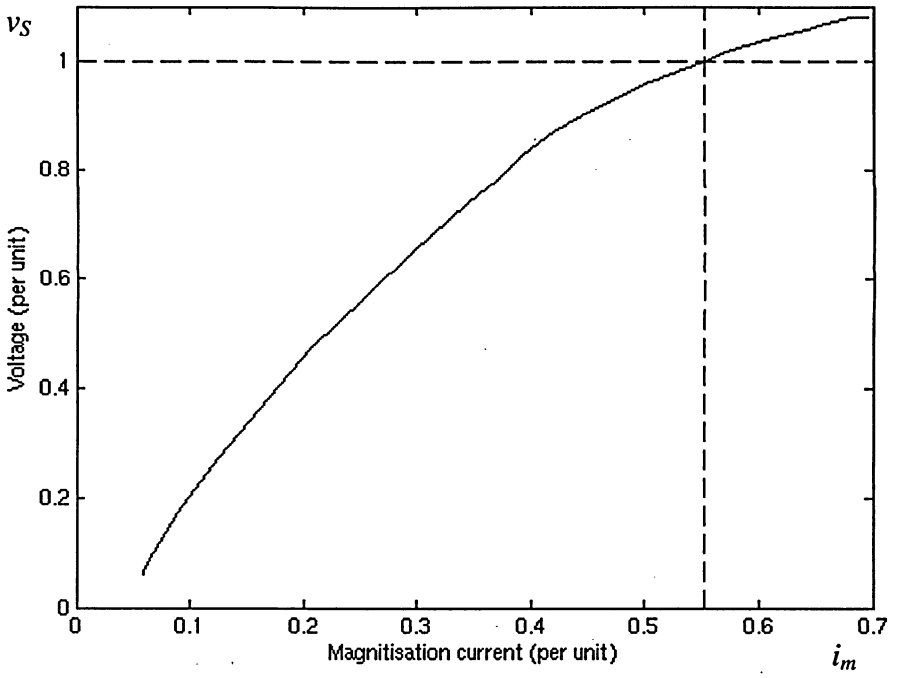

Figure 1-3: Induction machine excitation curve

The main issues with self excited induction machines are self starting and the power factor due to the magnetizing current. Self starting can be handled by adding an in situ battery or small combustion generator specifically set up for this purpose [37]. It is also possible to drive small machines at a higher than nominal speed to get them going, a probabilistic event that likely cannot be relied upon in larger installations. One paper that provides an overview of SEIGs lists numerous papers that provide methods of calculating the minimum required capacitance for self-excitation [38]. The capacitors attached to provide the reactive power a SEIG requires should be Δ-connected since Y-connected capacitors would require a larger value for the same effect with no benefits [39]. The re-excitation of an induction machine, following a complete voltage collapse that leaves minimal residual magnetism, is difficult [39]. It has been found that a machine self-excites under minimal load conditions prior to reaching rated speed if the attached capacitance is double the optimum value calculated in the next chapter. In addition, other methods are conceivable that could be used to augment the chosen capacitance for initial excitation [40]. If a severe voltage collapse has not been experienced the minimally loaded machine will self-excite without the additional capacitance.

The power grid as a whole needs to provide reactive power due to the fact that induction

machines are so common as well as due to the additional inductive loading of transmission lines and transformers. As discussed above and reiterated in other papers induction generators also require reactive power [16, 17]. A distributed method of handling reactive power is to make sure every machine has capacitors that match its load. In the case of an induction generator this would take the form of excitation capacitors. Using relays, capacitor banks can be switched in to provide the power factor and excitation desired. To operate on the knee of saturation, the magnetizing current is to be constant for constant *v/f*. Since capacitance is proportional to frequency the amount of capacitance required at low frequency to maintain this excitation current is quite large. Figure 1-4 is produced by the "capacitance_rpm.m" script in the appendix to illustrate the relationship between stator frequency (ω_S) and capacitance (C) required to ensure unity power factor for the power flowing from the terminals to the next part of the circuit.

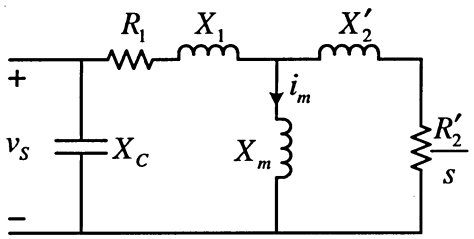

(a) Induction machine equivalent circuit with an excitation capacitor

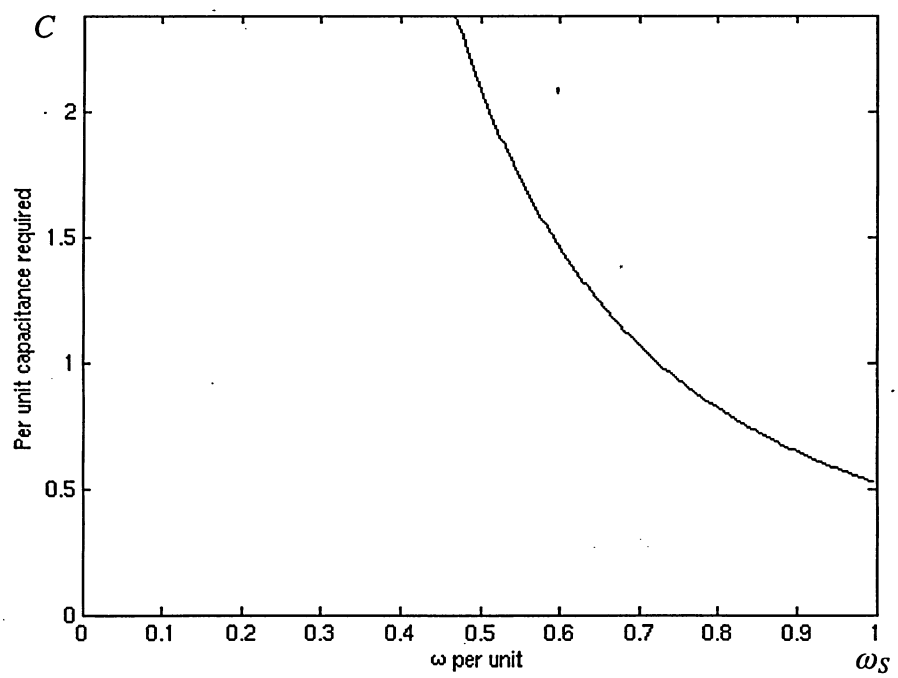

(b) Excitation capacitance versus ω_S

Figure 1-4: Capacitance required to provide the excitation current for an induction machine

However, to ensure the power system is well compensated it is helpful for the reactive power provided by the energy conversion system to be dynamic. Hence, power electronics come into play. Utilization of solid state control of the compensation for an induction generator results in a local pseudo substation.

1.4 Interconnection methods

A turbine can capture the kinetic energy in a fluid and transfer it to a rotating shaft. This rotating shaft can be used to turn an electrical generator. A number of different methods can be used to manipulate the output of an electrical generator to provide electrical energy in an acceptable format to society. The energy is general transferred via a grid connection. Different electrical generators and the respective methods used to convert wind energy to useful electricity are discussed in this section to provide the background which lead to the choice of components used for the research described by this thesis.

There are many factors influencing the method used to convert wind energy to electricity such as reliability, efficiency, variable-speed considerations, and cost. The type of converter used greatly depends on the type of electrical generator used. Single turbine systems, of which several of the same type can be combined to create a wind farm, are examined in more depth.

In order to reduce the cost of a wind energy system, it is effective to reduce the cost of its electrical components. In reducing the capital cost, one must consider a number of factors. These include machine design, grid connection requirements, and maintenance. Machines for wind energy systems must be efficient at partial power and be able to handle the large torque required for power transfer at slow speed. In addition, machine design specifications may include components such as magnets and dual winding sets. When developing a grid connection strategy, one must consider how much of the power the power electronics are expected to bear and the related substation requirements. The use of wound rotors increases both upfront and maintenance cost due to the inclusion of brushes and slip rings.

It is possible to derive a market comparison of which concepts are more prevalent based on which technology companies use [41]. Analyzing the data found in a market report, it can be estimated whether the relatively recent concept of doubly-fed machines dominated the market in

2003 [42]. Vestas using wound rotor technology only to provide adjustable field resistance and Enercon with their direct drive technology are the main suppliers, along with others accounting for about 41% of the market that does not use doubly-fed technology. To obtain an idea of what each company offers each of their literature was reviewed:

- GE's line up of turbines is doubly-fed with their largest offerings defined as "ac with IGBTs".
- Gamesa's European offerings are doubly-fed while their North American ones are denoted as variable slip asynchronous.
- NEG Micon's large turbines are doubly-fed while their other offerings are "asynchronous".
- Bonus (now Siemens) offers asynchronous with a double winding set.
- RePower offers double speed asynchronous with their large offerings providing a maximum of 20% of the power through the rotor through an inverter.
- Made Tecnologias Renovables offers variable speed synchronous machines with IGCT converters using single devices for full power.
- Nordex has asynchronous liquid cooled generators with some marked as double fed.
- Mitsubishi has an old sub MW line of induction generators and a new MW line of PM synchronous machines.
- Suzlon's offerings (2.1% of the market) are all pole switching asynchronous.

The research comparing the various merits of different designs has yet to mature. This and the foresight of identifying designs which will find future success confirm the validity of continued research and the design and development of an optimum system allowing variable speed operation.

Inevitably a controller or converter is required in all wind driven electrical generation systems. A small dc turbine used for charging batteries has to be disconnected and the rpm limited or stopped once the batteries are charged. A directly connected machine has to be synchronized to be hooked up to the grid and then disconnected from the grid when the wind dies to keep it from turning into a big fan. To a large extent the choice of the topology drives the selection of the converter and with converter prices ever reducing more flexibility is available.

1.4.1 Direct connection

Connecting the output of the generator directly to the grid is the simplest connection. Figure 1-5 depicts this directly connected configuration [43].

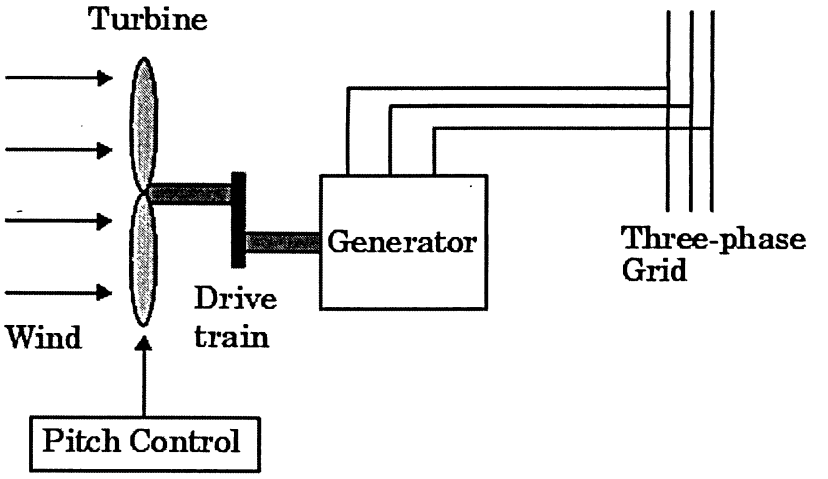

Figure 1-5: A wind energy system with a direct grid connection

The generator is directly connected to the grid in the same way as traditional generation. As we know wind is not as predictable and reliable as say steam from a thermal plant or water from a reservoir. Thus it is more difficult to from the control aspect to spool up the generator, synchronize it and finally connect it to the grid. Using an asynchronous generator eases these aspects especially if it is possible to guarantee no self excitation to allow connection to take place as long as the machine is near synchronous speed at the time of connection. Nonetheless the machine must still run in a fairly narrow speed range. To expand the range of the generator while still adding energy into the grid some generators can operate with an increased number of poles for low speed. This is comparable to changing gears.

1.4.2 Doubly-fed

Currently the majority of the market share is in the hands of the doubly-fed topology that uses power devices in 25-30% of the power path [25]. It provides some accommodation for variable speed. In the past wind turbines did not provide any reactive power support which the, now widely used, doubly-fed machine can. Figure 1-6 depicts this configuration which can be used to decouple the frequency of the field of the rotor from the machine frequency [43].

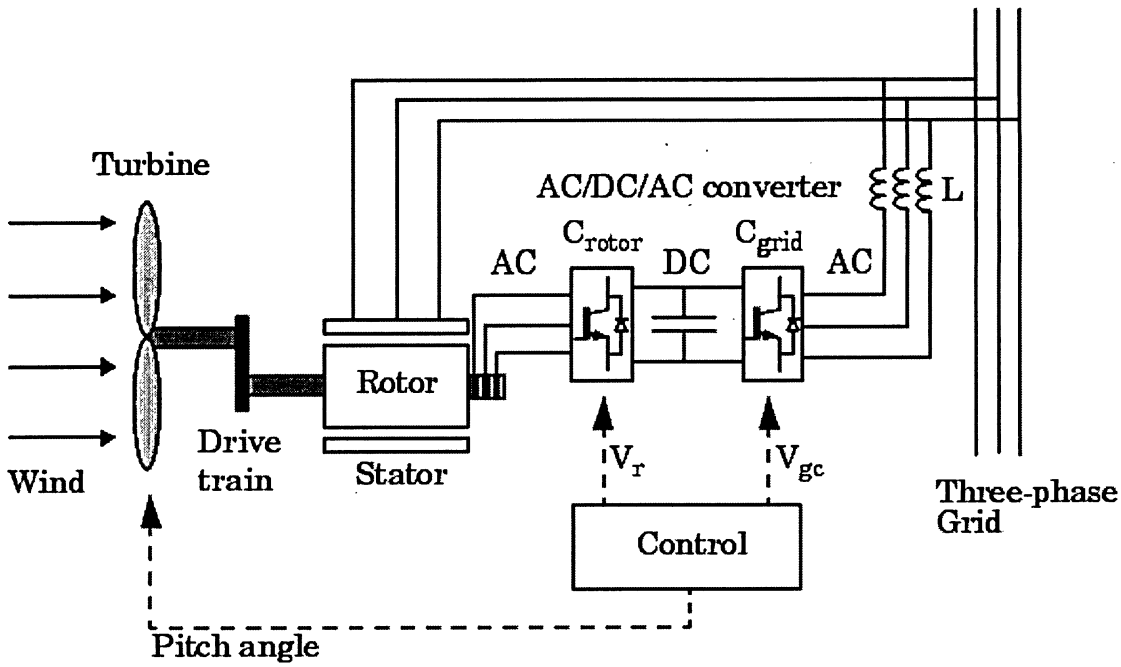

Figure 1-6: A wind energy system with a doubly-fed induction machine

It provides some decoupling benefits however it can be predicted that as the price of converters continues to decrease that utilizing a converter in the full power path is going to be the way to go. A doubly-fed example is GE's 1.5 MW machine with 3 pairs of poles that operates from 800 to 1440 rpm at the machine, about 0.67-1.2 per unit rotational speed [44].

The approach of taking the most efficient machine for generating electrical power and adapting it for wind turbines is not simple. Most efficient electrical machines operate at much higher speeds than wind turbines. As pictured many multi-megawatt designs use gearboxes. The alternative would be increasing the speed of the turbine. This has limits as they become noisy and more importantly, as the diameter increases, the tip speed must be kept low enough that it actually aids in power production. Eliminating the gearbox thus requires the use of a high torque, low speed "direct drive" generators which are becoming more common. However slow speed generators are of custom design and thus efficiencies are tough to compare especially as the remainder of each system also depends on the generator design. To strike a balance the Finnish "multibrid" design cuts back on the torque involved while also reducing the mechanical issues found in the higher speed stages of gearboxes by using a single stage gearset which still results in the use of a

relatively low speed permanent magnet synchronous generator [45, 46]. Regardless of gearbox usage, the speed of the blades and hub are coupled to the generating machine's rotor.

The rotating field of the rotor produces a current on the stationary (a.k.a. stator) windings of the machine. Rectifiers are used to convert this sinusoidal alternating current (ac) similar to that available at a typical outlet to direct current (dc) as available from a battery. There are different methods of achieving this conversion and passive converter designs are discussed followed by active designs which can be controlled.

1.4.2.1 Passive rectifiers

Simple rectifiers are built using passive diodes. These devices only allow current to flow in one direction. On the output a capacitor is used to smooth the output voltage. Using a single diode in a circuit allows one half of the sinusoid to be conducted. This results in a single pulse per cycle. The Total Harmonic Distortion (THD) and efficiency of this design is low. Using a 4 diode bridge design a single ac phase can be rectified such that the output appears as the absolute value of the input resulting in 2 pulses per cycle. Using a 3-phase input and a 6 diode bridge one can have a six-pulse output. Other multi-pulse designs make use of phase shifting transformers to accomplish even more pulses approximating a steady current even more closely. The amount of current that flows depends on the load with respect to the source. The shape of this current is topology dependent. All passive designs have operation contingent lagging power factor.

1.4.2.2 Active rectifiers

The simplest active design is the Silicon Controlled Rectifier (SCR) which uses thyristors instead of diodes. The point at which thyristors turn on can be delayed thus allowing a controlled reduction of the energy which flows to the load. This process however reduces the power factor by causing the current to lag the voltage of the source even more. The theory and simulation of a PWM rectifier which can control the degree to which the current either lags or leads the voltage has been discussed in a previous paper [47]. While another paper experimentally verified a different controller many years earlier providing transfer functions for the PWM rectifier in state-space form [48]. The challenges in designing a PWM rectifier include measurement issues such as multiple zero crossings due to noise and that the detection of phase of a low magnitude current is difficult to discern [49]. Also, when a typical ac-dc-ac motor drive is run in regenerative mode it is susceptible to resonance. As a PWM rectifier acts as a boost converter, it

can also provide a constant voltage power source for off the shelf inverters approved for grid connection.

The reason a dynamic rectifier is chosen over a passive rectifier is that using a PWM rectifier is more efficient and will be more cost effective, if not now, then soon. The reasons this is the case is that a PWM rectifier: provides lower THD and thus greater machine efficiency and longevity by approximating sinusoidal current, facilitates variable speed operation, and provides a constant dc voltage output allowing the use of off the shelf approved inverters.

1.4.3 Indirect connection

An absolutely variably transmission can be accommodated by using an indirect connection. Figure 1-7 shows a topology that utilizes a dc link to decouple machine frequency from grid frequency.

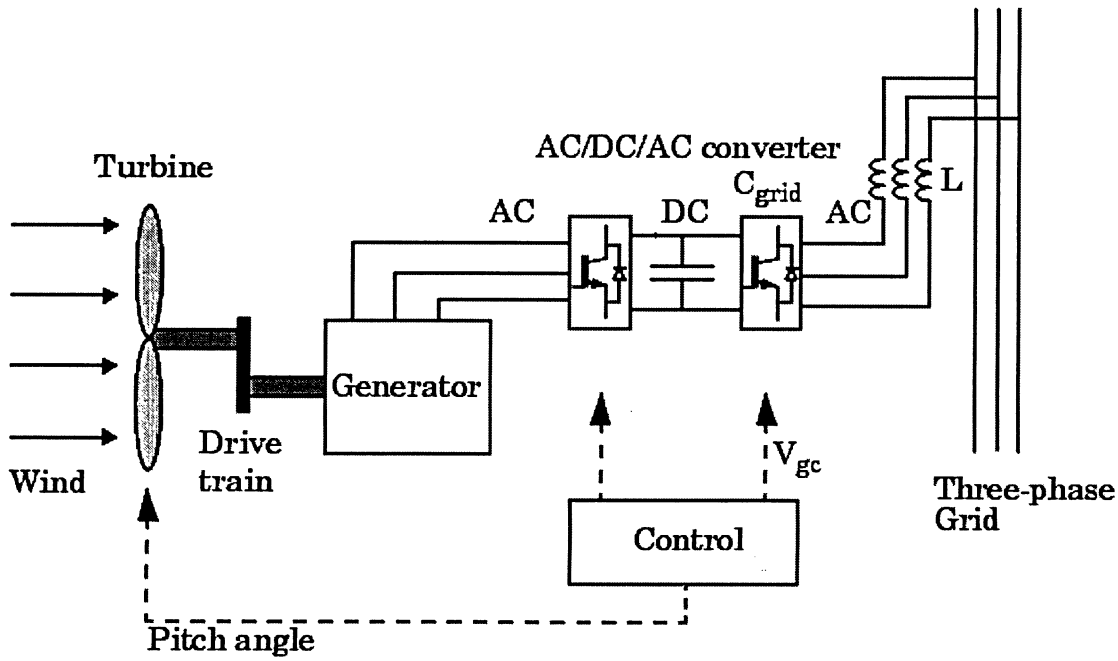

Figure 1-7: A wind energy system with a full power path converter

The Danish Wind Industry Association provides an excellent introductory animation of the above converter. The variable speed operational range of the topology shown in Figure 1-7 is greater than the "about 0.7 to 1.3 per unit" of doubly-fed induction machines [50]. A turbine that

drives a direct drive synchronous generator which uses a back-to-back converter has been shown to achieve 0.3-1.1 per unit variable speed operation [51]. Its specifications are: cut-in wind speed 3 m/s, nominal wind speed 12 m/s, cut-out wind speed 25 m/s during 1 min, cut-out wind speed 30 m/s during 0.1 s, and survival speed 70 m/s.

In theory there are direct ac to ac converters, however the topologies are not competitive with those with a dc link. Not only do ac-ac matrix converters require more devices than a dc link, but the devices have to be bi-directional. Bi-directional devices tend to have smaller ratings and the topology also tends to have over voltage problems. A dc link can be used for High Voltage dc (HVdc) transmission and can also easily interface with energy storage. As for generator selection a synchronous machine may be used instead of an induction machine to avoid the starting and excitation issues experienced in the case of induction machine. In addition, if the machine is large enough in diameter it may render the gearbox unnecessary. When operating a wind driven induction generator at variable speed, the power factor reduces drastically. This is due to the fact that while variable speed wind turbines should have real power flow proportional to the cube of the rotational speed, the magnetizing current must remain constant throughout the operational range. Thus the ratio of real power to reactive power, or power factor, is low for low frequency as is plotted with respect to stator frequency in Figure 1-8.

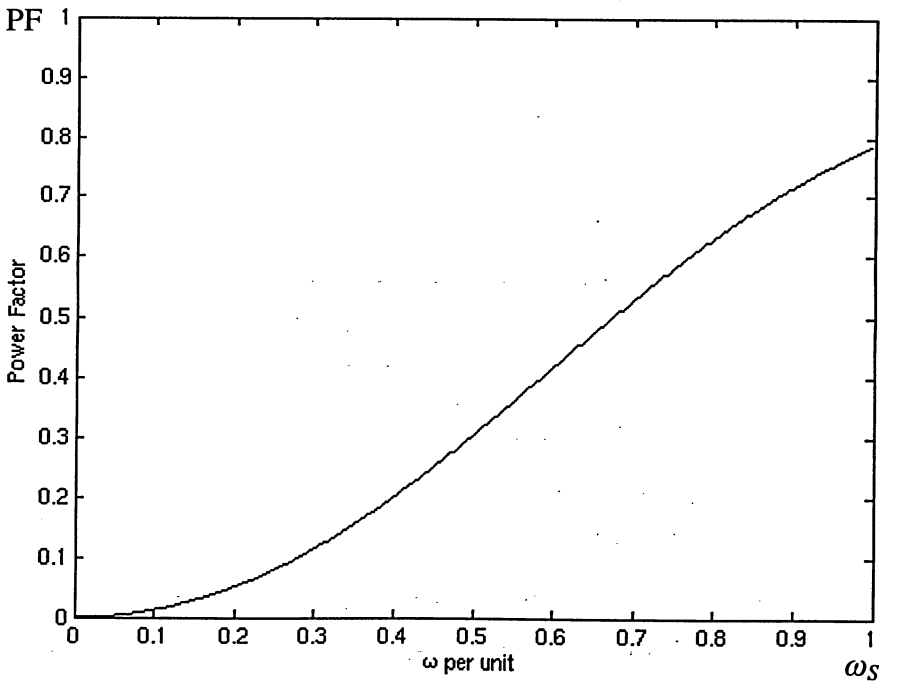

Figure 1-8: Power factor of a wind driven induction generator

Using a full power path converter not only allows for variable speed, it allows for control of real and reactive power control on both sides of the converter. Thus it is an excellent match for an induction machine. The reactive power control can ensure proper excitation while the balance of the real power equations determines the acceleration and thus the control of the speed of the wind turbine. Once output power is subtracted from input power captured from the wind the remainder primarily influences the rotational acceleration of the turbine. Acute transients may be stored in the various electrical components. However, if the dc link does not contain a purposely designed long term storage element the incident energy is transferred to the output with a slight loss at the effective rate of the switching frequency of the power converter.

1.5 Design specifications

The preceding sections have introduced various concepts about wind turbine systems. This section takes that knowledge and describes the objectives of the technical work detailed by this thesis. The primary design objectives of a wind turbine system are to reduce the overall cost and to improve its efficiency. The method taken to solve this problem is to use the inexpensive induction generator to provide power and to make use of a flexible PWM rectifier to be able to run it at variable speed. The converter criteria expected to be within the PWM rectifier's range of controllable performance.

To this end, a variable frequency PWM rectifier has been developed for wind driven induction generators. An induction machine requires the least capacitive reactive power support at high speed while additional capacitance is required at low speed. The application of a PWM rectifier can maintain an induction machine's excitation at varying frequencies even with a static capacitance value. The design goals below center on the input and output requirements of the rectifier. How these goals can be met is covered in the theory chapter along with how to choose the capacitance value such that the rating of the converter can be minimized.

Top-level converter requirements include high reliability at a reasonable cost and optimization for the operational range. Specific to this application is effectivity while partially loaded. Let us consider the detailed criteria for the input and output sides of the converter. The next chapter also discusses the converter's steady state operational theory as well as its control.

1.5.1 Input criteria

The input criteria are determined by the source which is a wind turbine driven self-excited induction generator (SEIG). For effective operation a wind turbine is to have variable speed and respectively, variable power capability. Since the aerodynamically optimum rotational speed increases linearly the output power available increases roughly as a cube. For effective operation at variable frequency as required by a variable speed turbine, a SEIG requires reactive power support for excitation. A SEIG produces a variable output voltage dependent on excitation, rotational speed, and loading. Allowances also have to be made for the frequency dependent characteristics of the reactive elements whether contained within the SEIG, the line inductances, the excitation capacitors, or other less significantly affected components. In addition, Low Total Harmonic Distortion (THD) is desired in the line current on the machine side to retain efficiency and to reduce Electromagnetic Interference (EMI).

Although the input power has a number of variable characteristics, there is a specific steady state operating scenario given a particular wind speed. The wind speed dictates the available output power along with the optimum rotational speed which, depending on machine characteristics, dictates the electrical frequency. For a specific frequency and power output, the SEIG requires a specific amount of reactive power for excitation for an acceptable output voltage. The PWM rectifier's variable power factor capability will be used in order to independently control the reactive power flow related to excitation. Transient considerations include maintaining excitation and deviation from steady state power draw in order to slow down the turbine or to allow it to speed up. Note that if the deviation is too large it is possible that power will be drawn by the machine. Excitation is also important for initial startup. Depending on the amount of residual magnetism in the rotor, significant reactive power compensation may be needed to get a measurable output voltage from a SEIG.

1.5.2 Output criteria

The primary output goal is to be able to connect reliably to the remainder of the electrical system. The easiest way to accomplish this is to provide a steady dc output voltage such that an off the shelf approved voltage source inverter can be used to connect to the grid. The output requirement then boils down to providing a variable power constant voltage dc with 10 to 15% ripple. Real and reactive power flow to the grid is also important as is consideration for grid

faults. Bearing this in mind the approved inverter can be used as a dynamic reactive power compensator in addition to transferring real power. Faults are traditionally handled in wind power installations by simple disconnecting. Transients are an issue in case of disconnection as they expose gearboxes to possibly significant transient torque [52].

1.5.3 Existing designs and design challenges

The design considered utilizes a squirrel cage induction machine, as a generator. Since the fact that this is the least expensive machine type is a well known fact, some of its features are also well known. As mentioned earlier, these machines require excitation current. Excitation capacitors are known to become ineffective at low frequency, thus a gearbox of at least one stage is considered a requirement to help increase speed and thus frequency. The mechanical costs involved with using an SEIG are minimized by using the machine with the lowest manufacturing cost and choosing the ideal balance of speed (accompanied by more gearing) versus torque (accompanied by more mechanical stress) to harness the power. It is then left to the converter and its controller's design to complete the conversion of wind power to a high quality dc source which an "off the shelf" inverter can link to the electrical grid. This is done by developing the Pulse Width Modulated (PWM) rectifier and related Digital Signal Processing (DSP) control system for such systems. The use of a capacitor supported dc link dictates the use of voltage source topology, which has the added benefit of energy storage capability. Various types of PWM have been used. In this case, Sinusoidal Pulse Width Modulation (SPWM) is used in the simulation since it requires less computation and thus the simulation time is manageable. In the real system Space Vector Modulation (SVM) is used to provide a greater range of operation while eventually Selective Harmonic Elimination (SHE) could be incorporated to further reduce THD.

In order to understand the challenges of this design, previous efforts that have developed various aspects of the desired design are considered. These efforts have been researched along with problems that have been encountered. One of the first to suggest an idea such as this design was limited by the devices available at that time [53]. Others have come up with a variety of designs but they have not been verified experimentally [54]. A design which has been experimentally verified, though the controller shown in makes use of the grid side converter to control the dc voltage, is said to be able to function independently as well when connected to the grid [55]. It

would be of interest to try the actual system constructed to provide the grid-connected results in standalone mode. In the case of an isolated system, initial start-up excitation is not possible without excitation capacitors when the dc link is starting from a discharged state. The use of a battery in an isolated system has been suggested for charging the dc link, however experimental evidence of a stable system using this technique has not been found [56]. It has been found that for larger sampling time steps such as 10ms a cross-coupled controller works however when using more modern, shorter, sampling time steps such as 0.2 ms it is necessary to use a direct PI controller in order to achieve the most stable system [57]. It should be noted that the setup used for these findings included a significant resistive component in the line impedance [58]. Typically a converter must be 30%-50% oversized with respect to rated power in order to supply the required magnetizing current [59]. Excitation capacitors can remedy this rating requirement while at the same time easing startup issues. A capacitance value can be calculated for rated operation by compensating an induction machine's magnetizing inductance by considering a parallel capacitance. Simply ignoring the remainder of the circuit, which does in fact have a noticeable effect, one arrives at a ballpark value of 0.7832 pu excitation capacitance. Various papers have discussed the choice of the excitation capacitance however they seem to provide erroneous calculations such as providing a value for X_m from other parameters that does not line up with the actual value [16]. One paper even provides 2 methods of calculating the same value that produce different results [60]. The first method does not provide the value in their example while the second does but provides a value that is too low: 0.3444 pu. Involved calculations are required and if the value is perhaps the delta connected value, then multiplying by 3 to get the Y-connected equivalent value, it becomes reasonable. It must be noted however that it was very useful when an author provided a numerical example to be able to at least verify (calculation scripts used provided in the Appendix) that formula transcription errors do not cause unintended values to be mistakenly calculated and attributed.

A successfully verified SEIG variable speed generation system that is able to control the excitation and dc link via the rectifier (ie. appropriate for isolated operation) has not been found. Moreover, one that optimizes the choice of capacitance to minimize the converter's rating has not been found. There is also a lack of clarity in discussing the steady state operation of a PWM rectifier and how it compares to the successful dynamic control of one. Thus this thesis and the paper accepted by IECON'06 which sums it up represent an accomplishment that has not been

done before [61].

1.6 Thesis Outline

This chapter has provided a background of the field covering the use of wind turbines to convert the energy in wind into an electrical form that can be added to the grid. It has also introduced the concept of the use of an SEIG along with a variable frequency PWM rectifier. Previous systems and the challenges they face have been presented as well. The remainder of this thesis details an endeavour to develop an improved system.

The second chapter specifically details the development of the system theory. Equations are derived to select an optimum value for the excitation capacitors to minimize the required rating of the front end of the power converter. In addition, a derivative of this development is the clarification of PWM rectifier control strategies.

The construction of a mathematical model and its simulation are discussed in chapter three. The first set of steps include assembling the power component models. This is followed by the construction of the control system blocks. The last step of the model construction was adjusting the controller parameters. After discussing the control parameters the 1MW SPWM rectifier simulation results are presented.

The fourth chapter details to the construction of a prototype. It describes how each subcomponent was tested and then integrated. The successful experimental results verifying the theory are provided along with matching simulation results.

In closure, the benefits of the accomplishments described by this thesis are summed up in the conclusions chapter. The contribution of a formula to calculate the value of excitation capacitors that allow the use of a rectifier rated only for the real power provided by a wind driven SEIG is discussed. In addition, shortfalls of extremely low rotational speed operation of an isolated SEIG system are discussed. It is also highlighted that for successful control a direct-coupled controller should be used instead of a cross-coupled controller. A brief discussion of relevant future work follows.

The appendix contains a listing of the Matlab scripts that were used for the calculations and creating the figures discussed in the thesis. The final pages are a list of references.

Chapter 2 – PWM Rectifier Theory for SEIG Applications

This chapter develops the theory for variable frequency Pulse Width Modulated (PWM) rectifiers for wind driven Self-Excited Induction Generators (SEIG). The first section in this chapter describes the use of SEIGs in wind energy conversion systems. The second section develops the mathematical equations for the selection of an excitation capacitance which minimizes the required rating of the PWM rectifier. Then a PWM rectifier's theoretical control strategy is covered by discussing the ideal system. This is followed by an explanation of the self adjusting cross-coupled controller that is modified to provide the functional direct-coupled controller. In conclusion, these concepts are brought together describing the contribution of this solution.

2.1 System overview

The primary design objectives of a wind energy system are to reduce the overall cost and to improve its efficiency. The proposed topology reduces overall cost by using a SEIG as shown in Figure 2-1.

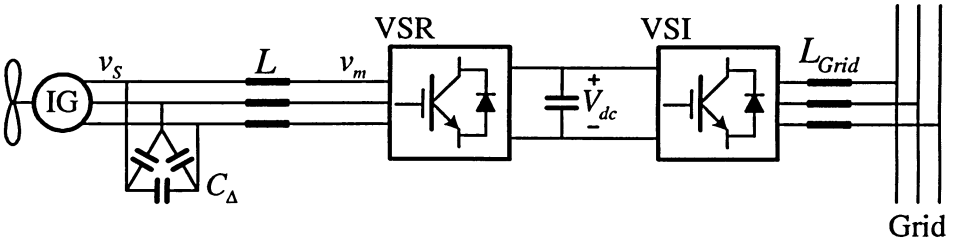

Figure 2-1: Block diagram of SEIG system

This wind energy conversion system is composed of the following components: the wind driven generator, the front-end converter, and the respective connection to the grid. The wind driven generator is comprised of a wind turbine, which could include a gearbox, which drives a SEIG. The source output voltage of the SEIG is designated v_S. The front-end converter is based on a Voltage Source Rectifier (VSR) with input voltage v_m. On the ac input side of this converter a line inductance (L) is added in order to allow a machine with excitation capacitors (C) to be

connected to a voltage source converter. The dc output voltage (V_{dc}) of the converter is filtered by a dc capacitor. The last component in the power path is comprised of a Voltage Source Inverter (VSI) to make the grid connection.

As stated, the SEIG is the least expensive generator option. The SEIG is paired with a PWM rectifier of minimized Volt-Ampere (VA) rating to further reduce the cost. System efficiency is maintained by providing for variable frequency operation. Machine efficiency is improved by the line inductance which reduces its Total Harmonic Distortion (THD). The novel component of this system composition is the minimization of the rectifier rating. The strategy hinges on the choice of the excitation capacitance. A voltage source rectifier is used in order that an off-the-shelf approved voltage source inverter can be used to connect to the grid. It is developed specifically for implementation with wind driven SEIGs with an intended machine size in the range of 1MW/690V.

2.2 Capacitance value calculation

In order to minimize the rating of the rectifier it should operate at unity power factor for rated power. An excitation capacitance can be determined using the calculations that follow. Figure 2-2 shows the single phase diagram, a single phase equivalent of the three-phase portion of Figure 2-1, from which the relations are developed.

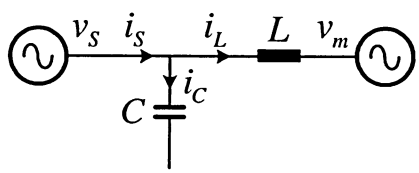

Figure 2-2: Single phase diagram of PWM rectifier system

The following parameters are marked on the single phase diagram where:

v_S represents the source voltage,

i_S represents the source current,

C represents the excitation capacitance,

i_C represents the capacitor current,

L represents the line inductance,

i_L represents the inductor (and VSR) current, and

v_m represents the VSR voltage.

Equations can be used to represent the component relationships in Figure 2-2. $\vec{I}_C$ can be expressed as a relationship between $\vec{V}_S$, C, and ω (which represents source frequency). It follows that C can be expressed as also shown in (2-1).

$$\begin{aligned} \vec{I}_C &= \vec{V}_S j\omega C \\ C &= \frac{I_C}{V_S \omega} \end{aligned} \tag{2-1}$$

V_S is expressed in (2-2) in terms of V_{LL} and k_{vf}, where:

V_{LL} represents the line-to-line voltage of the source and

k_{vf} represents the ratio of terminal voltage to rotational speed for a specific machine.

$$\begin{aligned} V_S &= \frac{V_{LL}}{\sqrt{3}} \\ &= \omega k_{vf} \end{aligned} \tag{2-2}$$

Using (2-2) the current into the capacitance from (2-1) can be expressed as:

$$I_C = \omega^2 C k_{vf} \tag{2-3}$$

Given the aforementioned electrical topology, a number of steady-state relationships hold:

$$\vec{I}_L = \vec{I}_S - \vec{I}_C \tag{2-4}$$

$$\mathrm{Im}\{\vec{I}_L\} = \mathrm{Im}\{\vec{I}_S\} - I_C \tag{2-5}$$

Note that $\vec{V}_L$ (the voltage across the inductor) can be expressed as:

$$\begin{aligned} \vec{V}_L &= \vec{V}_S - \vec{V}_m \\ &= \vec{I}_L j\omega L \end{aligned} \tag{2-6}$$

Notice that:

$$\begin{aligned} V_L &= I_L \omega L \\ I_L &= \frac{V_L}{\omega L} \end{aligned} \tag{2-7}$$

Note that since the purpose of the line inductance L is used to couple the SEIG to the rectifier it is reasonable to assert the constraint:

$$V_L < V_S \tag{2-8}$$

Also note that $\mathrm{Im}\{\vec{I}_S\}$ is a machine dependent constant magnetization current as explained in the

introduction. Since $\vec{V}_S$ is a measurable quantity while $\vec{V}_m$ is a chopped waveform we will set the angle of $\vec{V}_S$ as the reference, i.e. 0°. $\vec{V}_m$ can theoretically be set by the converter and is thus our controlled quantity with angle -γ. The rectifier's complex power ($\vec{S}$) can be expressed as:

$$\vec{S} = \vec{V}_m \vec{I}_L^{\,*} \tag{2-9}$$

With the real component:

$$P = \mathrm{Re}\{\vec{S}\} \tag{2-10}$$

and the imaginary component:

$$Q = \mathrm{Im}\{\vec{S}\} \tag{2-11}$$

The power factor providing the proportion of real power to complex power can be expressed as:

$$\mathrm{pf} = \frac{P}{S} \tag{2-12}$$

As the most typical case of reduced power factor is when current lags voltage we will distinguish the case of current leading voltage by assigning its power factor a negative sign. As the design criteria for rated power is unity power factor the rectifier current $\vec{I}_L$ is to have the same phase angle (-γ) as $\vec{V}_m$:

$$\begin{aligned} \vec{I}_L &= I_L \angle -\gamma \\ P &= V_m I_L \end{aligned} \tag{2-13}$$

The representative vector diagram is depicted in Figure 2-3.

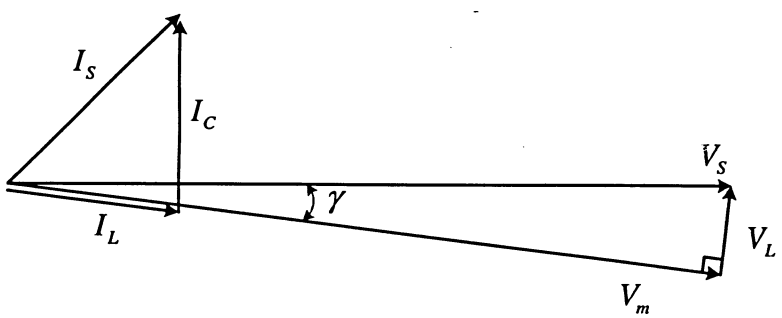

Figure 2-3: Vector diagram of rated power operation

For unity power factor operation at rated power, $\vec{I}_C$ has a specific value. Thus, the value of the capacitance can be determined for this specific situation.

Using the Pythagorean theorem:

$$V_m{}^2 + V_L{}^2 = V_S{}^2 \tag{2-14}$$

and rearranging:

$$V_m{}^2 + V_L{}^2 - V_S{}^2 = 0 \tag{2-15}$$

Then incorporating (2-7) and (2-13):

$$V_m{}^2 + \frac{(P\omega L)^2}{V_m{}^2} - V_S{}^2 = 0 \tag{2-16}$$

Multiplying $V_m{}^2$ through:

$$V_m{}^4 - V_S{}^2 V_m{}^2 + (P\omega L)^2 = 0 \tag{2-17}$$

and solving for V_m:

$$V_m = \sqrt{\frac{V_S{}^2 \pm \sqrt{V_S{}^4 - 4(P\omega L)^2}}{2}} \tag{2-18}$$

Equation (2-18) provides two roots. Note that other than by constraint (2-8), V_m and V_L have not been distinguished from each other trigonometrically and thus V_m is the larger of the two roots and V_L is the smaller of the two roots. Returning to Figure 2-3 we express:

$$\gamma = \arcsin\left(\frac{V_L}{V_S}\right) \tag{2-19}$$

Allowing the subsequent expression:

$$\begin{aligned} \mathrm{Im}\{\vec{I}_L\} &= -I_L \sin\gamma \\ &= -\frac{V_L}{\omega L}\sin\gamma \end{aligned} \tag{2-20}$$

Using Equation (2-5):

$$I_C = \mathrm{Im}\{\vec{I}_S\} + \frac{V_L}{\omega L}\sin\gamma \tag{2-21}$$

and incorporating (2-19):

$$I_C = \mathrm{Im}\{\vec{I}_S\} + \frac{V_L{}^2}{\omega L V_S} \tag{2-22}$$

followed by Equation (2-14):

$$I_C = \mathrm{Im}\{\vec{I}_S\} + \frac{V_S^{\,2} - V_m^{\,2}}{\omega L V_S} \tag{2-23}$$

Using Equation (2-18):

$$I_C = \mathrm{Im}\{\vec{I}_S\} + \frac{V_S^{\,2} - \frac{V_S^{\,2} + \sqrt{V_S^{\,4} - 4(P\omega L)^2}}{2}}{\omega L V_S} \tag{2-24}$$

Then recalling (2-1):

$$\begin{aligned} C &= \frac{\mathrm{Im}\{\vec{I}_S\} + \frac{V_S^{\,2} - \frac{V_S^{\,2} + \sqrt{V_S^{\,4} - 4(P\omega L)^2}}{2}}{\omega L V_S}}{\omega V_S} \\ &= \frac{\mathrm{Im}\{\vec{I}_S\}}{\omega V_S} + \frac{V_S^{\,2} - \sqrt{V_S^{\,4} - 4(P\omega L)^2}}{2\omega^2 L V_S^{\,2}} \\ &= \frac{V_S^{\,2} + 2\omega L V_S\,\mathrm{Im}\{\vec{I}_S\} - \sqrt{V_S^{\,4} - 4(P\omega L)^2}}{2\omega^2 L V_S^{\,2}} \end{aligned} \tag{2-25}$$

making use of (2-2) and where $\mathrm{Im}\{\vec{I}_S\}$ is the magnetizing inductance of the machine:

$$C = \frac{\frac{V_{LL}^{\,2}}{3} + 2\omega L \frac{V_{LL}}{\sqrt{3}}\mathrm{Im}\{\vec{I}_S\} - \sqrt{\frac{V_{LL}^{\,4}}{9} - 4(P\omega L)^2}}{2\omega^2 L \frac{V_{LL}^{\,2}}{3}} \tag{2-26}$$

Thus the above equation can be used to find an excitation capacitance that minimizes the rating of the rectifier by ensuring unity power factor operation for rated power. As a lower capacitance value, albeit with a higher voltage rating, can be used when capacitors are connected in delta instead of Y-configuration we remember to use the following formulae when converting back to the three-phase system from the single phase equivalent circuit:

$$C_\Delta = \frac{C}{3} \tag{2-27}$$

The following is a design example for a hypothetical 690V 60Hz 1MW machine. The machine's rated values are used as the base values. Thus $V_{ac-base}$ and ω_{base} are the per-phase rated voltage and rated stator frequency respectively while the base value for current is:

$$I_{ac-base} = I_{rated} = 858A \tag{2-28}$$

The magnetization current obtained via a calculation script included in the appendix is:

$$\mathrm{Im}\{\vec{I}_S\}=191A \tag{2-29}$$

The complex power of the machine includes the magnetization current and thus the magnitude of the complex power (used as the base value for power, S_{base}) at the rated operation point is greater than the rated power of the machine. The per-unit impedance, inductance, and capacitance base values are:

$$\begin{aligned} Z_{base} &= \frac{V_{ac-base}}{I_{ac-base}} = 0.464\Omega \\ L_{base} &= \frac{Z_{base}}{\omega_{base}} = 1.2mH \\ C_{base} &= \frac{1}{\omega_{base} Z_{base}} = 5700\mu F \end{aligned} \tag{2-30}$$

respectively. The line inductance using 0.14 per-unit inductors is:

$$L = 0.14 L_{base} = 0.17mH \tag{2-31}$$

Finally allowing the per phase capacitance to be calculated using (2-26):

$$C = \frac{\frac{690^2}{3} + 2\cdot 377\cdot\left(0.17\cdot 10^{-3}\right)\frac{690}{\sqrt{3}}191 - \sqrt{\frac{690^4}{9} - 4\left(\left(1\cdot 10^6\right)\cdot 377\cdot\left(0.17\cdot 10^{-3}\right)\right)^2}}{2\cdot 377^2\left(0.17\cdot 10^{-3}\right)\frac{690^2}{3}} \tag{2-32}$$

$$= 2000\mu F$$

This 0.36 per unit capacitance is compared to the 0.23 per unit capacitance needed for the case of no line impedance which using (2-1) is numerically:

$$C = \frac{191\sqrt{3}}{690\cdot 377} = 1300\mu F \tag{2-33}$$

The capacitance calculated using (2-26) is as expected since it has to have the additional ability to compensate for the line inductance used to connect to the rectifier which is to operate at unity power factor at rated power.

2.3 Variable frequency PWM rectifier operation

In the steady state case where $\vec{V}_m$ is free from external influences, i.e. disconnected from the inductance in this case, then the fundamental absolute values are as follows for modulation index m and dc link voltage V_{dc}:

$$\vec{V}_m = \frac{mV_{dc}}{2}\angle\gamma \text{ for Sinusoidal Pulse Width Modulation (SPWM)} \quad (2\text{-}34)$$

$$\vec{V}_m = \frac{mV_{dc}}{\sqrt{3}}\angle\gamma \text{ for Space Vector Modulation (SVM)} \quad (2\text{-}35)$$

Selective Harmonic Elimination (SHE) could eventually be used as a modulation technique as well. However, implementation of SHE is outside the scope of this project.

In the case that gating is not provided to the full bridge Integrated Gate Bipolar Transistor (IGBT) rectifier, the converter acts as a six pulse diode rectifier. The output of the rectifier in the heavily loaded case is similar to the output in the case of no output capacitor nor load:

$$V_{dc} = \frac{3\sqrt{3}}{\pi}\left|\vec{V}_m\right| \quad (2\text{-}36)$$

When the six pulse diode rectifier is loaded the current waveform is of a double hump shape that has a lagging power factor of approximately 0.86 changing for different loading conditions. This ball park figure is sufficient for the purposes here. Initially it was thought that the PWM rectifier could mimic the diode rectifier during initial transition from diode rectifier. However, the shape of the current waveform, initial controller values and converter transients were found to have a more significant impact on excitation than the actual power factor.

Once the PWM rectifier gating is engaged the system operates as per the depiction of the general case in Figure 2-4.

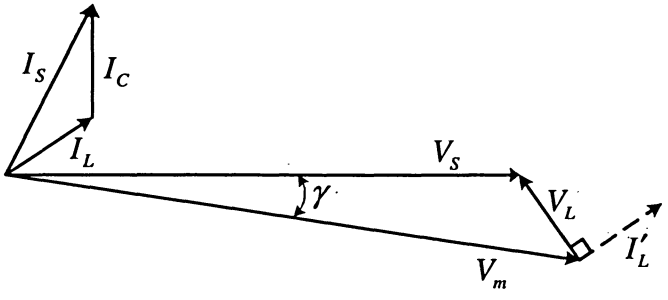

Figure 2-4: Vector diagram of system operation

As per the introduction to the use of variable speed wind turbines, power is related to the cube of the electrical frequency as follows:

$$P = \left(\frac{\omega}{\omega_{\text{base}}}\right)^3 \frac{\text{Re}\{S_{base}\}}{3} \qquad (2\text{-}37)$$
$$= \text{Re}\{\vec{S}\}$$

Equations (1-1) through (2-12) remain valid while rectifier current $\vec{I}_L$ now has the independent phase angle θ:

$$\vec{I}_L = I_L \angle\theta \qquad (2\text{-}38)$$

Also notice that:

$$\theta = \text{atan}(\frac{Q}{P}) \qquad (2\text{-}39)$$

$$pf = \cos\theta \qquad (2\text{-}40)$$

Taking the real part of (2-4):

$$\text{Re}\{\vec{I}_S\} = \text{Re}\{\vec{I}_L\}$$
$$= \frac{P}{V_S} \qquad (2\text{-}41)$$

and using (2-5):

$$\vec{I}_L = \text{Re}\{\vec{I}_L\} + j\,\text{Im}\{\vec{I}_L\}$$
$$= \frac{P}{V_S} + j\left(\text{Im}\{\vec{I}_S\} - I_C\right) \qquad (2\text{-}42)$$

Rearranging (2-6):

$$\vec{V}_m = \vec{V}_S - \vec{I}_L j\omega L$$
$$= \frac{V_{LL}}{\sqrt{3}} - \vec{I}_L j\omega L \qquad (2\text{-}43)$$

Combining (2-42), (2-43), then substituting in (2-3) and (2-37):

$$\begin{aligned}\vec{V}_m &= \frac{V_{LL}}{\sqrt{3}} - \left(\frac{P}{V_S} + j\left(\mathrm{Im}\{\vec{I}_S\} - I_C\right)\right) j\omega L \\ &= \frac{V_{LL}}{\sqrt{3}} - \frac{Pj\omega L\sqrt{3}}{V_{LL}} + \mathrm{Im}\{\vec{I}_S\}\omega L - I_C\omega L \\ &= \omega k_{vf} - \frac{\left(\frac{\omega}{\omega_{\mathrm{base}}}\right)^3 \frac{\mathrm{Re}\{S_{base}\}}{3} j\omega L}{\omega k_{vf}} + \mathrm{Im}\{\vec{I}_S\}\omega L - \omega^2 C k_{vf}\omega L \\ &= \omega k_{vf}(1-\omega^2 CL) + \mathrm{Im}\{\vec{I}_S\}\omega L - j\frac{\omega^3 \mathrm{Re}\{S_{base}\}L}{\omega_{\mathrm{base}}{}^3 k_{vf} 3}\end{aligned} \tag{2-44}$$

This equation for the general case provides an opportunity to produce an equation for the VA requirement of the rectifier at rated power that can be use to compare the choice of capacitance to alternative strategies. Considering only the magnitude of (2-9):

$$S = V_m I_L \tag{2-45}$$

and incorporating (2-2), (2-3), (2-37), (2-42), and (2-43) provides:

$$\begin{aligned}S = &\sqrt{\left(\omega k_{vf}(1-\omega^2 CL) + \mathrm{Im}\{\vec{I}_S\}\omega L\right)^2 + \left(\frac{\omega^3 \mathrm{Re}\{S_{base}\}L}{\omega_{\mathrm{base}}{}^3 k_{vf} 3}\right)^2} \\ &\sqrt{\left(\frac{\left(\frac{\omega}{\omega_{\mathrm{base}}}\right)^3 \frac{\mathrm{Re}\{S_{base}\}}{3}}{\omega k_{vf}}\right)^2 + \left(\mathrm{Im}\{\vec{I}_S\} - \omega^2 C k_{vf}\right)^2}\end{aligned} \tag{2-46}$$

Simplifying slightly:

$$\begin{aligned}S = &\sqrt{\left(\omega k_{vf}(1-\omega^2 CL) + \mathrm{Im}\{\vec{I}_S\}\omega L\right)^2 + \left(\frac{\omega^3 \mathrm{Re}\{S_{base}\}L}{\omega_{\mathrm{base}}{}^3 k_{vf} 3}\right)^2} \\ &\sqrt{\left(\frac{\omega^2 \mathrm{Re}\{S_{base}\}}{\omega_{\mathrm{base}}{}^3 k_{vf} 3}\right)^2 + \left(\mathrm{Im}\{\vec{I}_S\} - \omega^2 C V_{fconst}\right)^2}\end{aligned} \tag{2-47}$$

To optimize operation we use (2-26) to calculate the value of the capacitance. Then using (2-47) we can determine that for operation with no capacitance the converter has to be able to handle 50% more VA. Even if only the machine's internal inductance is used without additional line inductance, capacity for 30% more VA over the optimized case is required. This is presented in

Figure 2-5, maintaining the output power proportional to the cube of the rotational speed.

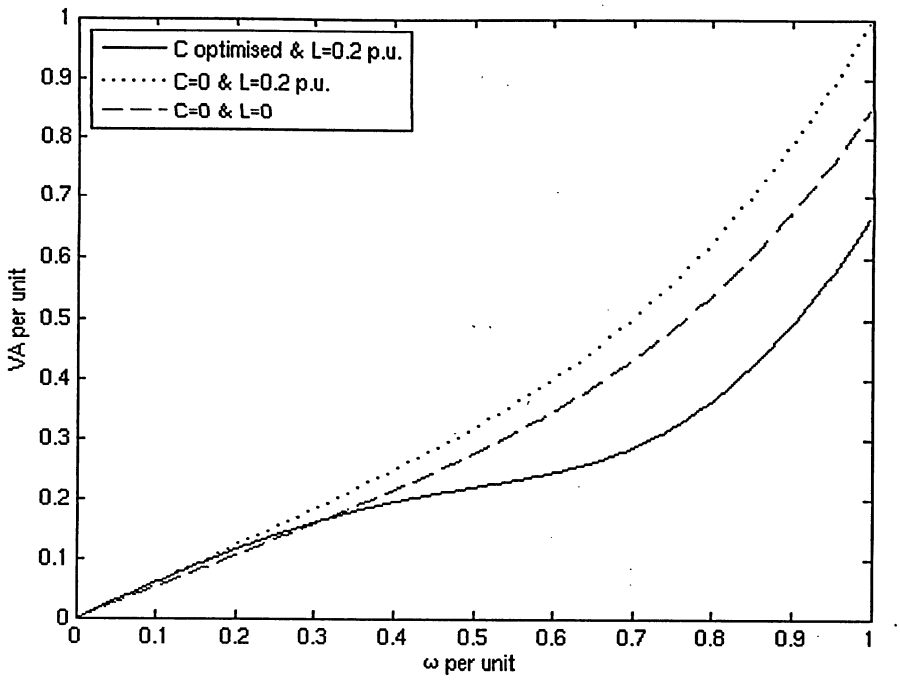

Figure 2-5: Plot of complex power flow through rectifier corresponding to ω

Notice that the required equivalent impedance of the rectifier:

$$Z_m = \frac{V_m}{I_L} \tag{2-48}$$

becomes unattainable at extremely low rotational speed. This is due to low rotational speeds corresponding to low input voltages while the magnetization current remains constant for constant *v/f*. In turn, the equivalent input impedance of the converter has to be extremely low. While a grid connected system could provide the required current, an isolated system cannot operate at extremely low rotational speed. Since the power is tied to the cube of rotational speed this occurs at a minimal power operation point.

2.4 Variable frequency PWM rectifier feedback control

This section details the development of PWM rectifier feedback control. This was successfully used to run the prototype after it was realised that a simple change was required for the controller shown in Figure 2-6. After describing the block diagram the operating principle is explained.

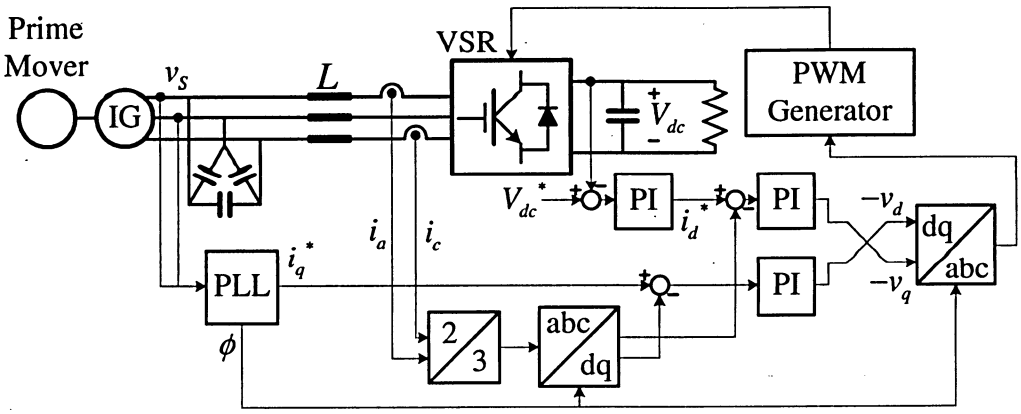

Figure 2-6: Block diagram of cross-coupled feedback control

There are two types of components in Figure 2-6: power components and control components. The power components include the prime mover, SEIG, capacitors, line inductance, VSR, and load as per Figure 2-1. The prime mover represents either a turbine or a motor which can be used to run the system in place of a turbine. In addition, there is a simple resistive dc load in place of a grid connected inverter. The control components include measurement transducers, control blocks, and signal lines. The measurement transducers (represented by dots) measure the line-to-line voltage of the source, the current into the VSR, and the dc voltage (V_{dc}). The line-to-line voltage is provided to the PLL while the currents (i_a and i_c) are provided to the 2/3 block that infers the current of the 3rd phase. The dc voltage is compared to the dc voltage command (V_{dc}*) and a Proportion Integral (PI) controller produces the direct-axis current command (i_d*) from the error. The PLL provides a source angle reference (ϕ) and the quadrature-axis current command (i_q*). The source angle is used by the abc/dq and dq/abc transforms to respectively convert time domain signals to the rotating reference frame and back again. The current commands are compared to their measured counterparts to provide error signals to PI controllers. These PI controllers produce the direct and quadrature-axis VSR input voltage commands v_d and v_q. The appropriate VSR gating is created from the time domain representation by the PWM Generator block.

The operating principle of feedback control relies on the use of PI controllers. Typically PI controllers are used to minimize the amount of calculations and eliminate the use of any specific parameter values for which error tolerances would affect the controller output. Thus instead of calculating a value, feedback is used to determine it. For example we can calculate that we need

a certain amount of current using $I=V/R$ for a situation where we have a desired voltage and an actual resistance that we know the value of to a certain tolerance. In the second case we use feedback to determine the value by increasing or decreasing the current until the voltage is as desired. This second method provides the correct answer regardless of the actual value of the resistance versus its known value or changes in its value due to heating. Transforms were used to decouple the direct and quadrature-axis currents. Correct operation of the PLL is very important for the transforms to work properly. If the reference angle is not generated properly the measured parameters will not be properly transformed into real (direct-axis) and imaginary (quadrature-axis) components. The transforms used to convert quantities into the reference frame of the phase A rotor voltage are somewhat different than those built into Matlab and thus the modified transforms are presented here. The transform used for current takes the three-phase rectifier currents ($\vec{i}_a$, $\vec{i}_b$, and $\vec{i}_c$) as inputs. In this case it is possible to measure just two of them as it is a balanced system and:

$$\vec{i}_a + \vec{i}_b + \vec{i}_c = 0 \tag{2-49}$$

If needed, only one could be measured creating the next one by using a 120 phase shift as in steady state:

$$\vec{i}_a = \vec{i}_b \angle -120° = \vec{i}_c \angle +120° \tag{2-50}$$

That however would result in a time delay of the feedback and was therefore not used. To provide the direct-axis and quadrature-axis currents, i_d and i_q respectively, from the values measured in the stationary time domain reference frame the following transforms are used:

$$\begin{aligned} i_d &= \frac{2}{3}\left(i_a \sin(\omega t) + i_b \sin(\omega t - \frac{2\pi}{3}) + i_c \sin(\omega t + \frac{2\pi}{3}) \right) \\ &= \frac{2}{3}\left(i_a \sin(\omega t) - i_b \left(\frac{1}{2}\sin(\omega t) + \frac{\sqrt{3}}{2}\cos(\omega t) \right) + i_c \left(\frac{1}{2}\sin(\omega t) + \frac{\sqrt{3}}{2}\cos(\omega t) - \sin(\omega t) \right) \right) \end{aligned} \tag{2-51}$$

$$\begin{aligned} i_q &= \frac{2}{3}\left(i_a \cos(\omega t) + i_b \cos(\omega t - \frac{2\pi}{3}) + i_c \cos(\omega t + \frac{2\pi}{3}) \right) \\ &= \frac{2}{3}\left(i_a \sin(\omega t) - i_b \left(\frac{1}{2}\cos(\omega t) - \frac{\sqrt{3}}{2}\sin(\omega t) \right) + i_c \left(\frac{1}{2}\cos(\omega t) - \frac{\sqrt{3}}{2}\sin(\omega t) - \cos(\omega t) \right) \right) \end{aligned} \tag{2-52}$$

The outputs are then passed through 2nd order 200 Hz low pass filters providing the controller with feedback of i_d and i_q. i_d is related to P which is related V_{dc} while i_q is related to pf. Thus the desired i_d (i_d*) can be calculated:

$$i_d^* = \frac{\sqrt{2} \cdot V_{dc}^{\ 2}}{3 V_{an} R_{load}} \tag{2-53}$$

However, since PI controllers are to be used this equation is only used for calculating an expected value. The PI controllers produce respective voltage commands to correct the current errors which they are provided. Once these desired d and q axis voltages commands (V_d and V_q) are ascertained they are converted back into the time domain 3-phase voltages (V_a, V_b, and V_c) by the following additional transforms:

$$v_a = v_d \sin(\omega t) - v_q \cos(\omega t) \tag{2-54}$$

$$\begin{aligned} v_b &= v_d \sin(\omega t - \frac{2\pi}{3}) + v_q \cos(\omega t - \frac{2\pi}{3}) \\ &= -v_d \left(\frac{1}{2}\sin(\omega t) + \frac{\sqrt{3}}{2}\cos(\omega t) \right) - v_q \left(\frac{1}{2}\cos(\omega t) - \frac{\sqrt{3}}{2}\sin(\omega t) \right) \end{aligned} \tag{2-55}$$

$$\begin{aligned} v_c &= v_d \sin(\omega t + \frac{2\pi}{3}) + v_q \cos(\omega t + \frac{2\pi}{3}) \\ &= v_d \left(\frac{1}{2}\sin(\omega t) + \frac{\sqrt{3}}{2}\cos(\omega t) - \sin(\omega t) \right) + v_q \left(\frac{1}{2}\cos(\omega t) - \frac{\sqrt{3}}{2}\sin(\omega t) - \cos(\omega t) \right) \end{aligned} \tag{2-56}$$

It is possible to transform this three-phase representation into a two axis representation. However, it is advantageous to use the following transforms instead to convert directly from the dq reference frame to the stationary two axis, v_α and v_β, representation:

$$v_\alpha = v_d \cos(\omega t) - v_q \sin(\omega t) \tag{2-57}$$

$$\begin{aligned} v_\beta &= v_d \cos(\omega t + \frac{\pi}{2}) + v_q \sin(\omega t + \frac{\pi}{2}) \\ &= v_d \sin(\omega t) + v_q \cos(\omega t) \end{aligned} \tag{2-58}$$

Since PI controllers are used to create desired quantities which are transformed back into the time domain for converter gating, reference values are required. i_d^* is provided by the V_{dc} PI controller. In order to provide the reference i_q^* for appropriate excitation current we notice the phase shift of the reference frame:

$$i_q^* = \mathrm{Re}\{\vec{I}_L\} \sin\gamma + \mathrm{Im}\{\vec{I}_L\} \cos\gamma \tag{2-59}$$

Using (2-42) and substituting in (2-3) and (2-37):

$$\vec{I}_L = \frac{\omega^2 \,\mathrm{Re}\{S_{base}\}}{\omega_{\mathrm{base}}^{\ 3} k_{vf} 3} + j\left(\mathrm{Im}\{\vec{I}_S\} - \omega^2 C k_{vf}\right) \tag{2-60}$$

i_q^* can now be calculated by the PLL block in Figure 2-6 and is plotted in Figure 2-7 with respect to frequency.

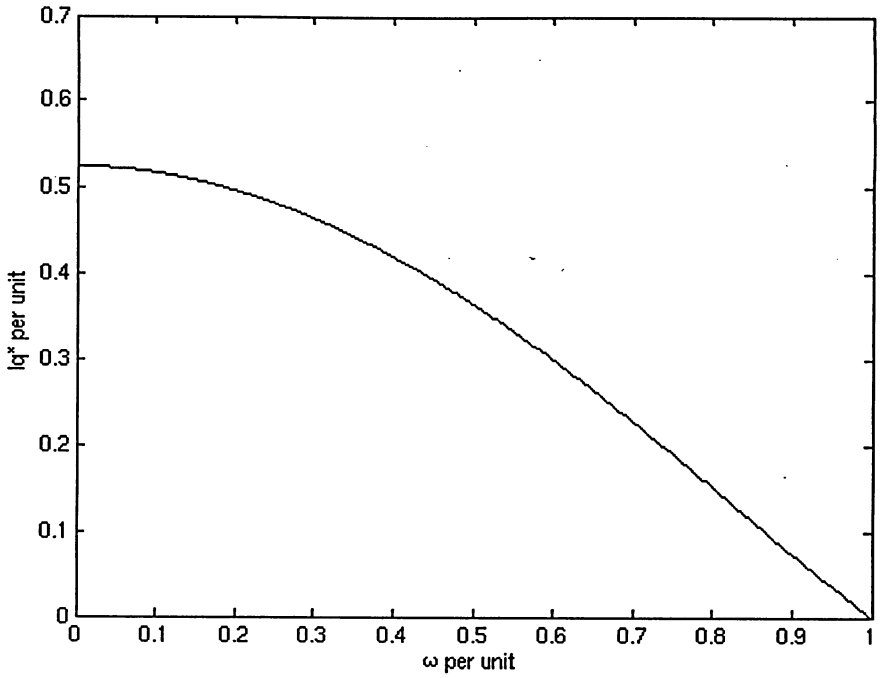

Figure 2-7: Iq command

Use of cross-coupled PI controllers for i_d and i_q would follow standard principles. However, direct coupled control is required for systems where the controller time-step is less than 200μs. Thus the control lines in Figure 2-6 are simply uncrossed linking v_d to i_d and v_q to i_q. This strategy handles the current transients in the system better resulting in more stable control.

2.5 Conclusions

This chapter has presented PWM rectifier theory for wind driven SEIG applications. The theory presented includes an equation to determine the optimal excitation capacitance to be used with a SEIG. It also provides details of variable frequency PWM rectifier operation. Following the details of PWM rectifier operation, a control strategy is developed.

The equation provided calculates the value of the delta connected excitation capacitors required to minimize the VA rating requirement of the converter. The use of these capacitors allow the use of a rectifier rated only for the real power provided by a wind driven SEIG. Without the use of the optimized excitation capacitance the rating of the converter will have to be at least 30%

greater.

In addition to the capacitance formula, close examination of PWM rectifier operation led to the identification of a limitation and a concept. Examination of the function of a PWM rectifier reveals limitations in its operation in isolated SEIG systems rotating at extremely low speeds. Direct coupled control is required for systems where the controller time-step is less than 200μs.

The simulation of these contributions is discussed in the following chapter while the proof of concept built to experimentally verify it is detailed in the subsequent chapter.

Chapter 3 – Simulation of a PWM Rectifier for Wind Driven Induction Generators

This chapter describes the verification of the wind driven SEIG fed PWM rectifier feedback control scheme developed in chapter 2 by simulation. In addition to using computer aided analysis to verify the theoretical controller proposed, further investigation into the response of the controller is detailed. The first section in this chapter describes the construction of the model used in simulation. It provides details about both the electrical and the control components. The second section presents the simulation results as evidence that the variable frequency PWM rectifier controller discussed in chapter 2 responds as intended. Six subsections present simulation results with each focusing verifying a different aspect of the controller. The first subsection demonstrates that PLL lock is achieved and that appropriate gating is generated by using a diagram to depict the source and rectifier voltage. The second subsection investigates control of the dc output voltage which will be maintained at a constant value. The third subsection verifies stable unity power factor operation at rated power. The fourth subsection confirms that the transient performance of the controller is acceptable for the transition from rated to half power. The fifth subsection verifies stable steady state operation at half power, an operation point at which excitation current is provided by the rectifier. The sixth subsection confirms that the transient performance of the controller is acceptable when transitioning from half to rated power. The conclusion is that the controller, as described in chapter 2, has been verified by simulation.

3.1 Model Construction

The intended system parameters and control systems were built in Mathworks' Matlab Simulink simulation environment. The controller block diagram presented in Figure 2-6 was used as a guide for building the direct-coupled controller shown in Figure 3-1.

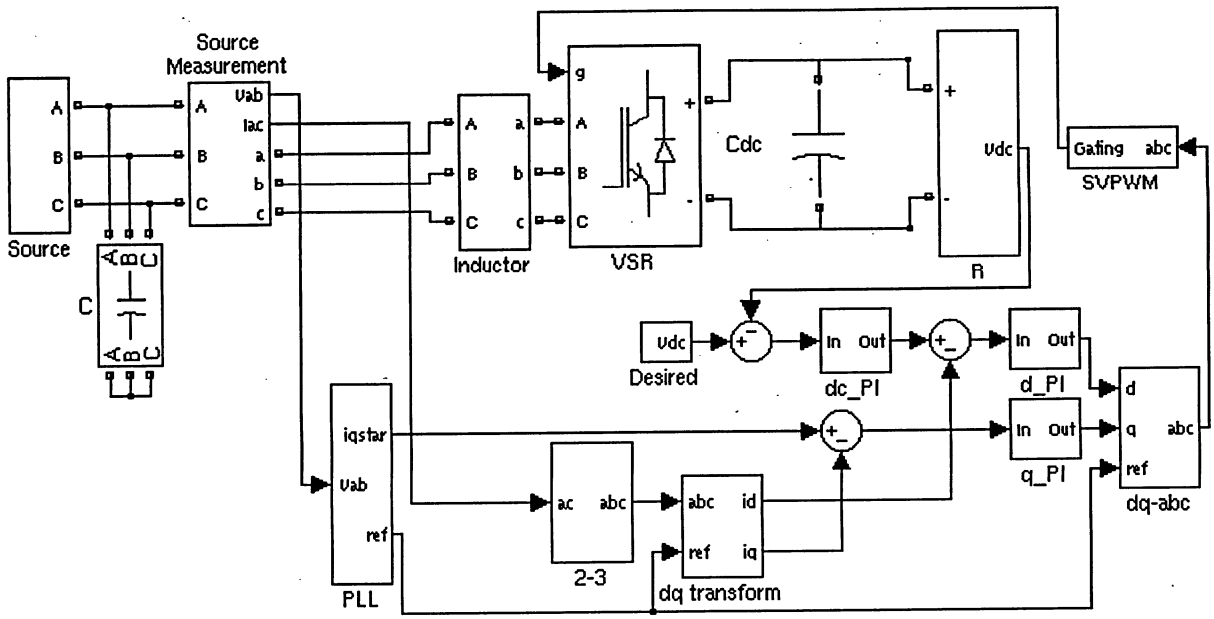

Figure 3-1: Simulink simulation top level block diagram

The details of how the various blocks of the simulation were constructed are described in the following subsections. The Source is a voltage source which is used to represent the SEIG. Excitation capacitors (C) are attached as per (2-26). The output of the Source is measured by the Source Measurement block which provides v_{ab} to the PLL as well as i_a and i_c for the transforms. The three-phase power then flows through the three-phase line Inductor to the Voltage Source Rectifier (VSR). The gating of the VSR is provided by the Space Vector Pulse Width Modulation (SVPWM) block which takes a three phase time domain input from the dq-abc transform block. The dc output of the VSR is supported by the dc capacitance C_{dc} and connected to the resistive load R. The PLL locks on to v_{ab} and calculates the appropriate quadrature-axis current command (i_q*). It also provides the reference phase angle (ref) to the transforms. The third unmeasured phase can be derived from the two measured phases by the 2/3 block and provide the three-phase time domain currents to the dq transform block. The dc voltage is compared to the Desired V_{dc} and the Proportion Integral (dc_PI) controller produces the direct-axis current command from the error. The current commands are compared to their measured counterparts to provide error signals to the current PI controllers (d_PI and q_PI). These PI controllers produce the direct and quadrature-axis VSR input voltage commands v_d and v_q. The gains for the PI controllers are provided in the control parameters subsection. Each of the respective subsections expand on these explanations.

3.1.1 Source

Simulations of the entire proposed system, including the wind driven SEIG as the electrical source, would take the better part of a day to run. The ability to run the simulation in a shorter amount of time allows parameter changes to be tested more efficiently. Thus in order to simplify the simulation, the self-excited induction generator is approximated by a three-phase controlled voltage source. Figure 3-2 depicts the block diagram of the source used in the simulations.

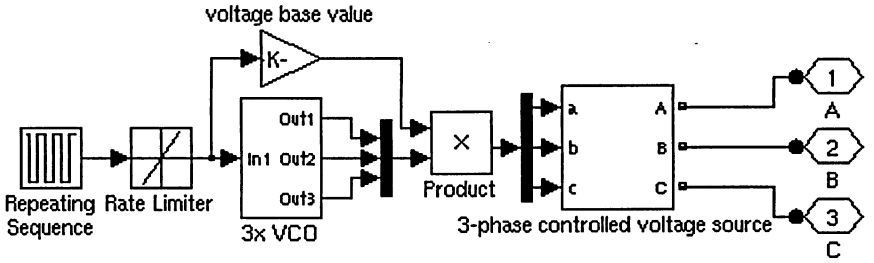

Figure 3-2: Simulink source block diagram

The source is composed of a number of blocks that produce a three-phase variable amplitude and variable frequency voltage source. The per-unit frequency command values are incorporated into a Repeating Sequence block. The repeating sequence block is used to start at a value, change to another, and then return to the original value during a 2 second simulation. The changes in the per-unit frequency command are limited by a Rate Limiter block. A step change is a good worst case test for a control system however a step change in this system causes the PLL lock to be lost. Thus the rate of change must be limited. This does not cause the simulation to model the system any less accurately since the rotational speed of a large wind turbine also has a maximum rate of change corresponding to the maximum torque it can handle. The resulting frequency command is provided to a block containing 3 Voltage-Controlled Oscillators (VCO). These oscillators are 120° out of phase with each other. Multiplication of the oscillator output by the voltage base value based on the per unit frequency command scales the output amplitude, using the product block, keeping the ratio of the voltage to the frequency of the source constant which keeps the air-gap magnetic flux of the generator constant. The final block is the 3-phase controlled voltage source which translates the voltage signals into their respective electrical representations and includes an equivalent total leakage inductance.

3.1.2 VSR and respective PWM gating

The voltage source rectifier is based on the 3-phase PWM Integrated-Gate Bipolar Transistor (IGBT) boost rectifier topology shown in Figure 3-3.

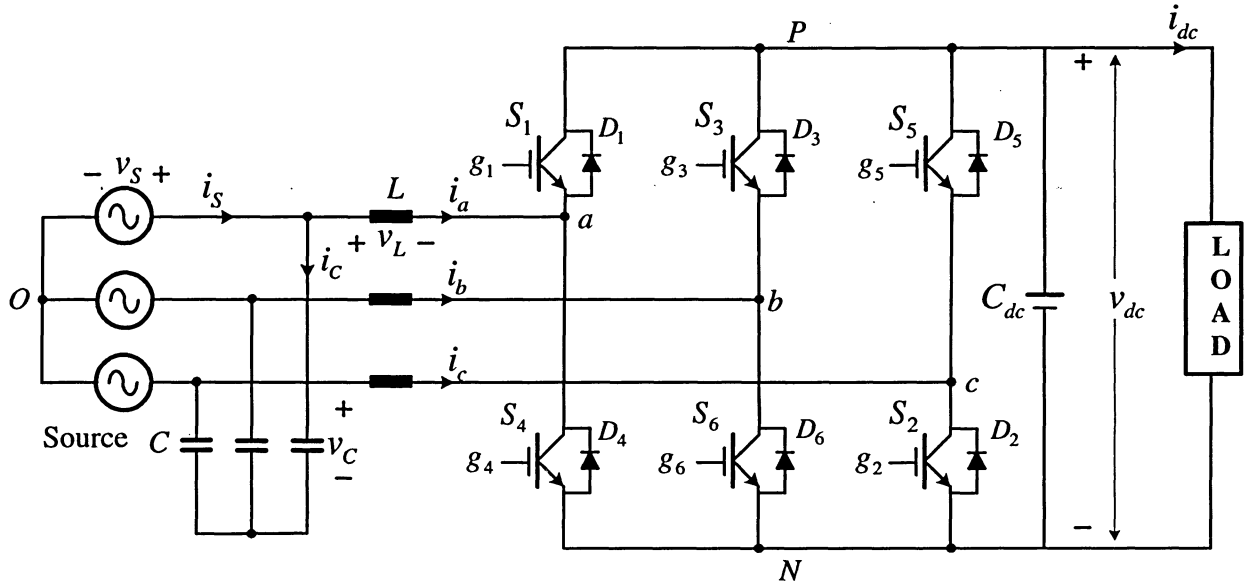

Figure 3-3: 3-Phase IGBT rectifier

The source is shown as 3 Y-connected sinusoidal voltage sources (v_S) with the output phase current of i_S. The excitation capacitors (C with current i_C) are also Y-connected to be able to designate the capacitor phase voltage v_C which is equivalent to the source voltage. The connection to the converter is made via line inductances (L) with the respective voltage drop of v_L. The converter consists of six IGBTs, each of which have a free-wheeling diode connected in parallel. The input current is represented by i_a, i_b, and i_c while the dc output voltage (v_{dc}) is filtered by the dc capacitance (C_{dc}) to provide the dc current (i_{dc}) to the load. The switching frequency of the rectifier (1080Hz) is 18 times its rated operation frequency of 60Hz. It is chosen to be 1080 Hz in order to be high enough to have low THD while low enough that the converter runs with reasonable efficiency. Each time the switches operate some energy is lost and if the switching frequency is much higher not only will energy be lost but it will have to be dissipated by an additional cooling mechanism to keep the switch from overheating. The gating for the switches is generated by using the SPWM technique, an example of which is shown in Figure 3-4.

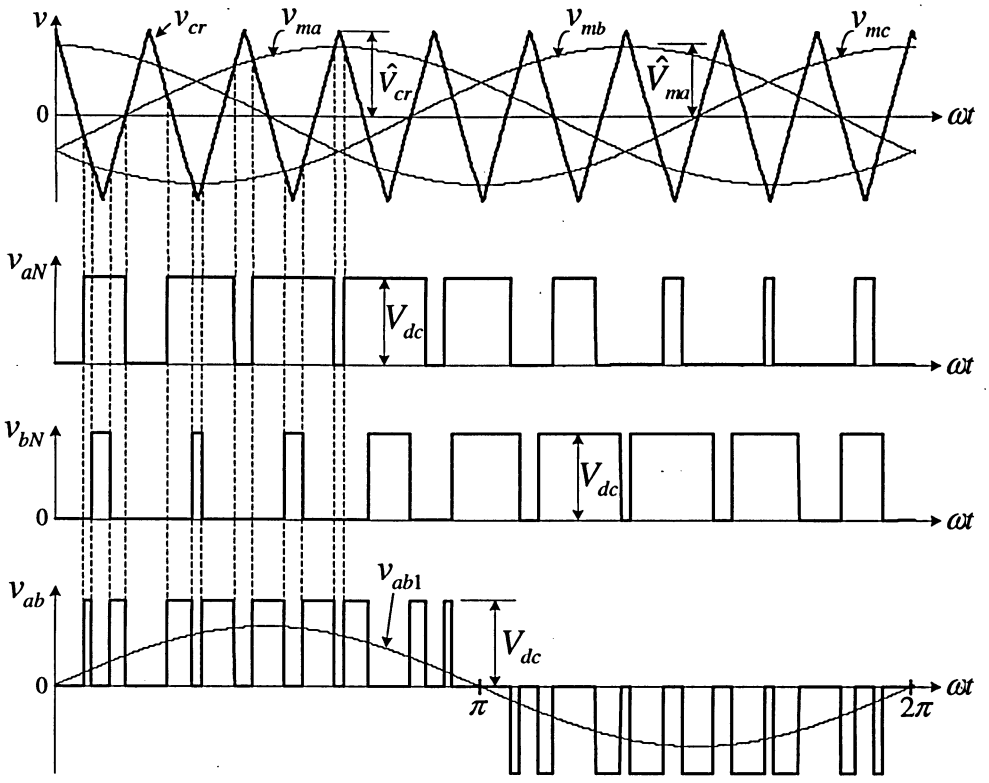

Figure 3-4: SPWM gating

The top axis shows the three-phase sinusoidal modulating waves (v_{ma}, v_{mb}, and v_{mc}) and the triangular carrier wave (v_{cr}). $\hat{V}_{ma}$ is the peak value of the modulating waves while $\hat{V}_{cr}$ is the peak value of the carrier wave (typically fixed). The amplitude of the fundamental-frequency component in the converter's three-phase voltage is controlled by the modulation index m which is the ratio of $\hat{V}_{ma}/\hat{V}_{cr}$. The converter's three-phase frequency varies with the frequency of modulating waves. The operation of switches is determined by comparing the modulating waves to the carrier wave. The switching pattern in Figure 3-4 is shown with a high modulation index and low frequency modulation (the ratio of the carrier frequency to the modulating frequency) for clarity. The leg a terminal voltage, the magnitude of which is equal to the dc voltage (V_{dc}), with respect to the negative dc bus (N) is shown on the v_{aN} axis. The switches in each leg operate in complementary manner such that when upper switch (S1) in inverter leg a is on for when v_{ma} is greater than v_{cr}, the lower switch (S4) is off. The leg b terminal voltage with respect to the negative dc bus is shown on the v_{bN} axis such that the converter's resulting line-to-line voltage (v_{ab}) can be displayed on its respective axis. Also provided on the v_{ab} axis is the waveform of its fundamental-frequency component (v_{ab1}).

3.1.3 Load

For the purposes of this research we aim to operate on the steady state peak power conversion curve as presented in the introduction. The load is a switched resistor load as shown in Figure 3-5.

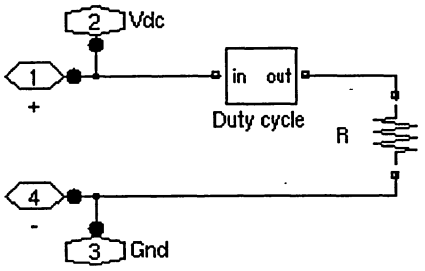

Figure 3-5: Switched load block

The full power load is attached for rated frequency and when the frequency changes a lower load is implemented by reducing the duty cycle from 100% by tying it to the cubic root of the per unit frequency. This is done such that the power curve presented in Figure 1-1 is followed for the constant dc voltage.

3.1.4 PLL block

This subsection describes how the PLL block shown in Figure 3-6 was used to track the source.

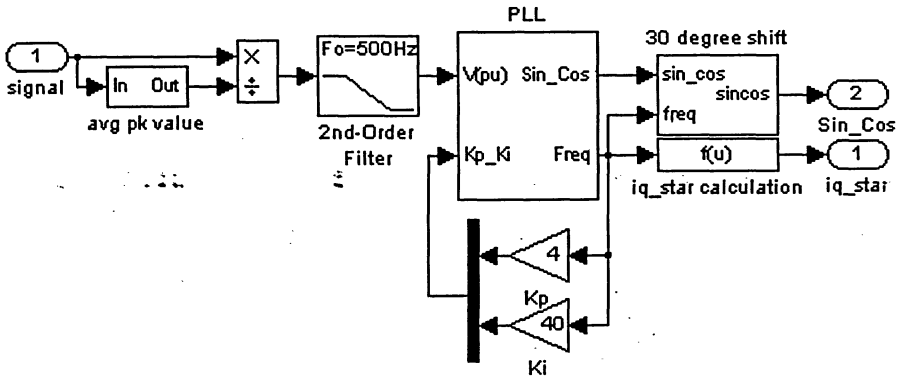

Figure 3-6: PLL Block

The first step is normalizing the input signal. This is done by dividing it by its average peak value. The result is filtered to remove noise from the signal prior to providing it to the PLL. The

PLL uses frequency dependant gain as shown with the proportional and integral gains set to 4 and 40 respectively. As $\vec{V}_{ab}$ is measured, a block is used to ensure a 30° phase shift is to have the sine and cosine accurately represent the angle of $\vec{V}_S$. (2-59) is used by the iq_star calculation block to provide i_q^*. As stated in the theory chapter, $\vec{V}_S$ is the reference and $\vec{I}_L$ is the quantity to be controlled by $\vec{V}_m$. The feedback controller uses the PLL to extract the phase angle for the transforms. In the case of the transforms we need to quantify the phase shift of the preceding blocks for the phase shift block to be able to provide the remainder of the shift required ($\Delta\varphi$). Part of the phase shift is due to the filtering of the input signal to the PLL and an additional component is due to how the remainder of the PLL functions. The phase shift of the filter, which is 9.7694° at 60 Hz as shown in Figure 3-7, is linear with respect to frequency f and is thus easily modeled.

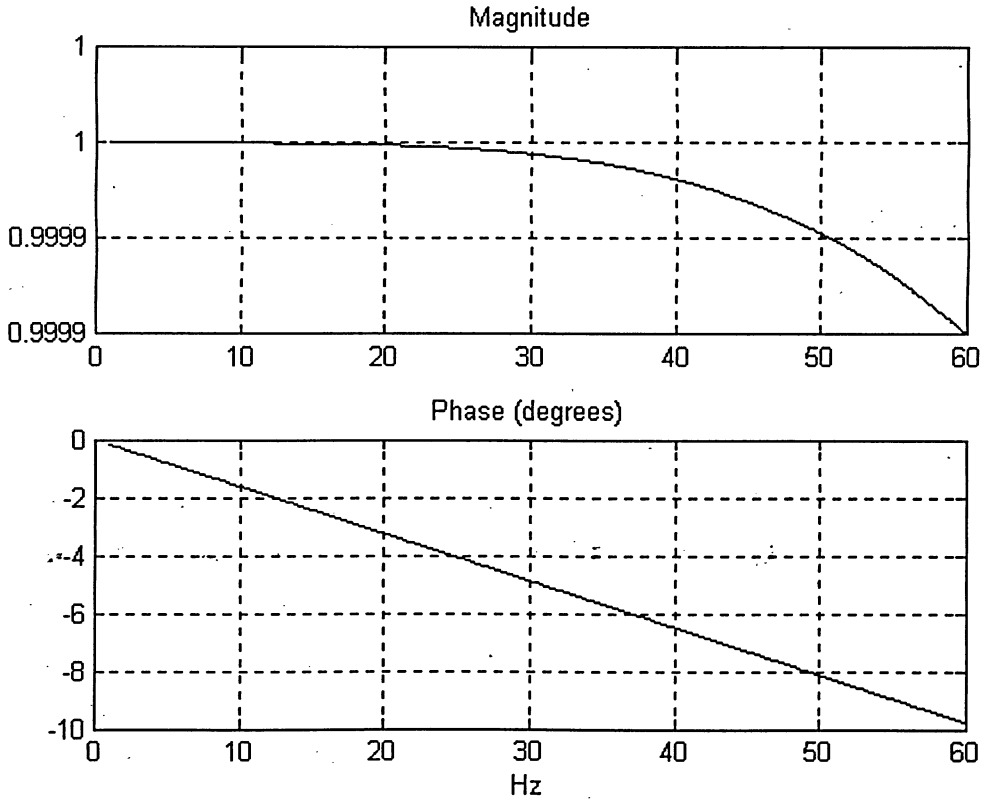

Figure 3-7: 500Hz 2nd order filter frequency response

Heuristically we find that the additional phase shift responds similarly and is approximately 4° at

60 Hz. Thus we delay the signal by the following additional quantity to produce the reference angle:

$$\Delta\varphi = 30° - kf$$
$$\text{where } k = \frac{9.7694° + 4°}{60Hz} \tag{3-1}$$

Additional filtering of the signals takes place after the transform to reduce the likelihood of any additional phase shift of the measured signals. Once transformed the signals are no longer sinusoidal values but representations of vector magnitudes which can be filtered.

3.1.5 Transforms

Direct-quadrature (dq) decoupling transforms were used allowing the use of separate feedback control of the d and q currents. They were presented in the theory section 2.4 Variable frequency PWM rectifier feedback control. The dq transform is implemented using (2-51) and (2-52). The abc-dq transform is implemented using (2-54), (2-55), and (2-56).

3.1.6 Control parameters

The main control parameters are the gains of the 3 Proportional-Integral (PI) controllers. They are used as described in section 2.4 Variable frequency PWM rectifier feedback control. Proportional gains provide feedback based on the magnitude of the error while the Integral gains integrate the error signal in order to eliminate steady-state error. Derivative gains use the slope of the signal to predict future output, however they are not used since not only do they reduce the effectiveness of the integral gain, in a real system the signal noise combined with the latency of the system tends to provide unproductive control output. The use of a per-unit control system allows easier transferal of the control system to installations of different sizes such as the scaled down system that is used for the experimental verification. The script files in the appendix do the groundwork of calculating the per-unit values and dependent system parameters. Both current feedback proportional gains are set to 0.13 while the integral gains are set to 2/3. The dc error gains, which provide the direct-axis current reference, are a proportional gain of 90 and an integral gain of 36.

3.2 1MW SPWM rectifier simulation

The system considered is a 1 MW, 60Hz 690V 3-phase wind turbine driven variable frequency PWM rectifier. The simulation results presented in this section provide evidence that the variable

frequency PWM rectifier controller discussed in chapter 2 responds as intended. The scope outputs from the simulation scopes have been captured for the voltages on either side of the input inductance. The rectifier input currents and the output voltages in different conditions have been plotted. The scope outputs have been captured to show the steady state operation at full power, the transition to half power, steady state operation at half power, and the transition back to full power. In addition, the Fast Fourier Transforms (FFT) of the currents at the steady state operation points are considered to be able to construct vector diagrams from the fundamentals of the current. These vector diagrams demonstrate operation as discussed in chapter 2. The system parameters are presented in Table 3-1.

Table 3-1: 1MW system component parameters

1MW SEIG	60Hz 690V	f_{sw}	1080Hz
Rated Current	858A	Magnetizing current	191A
L	0.17mH	C	2000 μF
V_{dc}	1260 V	C_{dc}	68 000 μF

3.2.1 Source and rectifier voltage

The voltage across the line inductance is described by (2-6) to be the voltage drop from the source voltage to the rectifier voltage. The source voltage and the rectifier voltage are shown in Figure 3-8.

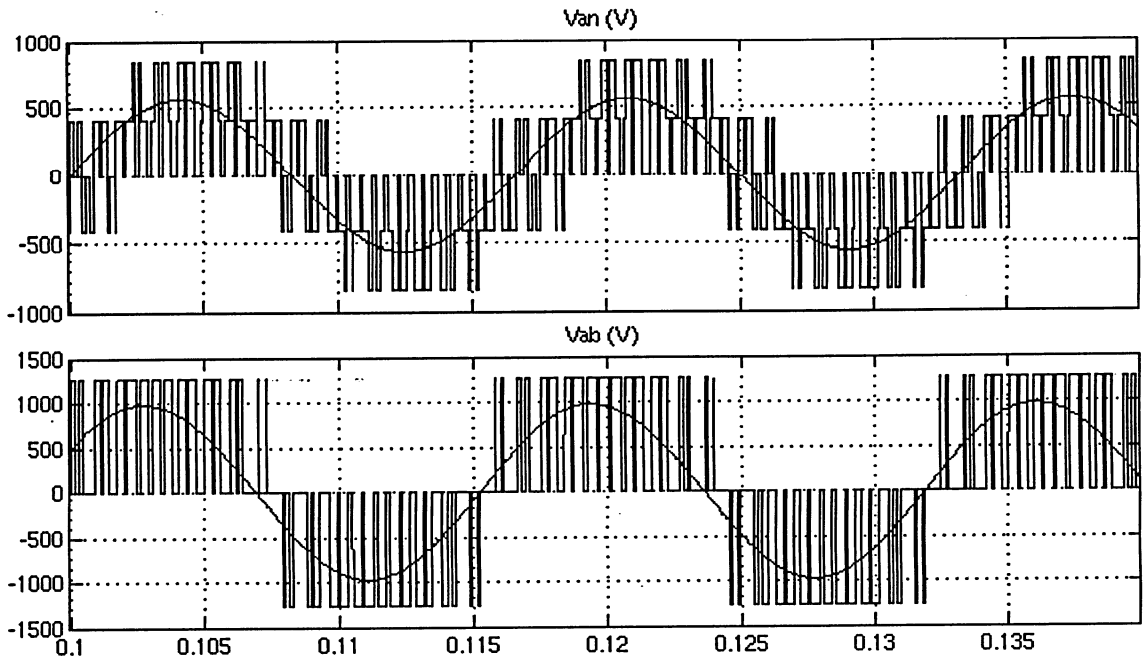

Figure 3-8: Source and rectifier voltages from simulation

Both the phase voltage (v_{an}) and the line-to-line voltage (v_{ab}) are shown. The sinusoidal source voltage (v_S) is a reference both for the PLL and for identifying whether the gating has been generated correctly. The chopped rectifier voltage (v_m) indicates switched voltage patterns demonstrating proper gating functionality including a PLL lock. Note how the phase shift across the inductor is visible by comparing the zero crossing points of v_S and v_m.

3.2.2 Output voltage

As discussed previously, a constant output voltage is desired such that an off-the-shelf approved inverter can be used for a grid connection. The rated voltage of the source and the type of modulation also determine the magnitude of the dc link voltage. The dc voltage is determined by the fact that the controller in use is of a boost configuration and thus is expected to have a value no less than that described by (2-36). The most suitable dc value is very near that obtained by a SPWM modulation index of 1 for the full power scenario. The numerical values are calculated by the scripts in the appendix. The response to a ramp change in the source, the respective voltage regulation, and the recovery time are detailed when conducting the ramp driven transition tests.

3.2.3 Operation at rated power

The key point to be verified during operation at rated power is that unity power factor is maintained at the rectifier as shown in Figure 3-9. The excitation capacitors provide the reactive power requirement of the induction generator at this operation point.

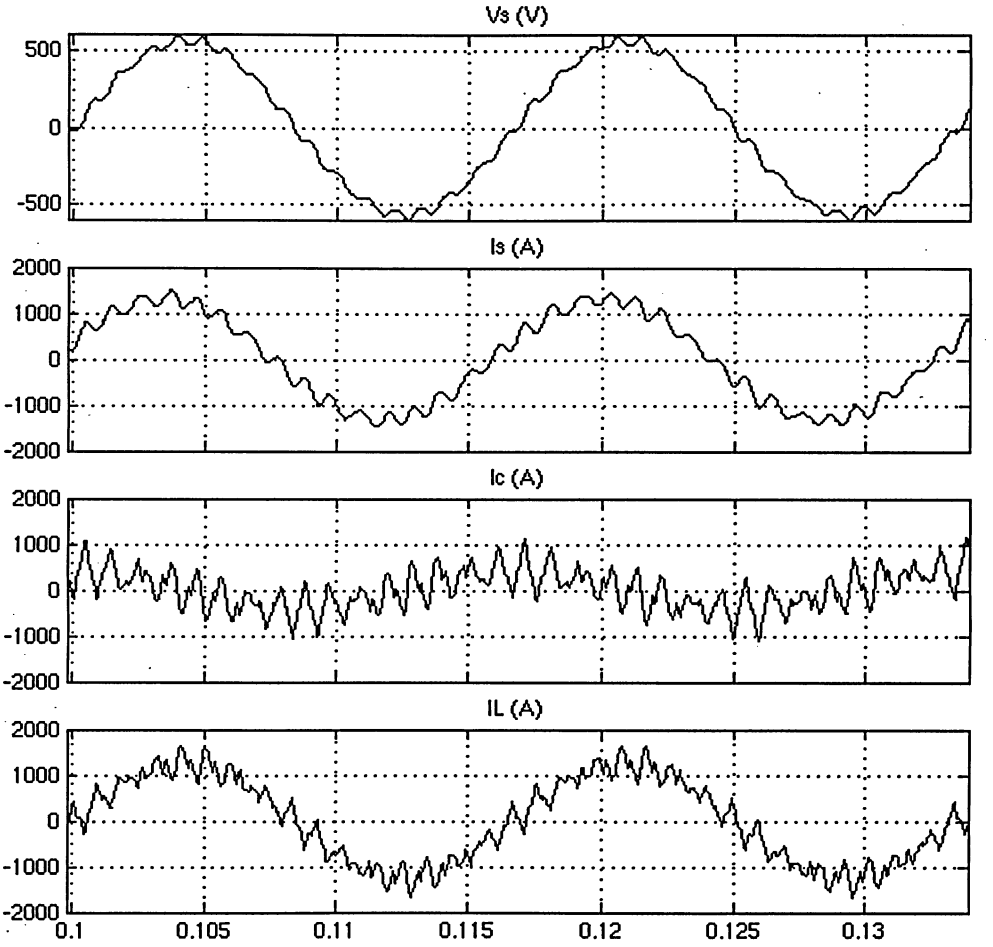

Figure 3-9: Simulation of rectifier operating at rated power

The simulation of the rated power and rated frequency operation is clearly identifiable to be at unity power factor. In order to demonstrate operation as discussed in chapter 2 more conclusively, the FFTs for the steady-state rated power operation are provided in Figure 3-10.

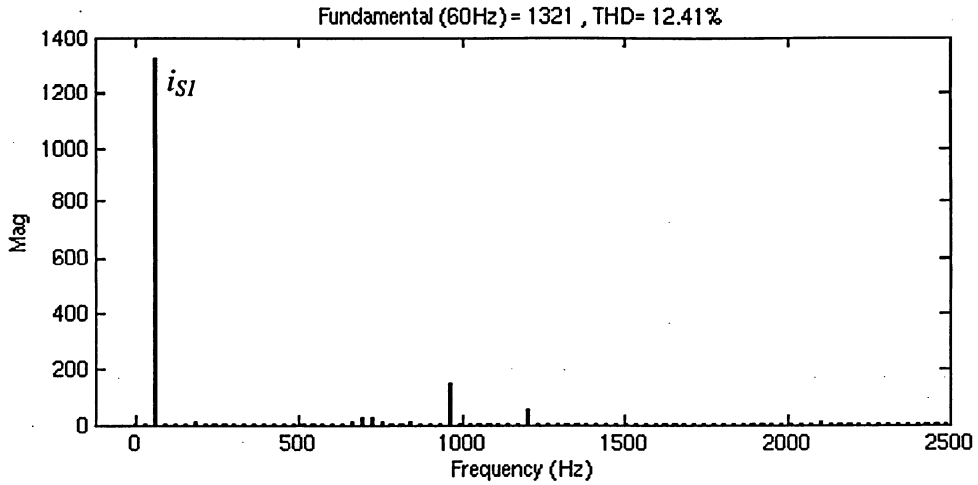

(a) Machine current, i_S

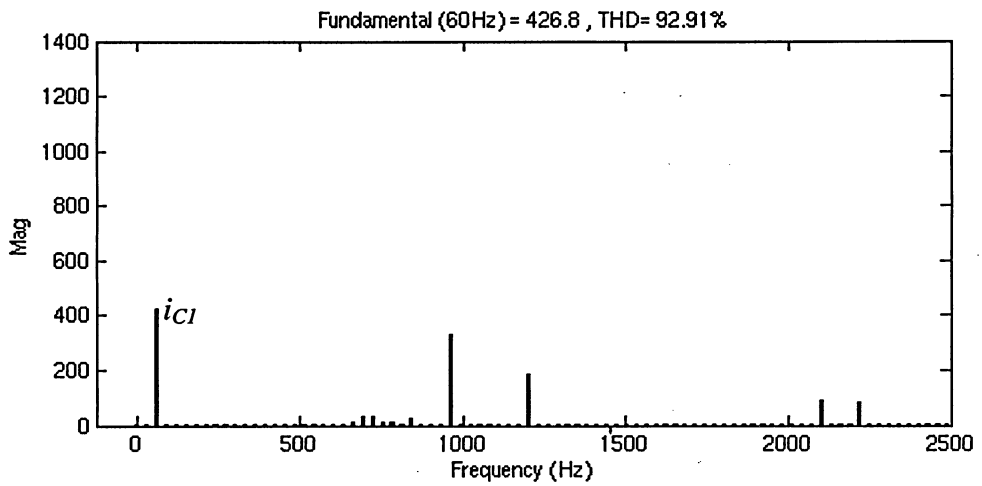

(b) Capacitor current, i_C

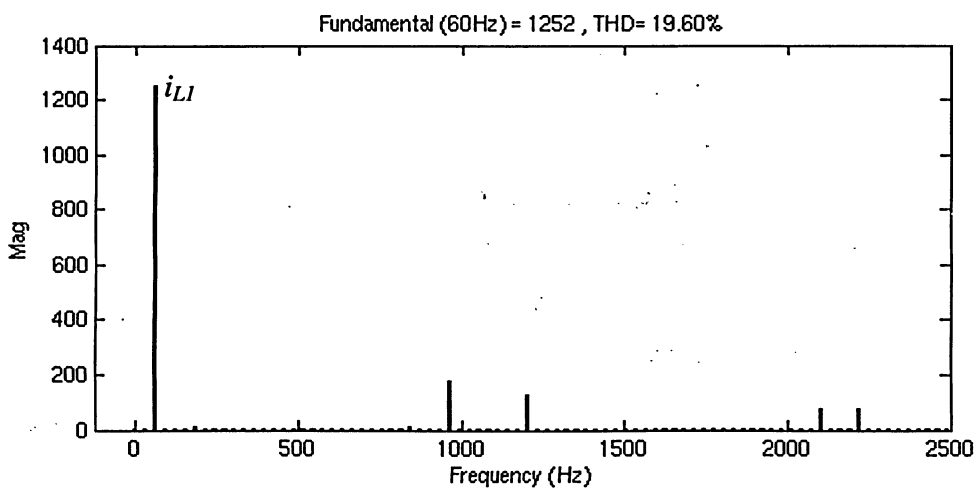

(c) Converter current, i_L

Figure 3-10 Per-unit peak value FFTs of current at full power, unity power factor operation

The machine current FFT shows that the machine experiences some partially filtered switching related current harmonics. Higher frequency harmonic currents created by the converter are completely filtered by the excitation capacitors. Thus, the THD experienced by the machine is reduced. The rms values of the fundamental currents are used to construct the vector diagram in Figure 3-11.

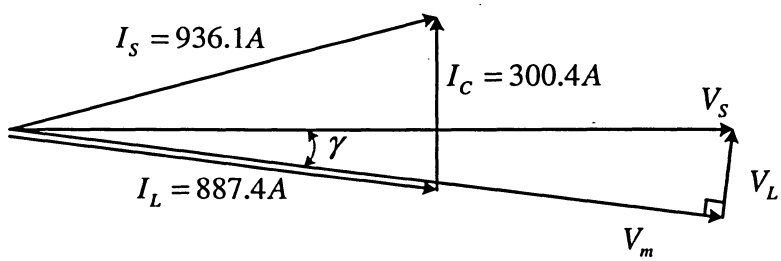

Figure 3-11: Resulting vector diagram of operation at full power, unity power factor

The vector diagram clearly indicates that the PWM rectifier operates at unity power factor by showing that the reactive current ($\vec{I}_C$) provided by the capacitance allows the rectifier input current ($\vec{I}_L$) to be in phase with the rectifier three-phase input terminal voltage ($\vec{V}_m$). Thus allowing the converter to only carry the real power.

3.2.4 Transition from rated to half power

The transition from rated to half power operation is considered in order to test the dynamic attributes of the controller. A ramp function is generated to simulate this transition to the half rated power steady-state operating point resulting in Figure 3-12.

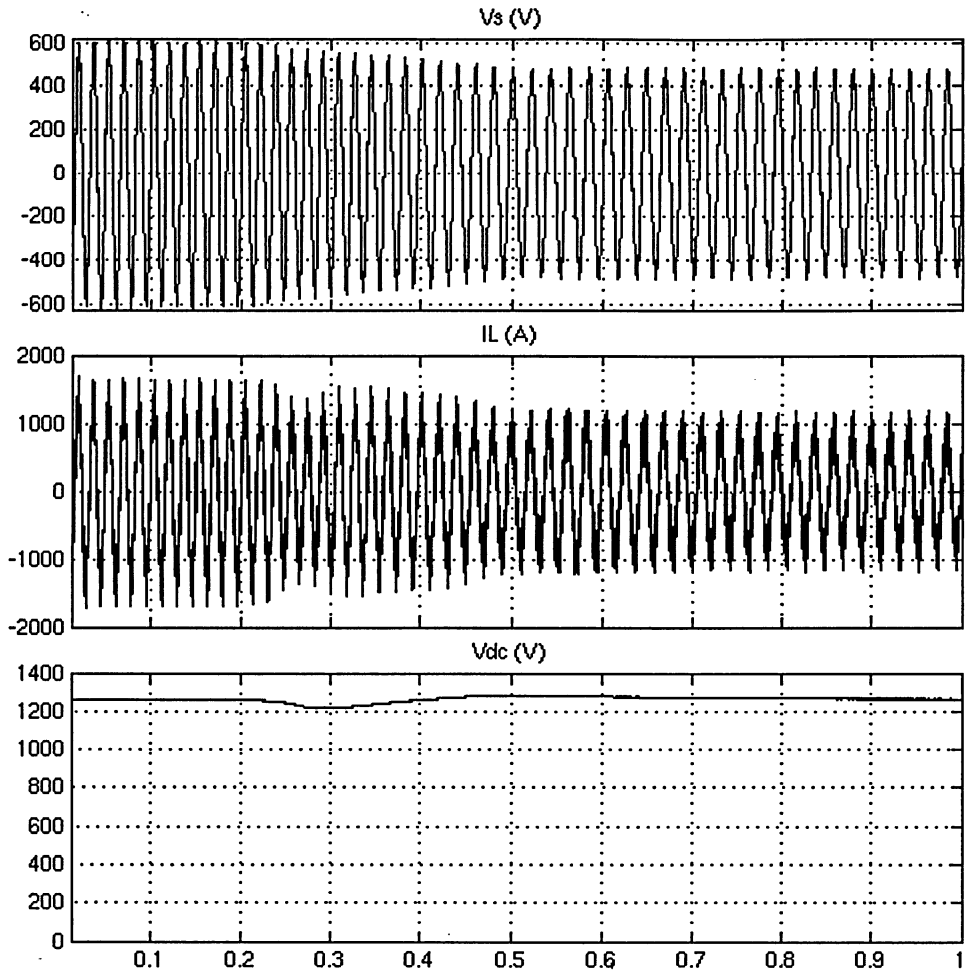

Figure 3-12: Simulation of rectifier transitioning from rated power to half rated power

There is a slight drop in dc voltage as the transition begins as since the power supplied drops before the PLL and the rest of the controller can react. Let us consider the time it takes the controller to recover from the change in the source. Once the ramp is applied to the system, the dc voltage recovers (to a tolerance of 2%) in 337ms. In addition, the voltage regulation (*VR*) is calculated by considering the dc voltages prior to (V_{rated}) and after (V_{half}) the transition:

$$\begin{aligned} VR &= \frac{V_{half} - V_{rated}}{V_{rated}} X\ 100\% \\ &= \frac{1264 - 1257}{1257} X\ 100\% \\ &= 0.56\% \end{aligned} \qquad (3\text{-}2)$$

This demonstrates the ability of the system to provide near constant voltage over a wide range of conditions. The power locus over rotational speed of these conditions is found in Figure 1-1

where the peak power transfer points are plotted. As per subsection 3.1.3 the load is varied to such that maximum power transfer is maintained at constant dc voltage for varying rotational speed.

3.2.5 Operation at half power

The key idea behind operation at power points other than at rated power is to provide the corresponding reactive power to the induction generator. The excitation capacitors provide less and less of the required excitation current when both the frequency and voltage are reduced as the power is reduced. The half power case was chosen to demonstrate the provision of this reactive power and the scripts in the appendix were used to determine the respective rotational speed, hence frequency. The simulation of the half rated power operation point confirms provision of reactive current. The leading current is most easily noticed by observing zero crossings in Figure 3-13.

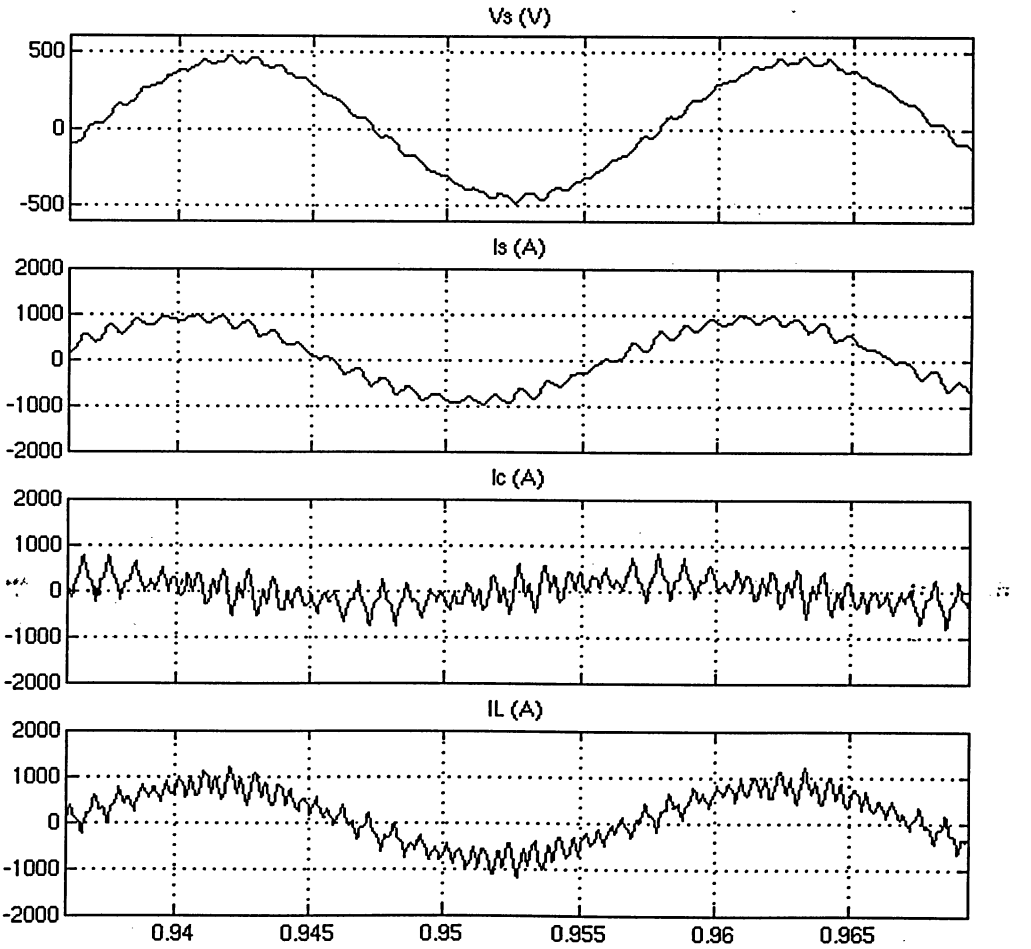

Figure 3-13: Simulation of rectifier operating at half rated power

The current FFTs for the steady-state half rated power operation are provided in Figure 3-14.

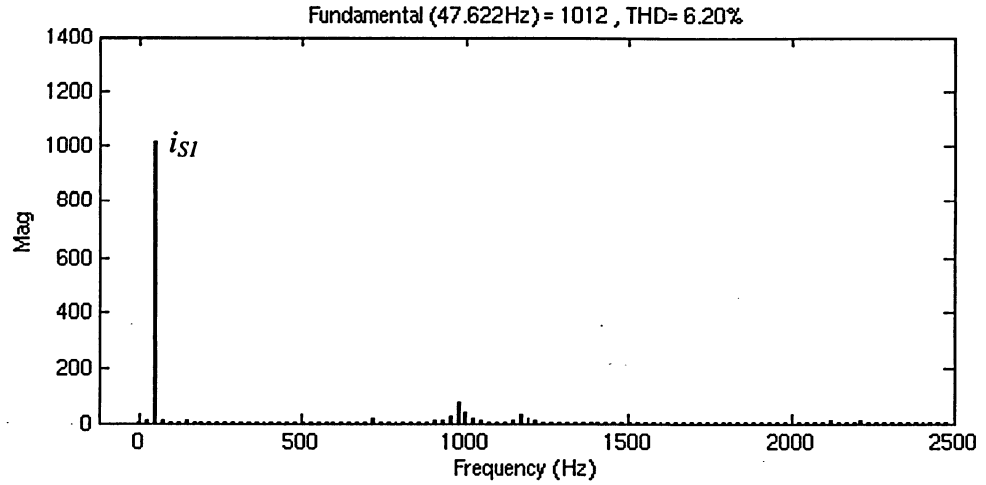

(a) Machine current, i_S

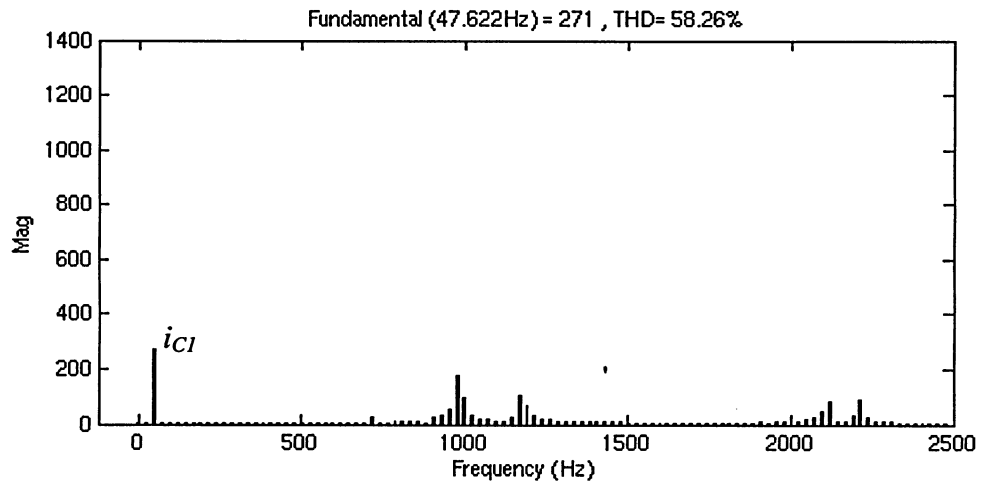

(b) Capacitor current, i_C

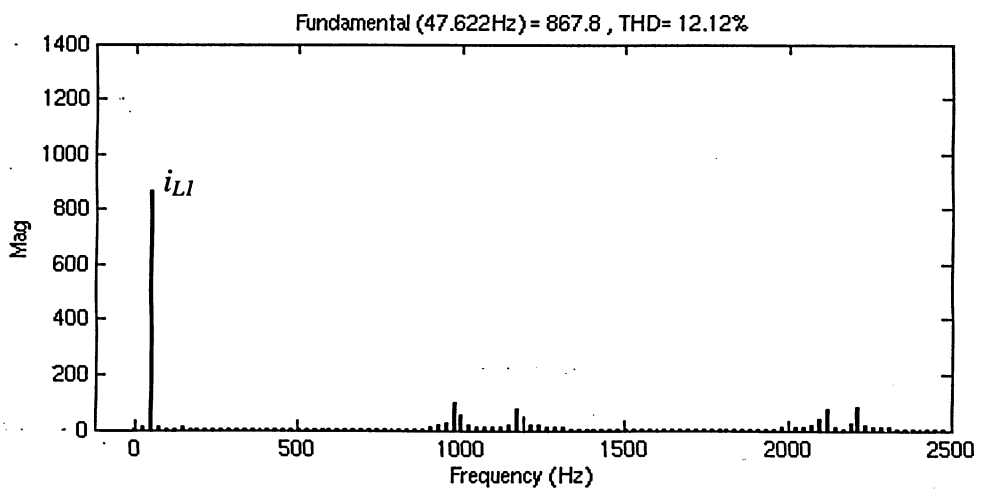

(c) Converter current, i_L

Figure 3-14 Per-unit peak value FFTs of current at half power, leading current operation

This half power case was chosen to demonstrate the provision of reactive current to the machine in order to demonstrate operation as discussed in chapter 2 more conclusively. The reactive current provided by the capacitors is reduced due to lower frequency and lower source voltage. Once again, the machine current FFT shows that the machine experiences some partially filtered switching related current harmonics. Higher frequency harmonic currents created by the converter are completely filtered by the excitation capacitors. Thus, the THD experienced by the machine remains low. The rms values of the fundamental currents are used to construct the vector diagram in Figure 3-15.

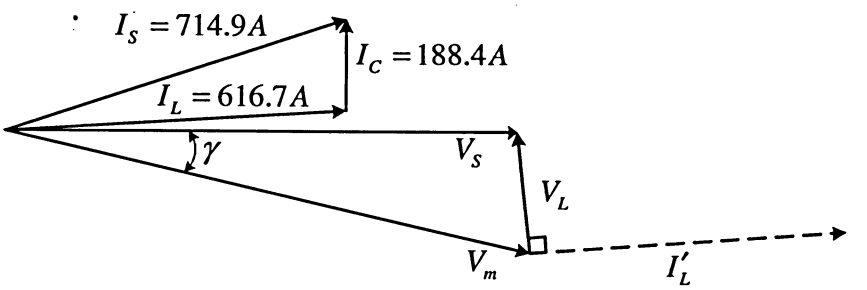

Figure 3-15: Resulting vector diagram of operation at half power, leading current

The vector diagram clearly shows that the PWM rectifier input current ($\vec{I}_L$) leads the the rectifier three-phase input terminal voltage ($\vec{V}_m$). Thus the reduction of the reactive current ($\vec{I}_C$) provided by the capacitance at lower frequency has been compensated for by the converter providing reactive current such that the machine is still provided the correct magnetization current. This verifies the correct operation of the control strategy described in chapter 2.

3.2.6 Transition from half to rated power

For completeness, the transition back to rated power from half rated power is considered. A ramp function is used again with the results depicted in Figure 3-16.

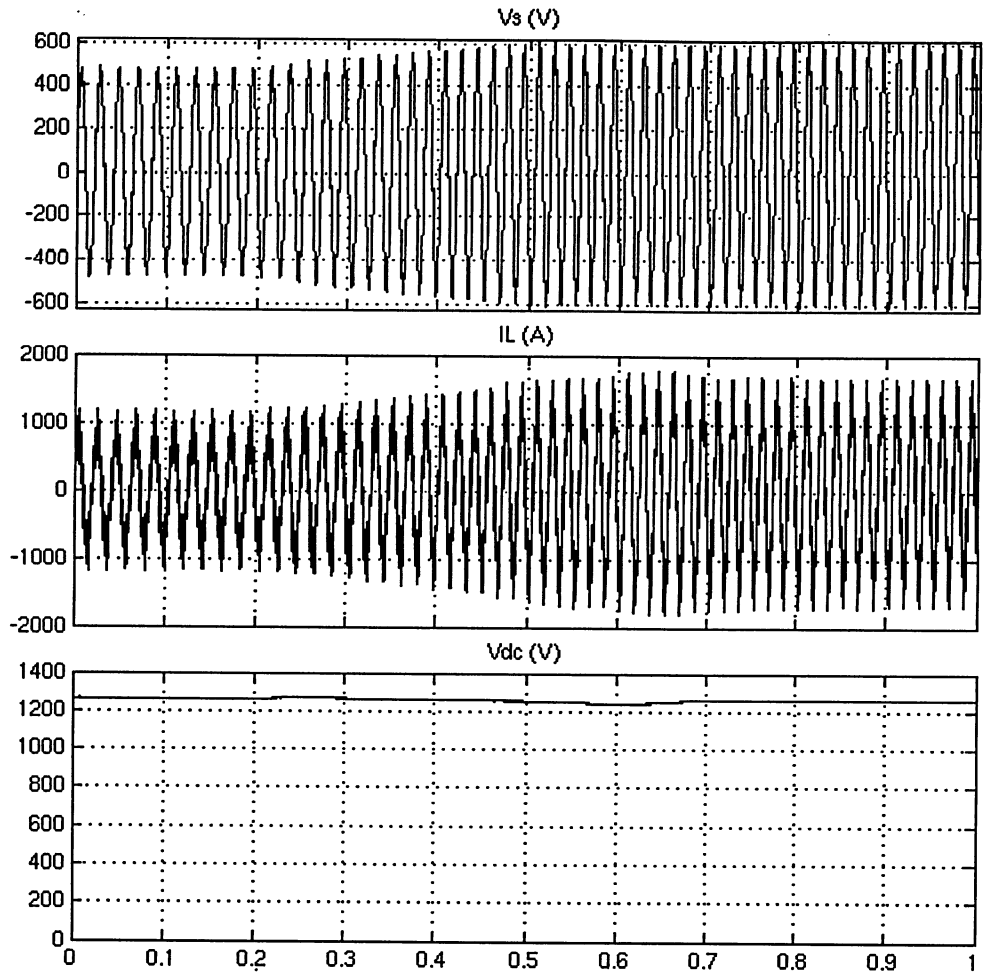

Figure 3-16: Simulation of rectifier transitioning back to rated power from half rated power

When ramping the power back up to rated power we notice a slight dip in dc voltage. This is due to the dc voltage controller spooling up a bit during the increase in power and recovering by undershooting the voltage once the power is no longer increasing. The dc voltage remains within a tolerance of 2% when the ramp is applied to the system.

3.3 Conclusion

The controller functions as intended; verifying the system described in chapter 2. The simulations confirmed that the variable frequency rectifier could operate at the intended steady state operation points. It was also used to confirm the ability of the PLL to track the nature of the input power. In addition a clearer understanding of the operation of a PWM rectifier for wind driven SEIG applications was garnered. Steady-state operation is analyzed both in the time-domain and the frequency-domain. The rated power operation point demonstrates unity power

factor operation ensuring that the converter only needs to carry the real rated power. While the half rated power operation point demonstrates that the converter is able to provide reactive current such that the machine is still provided the correct magnetization current when the reactive current provided by the capacitance becomes reduced. The operation point transition simulations show that the dc output voltage remains stable through the transitions. The next step was to experimentally verify the concept as discussed in the next chapter.

Chapter 4 – Experimental verification

This chapter discusses the experiments conducted to verify the theoretical wind driven SEIG PWM rectifier system. The main tests are the rated operation point test where unity power factor is desired and the half rated power test where additional excitation is provided to the SEIG by the converter. The scaled down experimental setup and the method used will be discussed followed by the results.

4.1 Experiment setup

A scaled down system was used for experimental verification. This section discusses the specific components from which it was built. Figure 4-1 shows the block diagram of the experimental setup.

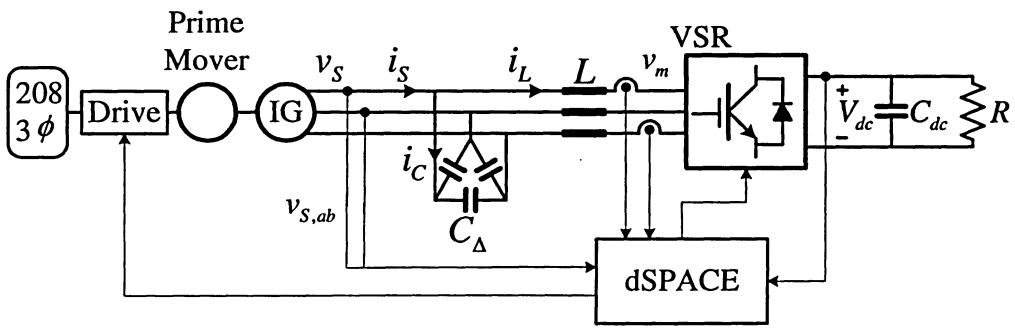

Figure 4-1: Experiment setup

The experimental system consists of the power components and the controls components. The power components include a drive which draws power from a 208V 60Hz 3-phase panel to turn the Prime Mover. The Prime Mover drives a capacitor (C_Δ with phase current i_C) supported induction machine (IG) which provides the current i_S to the remainder of the system. The power continues to flow through the line inductors (L) to a Voltage Source Rectifier (VSR, with input voltage v_m). The dc capacitor (C_{dc}) supported VSR output (V_{dc}) feeds a resistive load (R). The VSR control system is implemented in dSPACE which measures VSR input current (i_L), source voltage (v_s, initially as the line-to-line voltage $v_{S,ab}$), and output voltage (V_{dc}) via transducers. An overview of the experimental system parameters is provided in Table 4-1.

Table 4-1: Experimental component parameters

Prime Mover			
Machine Type	"Brushless" dc	Rated Power	5HP
Max Peak Current	30 A	Rated Current	21.4 A
Bus Voltage	320 V_{dc}	Rated Speed	1750 rpm
Induction Machine			
Rated Voltage	230V	Rated Power	7.5HP
Magnetizing Current	11A	Rated Current	21A
Rated Frequency	60Hz	Rated Speed	1750 rpm
System Parameters			
L	5mH	C_{Δ}	85μF
C_{dc}	3400μF	R	46Ω
Operating Conditions			
V_{dc}	420 V	f_{sw}	1080Hz

The power components are discussed in more detail first. The control system is discussed second.

4.1.1 Power components

The power components consist of the voltage source and the converter. The voltage sources used were initially the variac and then the drive and the machine set as pictured in Figure 4-2 along with the capacitor bank.

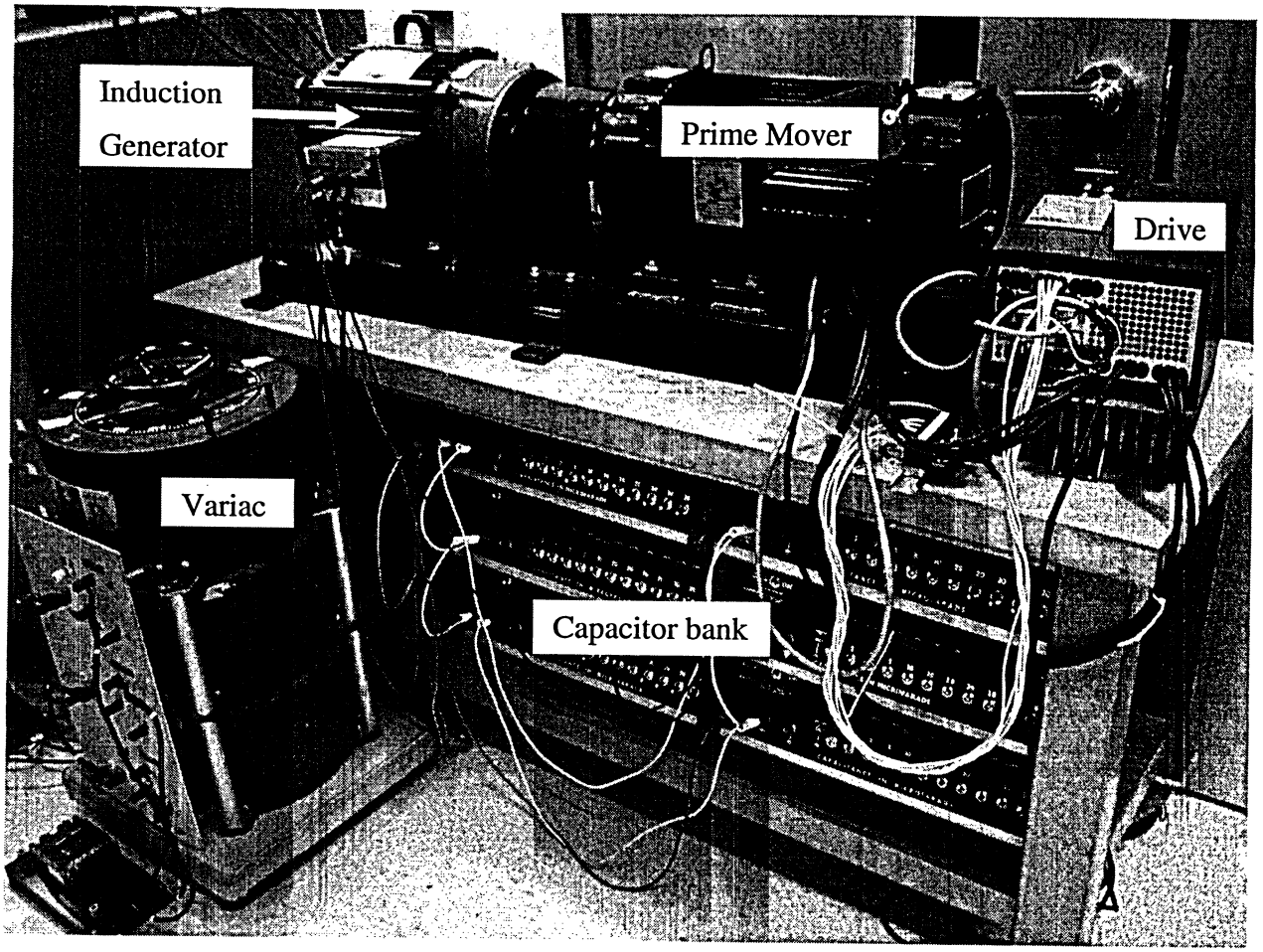

Figure 4-2: Experimental machine setup

The power components were assembled with all of the power drawn from a 208V 3-phase 60A panel through a 30A ac breaker. A common system ground was connected without creating any ground loops. The power was initially fed to a Variac and connected to the line inductors via a 10A ac breaker to test the rectifier. Later the power was instead fed to a PowerFlex PX-30 Drive that needed to be reprogrammed via a RS485 port to accommodate the Model #F184A1F0N002000 "Brushless dc" PowerTec permanent magnet machine (Prime Mover). A communication cable was acquired for this purpose as was an RS232 to RS485 converter to be able to use a desktop computer workstation to reprogram the drive. The drive's over current and over speed protection were then also appropriately set. The 5hp permanent magnet machine was used to drive the 7.5hp 4 pole 230V 60Hz Lincoln Motors inverter duty induction machine (Induction Generator) to form a machine set. The induction machine's rated excitation current and a real power value of 5hp was used to develop the per unit system as calculated in the appendix. The excitation of the induction machine is supported by 6 manually switched JJ Lloyd

Instruments Type No. C140 capacitor banks totaling up to a maximum of 280 delta connected uF.

The converter is pictured in Figure 4-3 with its related components.

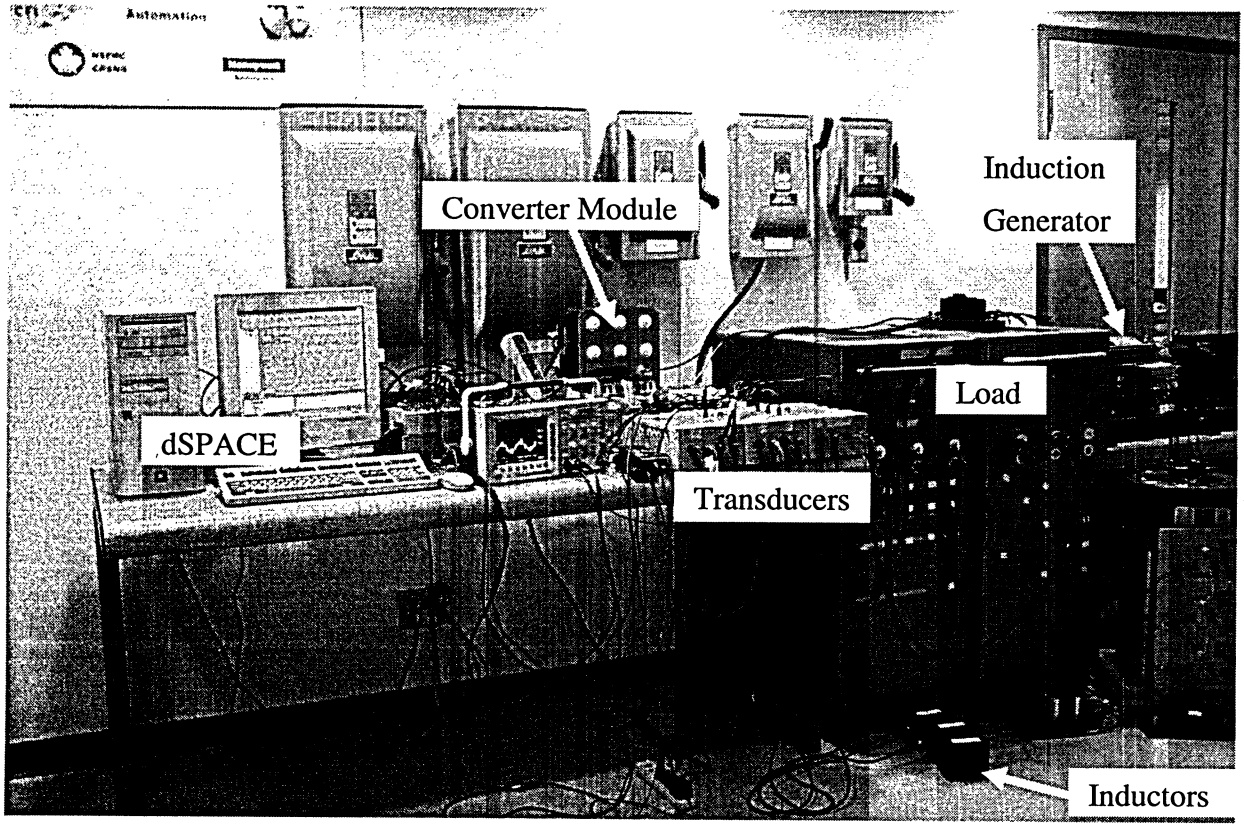

Figure 4-3: Experimental converter setup

The phase to phase voltage of the source is measured by a voltage transducer circuit which incorporates a Liaisons Electroniques-Mecaniques SA (LEM) LV 25-P Voltage Transducer. Similarly the rectifier input current, connected via a 20A breaker through 5mH per phase inductance to the rectifier, is also measured via LEM based boxes. These measured quantities are provided to the dSPACE rapid prototyping system that generates the corresponding gating for the rectifier. The rectifier is realized by using a Semikron 3-phase inverter as a rectifier. The Semikron SKiiP 342GD 120-3DU IGBT module has a 3400 uF dc link capacitance. The $420V_{dc}$ load is created from a manually switched resistor Load bank.

4.1.2 Real-time control

A dSPACE ACE Kit 1103 rapid prototyping system installed in a desktop computer workstation was used for real-time control. The Simulink block diagram was taken from the simulation block diagram shown in Figure 3-1 and the control system part of it was connected to real components and measurement transducers in place of their models. The control blocks ended up being rebuilt due to compatibility issues. The resulting block diagram as constructed for the experiment is shown in Figure 4-4.

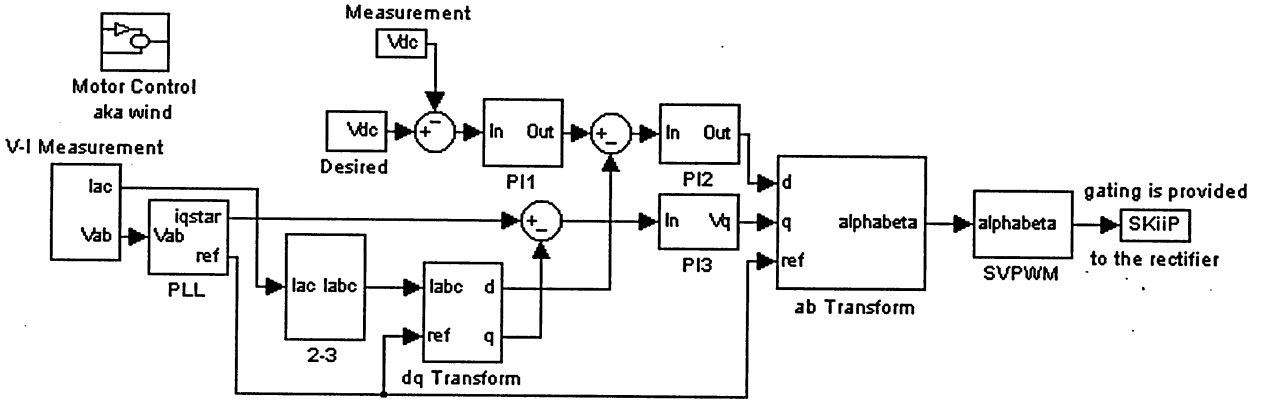

Figure 4-4: Real time control system top level block diagram

A 100μs time step was used for the real-time ACE kit PowerPC 750GX processor which also processed the inputs from transducers. The slave TI TM320F240 DSP generated 1080 Hz SVM gating signals with a 4μs deadband which were then amplified through hex level shifters to provide the signal level desired by the IGBT module.

4.2 Method

To verify the functionality of the experimental setup, each subcomponent of the SEIG fed PWM rectifier energy conversion system was individually verified prior to integration.

4.2.1 dSPACE interface testing

The first stage involved interfacing with the dSPACE system. Simple Simulink models were compiled and loaded as executables to capture sine waves from a function generator and provide corresponding sample output to an oscilloscope. During simulation, it was possible to manipulate slider bars in the Simulink diagram to manipulate system parameters. Once compiled and loaded

into the PowerPC board, real-time modification of the values was possible once the variable to be modified was connected to slider bars in the dSPACE ControlDesk layout. Figure 4-5 provides an example of the ControlDesk layout later in the development of the project.

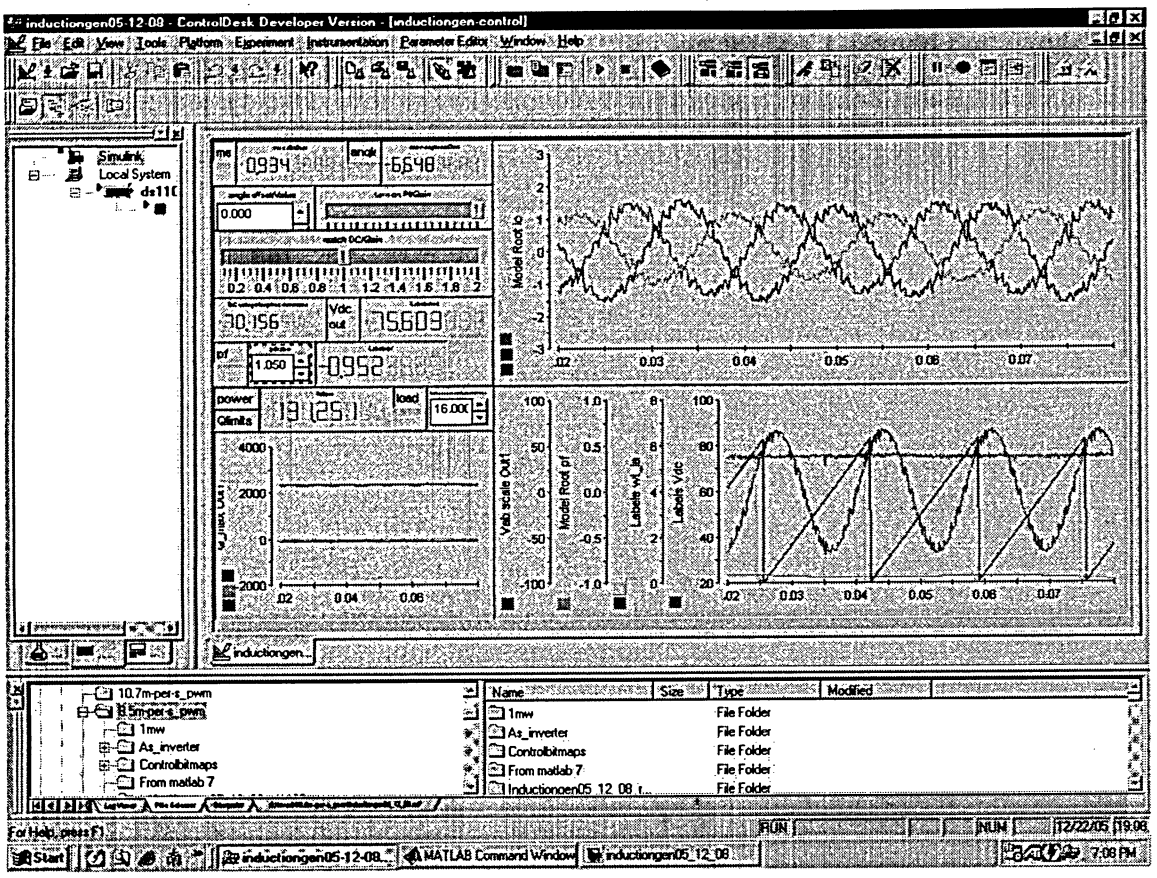

Figure 4-5: Screen capture of dSPACE ControlDesk

The next step was to load the full control system into dSPACE such that each I/O function could be tested. The continuous time Matlab version 7 simulink control system from the simulations was converted into a functioning fixed time step discrete Matlab version 6.1 simulink control system that could be executed in the real-time dSPACE environment. When the system cannot execute in real-time, the processor stops and retains static output values. This is not acceptable in many cases, especially when dealing with pulse width modulated gating. For reliable real-time operation it was important to reload the executable in case it had already been running for over an hour and to always maintain power to the transducers such that the inputs to the processor were well defined and in range.

4.2.2 PLL testing

Simulation demonstrated that the PLL was able to effectively track the source frequency and provide noise free reference sinusoids and instantaneous reference angles. Experimentally it was tested by using a Hewlett Packard DC-600kHz 8904A Multifunction Synthesizer as a variable frequency source. As previously mentioned, the PLL was tuned to have frequency dependent PI gains. It effectively tracked a low frequency signal all the way to 60Hz, however if provided a harmonic it will remain at the fundamental. Thus step changes are to be avoided.

4.2.3 Running the converter as an inverter

To test the converter and its gating, it was run as an inverter. This simplifies the control since the inverter does not have a boost characteristic nor does it need to be synchronized with a source. Nonetheless shoot-through (short circuit current that would flow should both devices in a converter leg be on at the same time) is still an issue. To avoid this, neither switch in a converter leg is on during a predetermined dead-time. 1080 Hz SVM gating signals are generated by the PowerPC's slave TI TM320F240 DSP for the 3 legs of the converter. The DS1103SL_DSP_PWMSV dSPACE control block that was used incorporates a dead-time setting which was set to 4μs of dead-time for the complementary switch pairs. While the SemiKRON driver has a 2.3 μs built in dead-time, 4μs was identified to be safer especially in the case of an experimental PWM rectifier. The dSPACE interface was not able to have a sufficiently high sample rate to identify the correct implementation of dead-time creation. A Tektronix TDS 3032B 300MHz 2.5GS/s oscilloscope was used to capture the waveforms and to identify all instances of dead-time generation throughout a cycle of the fundamental frequency. In order to connect the DSP digital output to the driver, CD4504B level shifters were used. Then the converter switching operation was verified by providing a dc source to the converter and comparing the output to Figure 3-8. An independent dc power supply was used to feed both the driver and the hex level shifter board.

4.2.4 Running the induction machine as a motor

Prior to coupling the machines, the induction machine parameters were verified as per the script included in the appendix. In addition, the induction generator magnetization curve in Figure 1-3 was created by running the machine at no load and measuring the armature current, plotting it as a function of terminal voltage [38]. The variac was used for this. The machine was then run at

various speeds by using the inverter to drive it allowing the parameters for Figure 1-2 to be calculated. The results of these calculations are compiled into Table 4-2.

Table 4-2: IEEE Parameters

Stator winding resistance	R_1=0.2Ω	Referred rotor resistance	R_2'=0.23Ω
Stator winding leakage inductance	X_1=0.45Ω	Referred rotor inductance	X_2'=0.45Ω
Magnetizing inductance	X_m=13.4Ω		

4.2.5 Running the converter as a rectifier

The 230V 60Hz 7kVA 20A 3-phase variac which was fed from the 208V 3-phase panel was used to test the rectifier operation. A 10A breaker was used on the output of the variac. The level of noise with increasing source voltage was surprising but since the three-phase currents were confirmed to be balanced, full voltage operation was achieved. Reactive power control was tested by commanding a range of sample power factor operation points. A cross-coupled controller did not provide acceptable transient currents. The control system was then set up in open loop configuration to identify the cause of this. It was then found that changing the control parameters demonstrated different transfer function relations than expected. A direct PI controller was found to be stable with more acceptable transient current. Eventually, the control parameters for steady-state operation were obtained for the direct-coupled controller discussed in chapter 2.

4.2.6 Running the machine as a generator (Full integration)

The machine was coupled to the dc motor whose speed was determined by an additional controller added into the Simulink model to provide the PowerFlex drive with a speed reference corresponding to a hypothetical turbine's conversion of wind energy to rotational energy. The dc machine torque can be monitored via the PowerFlex drive's armature current readout to ensure correct operation. For the case of an actively controlled mechanical system, we will assume that the turbine's yaw system keeps the turbine pointed into the wind and that its pitch control system keeps the blades at the optimum energy collection angle taking into account wind speed and rotational speed. When the PWM rectifier was connected the PI gains were reduced fourfold to accommodate the response of the real system.

In order to run the experiment, a start-up procedure was developed. The load could be increased in 12 steps, thus for initial start-up one load bank was engaged and the rectifier operated as a six-pulse rectifier. The modulation index was limited to remain near unity and likewise for the power factor. Then using feedback control the source was allowed to drive the generator through the self-excitation process with a command of 0.05 pu voltage. This is about three times the rms value of the transducer noise and allows the PLL lock to be verified. The lightly loaded machine will excite by around half rated frequency with excitation capacitors selected as per (2-26) for rated operation. In the case that residual magnetism has been lost, doubling the capacitance is sufficient to excite the machine prior to rated frequency at which point the additional capacitance can be removed. In the case of this experimental isolated system, initial start-up excitation is not possible without the capacitors since the dc link is starting from a discharged state.

The next step was to simultaneously reset the integral controllers and commence gating. After increasing the voltage command to 0.5 pu the modulation index limit was eased to about 0.7. Once the controller settled, the motor control was changed from voltage feedback to simply rotational speed and the modulation index limit was changed to about 0.2. This point of operation both without (left) and with (right) gating signals is shown in Figure 4-6.

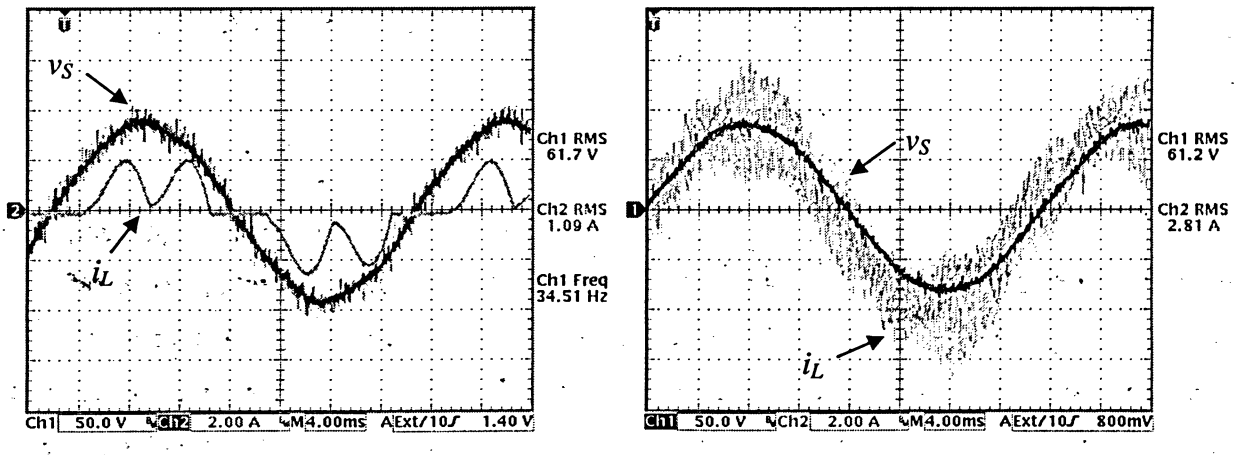

Figure 4-6: Measured waveforms during initial operation

Prior to engaging the gating, the current pulses (i_L) show that the bridge operation identical to a six-pulse diode rectifier. The source voltage (v_S) noise in both cases is due to noise from the prime mover's drive. Once the gating is engaged it is apparent that the bridge operates as a PWM

rectifier since the bridge current (i_L) then approximates a sinusoid.

To move to the actual half rated power operation point, the machine speed was set accordingly and the load was increased to six load banks. The dSPACE control panel was notified of this and the dc voltage was then commanded to be boosted from about 300V to the steady state operation point of 420V. To transition to full power, the machine speed was ramped up followed by the load. 0.05 pu speed command steps are used at times to avoid resonant operation points. At full power the chopped line-to-line v_m ($v_{m,ab}$) in Figure 4-7 was captured. It indicates a switched voltage pattern that demonstrates proper gating functionality including verifying PLL lock. The sinusoidal source voltage and the chopped rectifier voltage are on opposite sides of the line inductance. To ensure residual magnetism, the start-up procedure is reversed for shutdown.

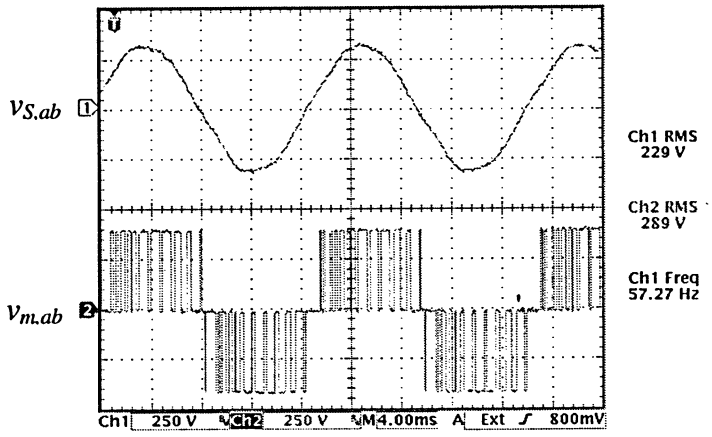

Figure 4-7: Experimental source and rectifier voltages

4.3 Results

This section discusses the results of the experiments conducted to verify the theoretical wind driven SEIG PWM rectifier system. The main tests are the rated operation point test where unity power factor is desired and the half rated power test where additional excitation is provided to the SEIG by the converter. The corresponding test results are shown after discussing initial experimentation.

4.3.1 Initial experimentation

To be able to properly compare the experimental 5hp variable frequency PWM rectifier system results to the simulations, additional simulations were conducted at 5hp. In initial tests there were

uncontrolled oscillations. There are a lot of possible contributors to resonance in this system. In all likelihood, the use of cross-coupled control versus the use of direct coupled control, the large input inductance, and the loading effects combined to create an unmanageable system. Of particular note was the periodic surging of power. It is possible that in addition to the issue of stabilizing the dc voltage via the rectifier, the PowerFlex drive's internal proportional controller compounded these effects.

Once the direct-coupled feedback control was implemented, the system was much more stable. The excitation capacitance was reduced from that prescribed by equation (2-26), to run a test attempting standalone operation of the topology without excitation capacitors. However the system tended to lose stability and once the capacitance was reduced ten-fold, the system went out of control. Nevertheless, the system functioned properly for the verification of the intended theory as depicted in the following figures corresponding to operation at full and half rated power.

4.3.2 Operation at full rated power

At full rated power the converter is only handling the real component of the machine power. Full rated voltage of 230V and full real current of 10A is expected for a dc load of 46Ω. It is clear that the converter is operating appropriately at unity power factor in both the simulation and experimental results shown in Figure 4-8 and Figure 4-9 respectively.

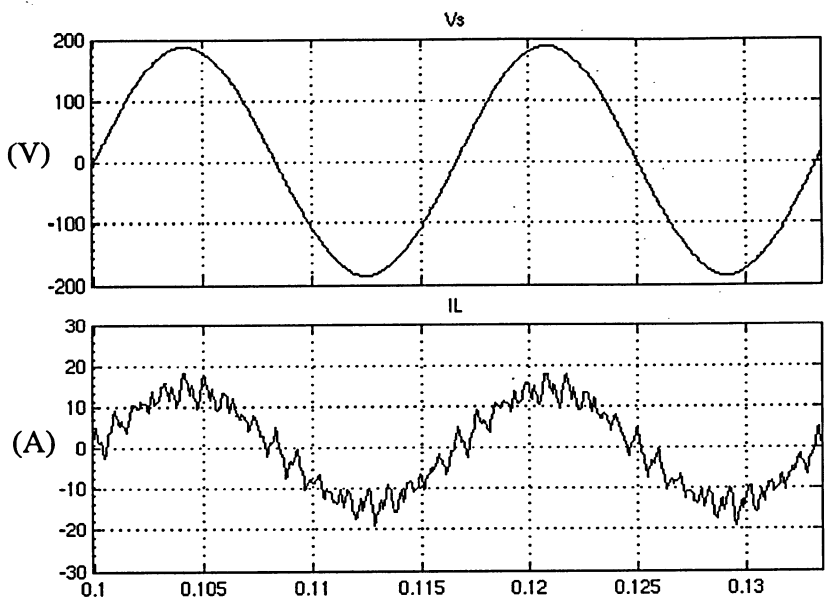

Figure 4-8: Simulation of full power, unity power factor

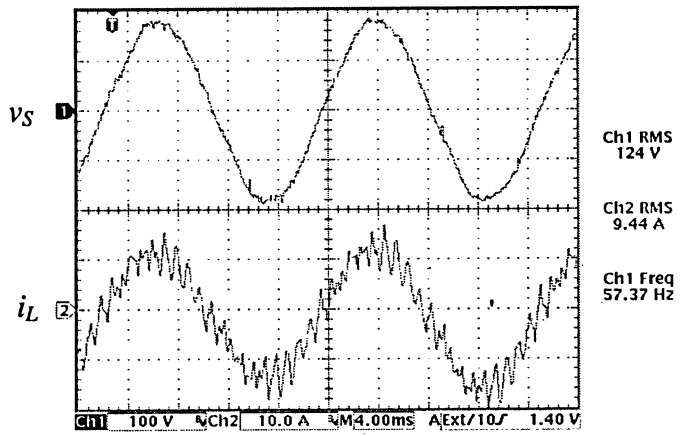

Figure 4-9: Experimental system operation at full power, unity power factor

In order to demonstrate operation as discussed in chapter 2 more conclusively, the Fast Fourier Transforms (FFT) for the steady-state rated power operation are provided. Figure 4-10 shows the FFTs of the currents at the node where the capacitor is connected.

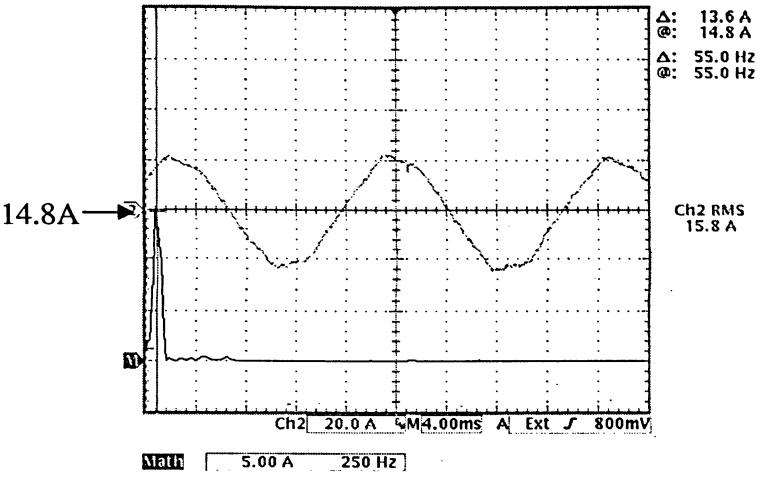

(a) Machine current, i_S

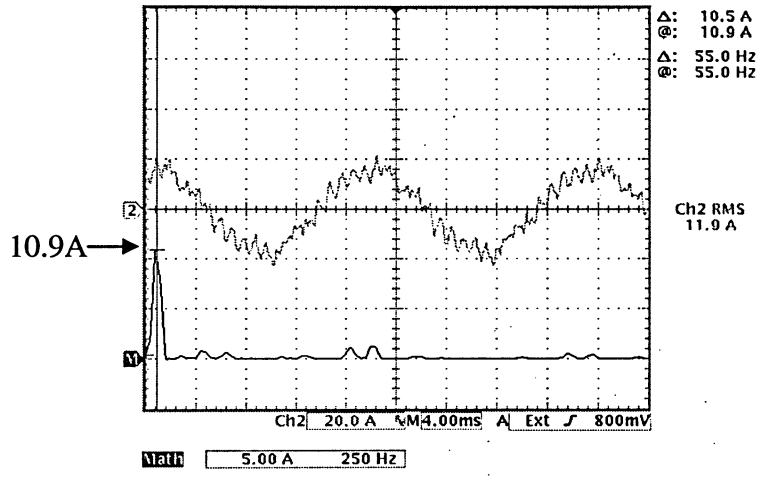

(b) Capacitor current, i_C

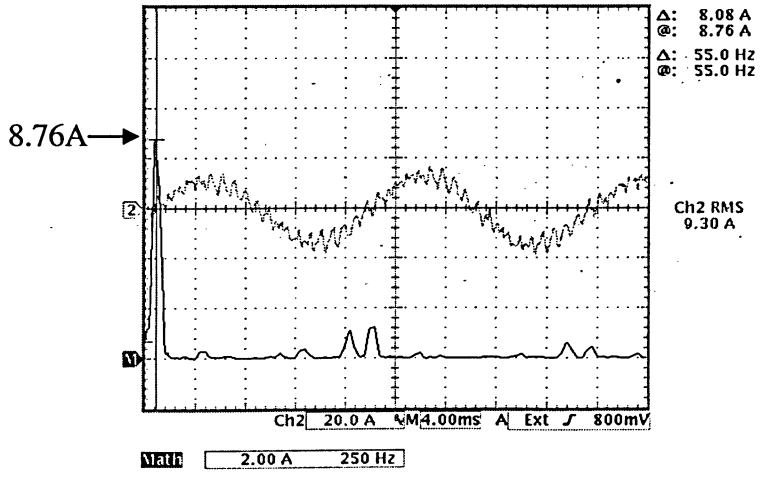

(c) Converter current, i_L

Figure 4-10: FFTs of current at full power, unity power factor operation

Recalling Figure 2-3 and placing the fundamental of the respective measured currents on the

phasor diagram provides Figure 4-11.

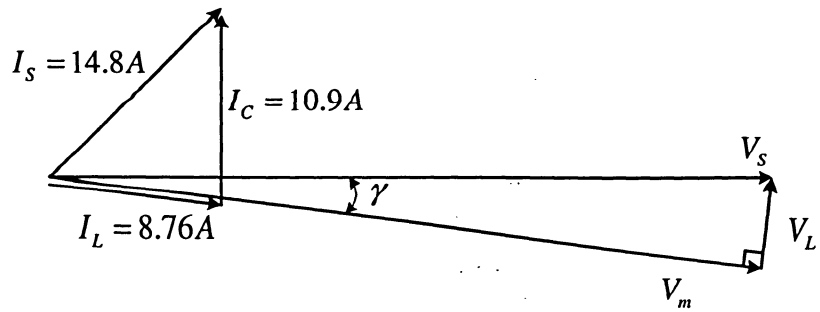

Figure 4-11: Resulting vector diagram of operation at full power, unity power factor

The vector diagram clearly indicates that the PWM rectifier operates at unity power factor by showing that the reactive current ($\vec{I}_C$) provided by the calculated capacitance allows the rectifier input current ($\vec{I}_L$) to be in phase with the rectifier three-phase input terminal voltage ($\vec{V}_m$). Thus allowing the converter to only carry the real power. $\vec{I}_L$ is a bit smaller than expected. This is due to all of the operation parameters, including dc voltage and most importantly the load, being slightly less than rated.

4.3.3 Operation at half rated power

When operating at half rated power, the current is leading the voltage meaning the converter is providing some of the reactive excitation current. A line to line RMS voltage of 183V is expected for the dc load of 100Ω. It is clear that the converter is providing reactive current in both the following simulation and experimental results shown in Figure 4-12 and Figure 4-13 respectively. The leading current is most easily noticed by observing zero crossings in the figures.

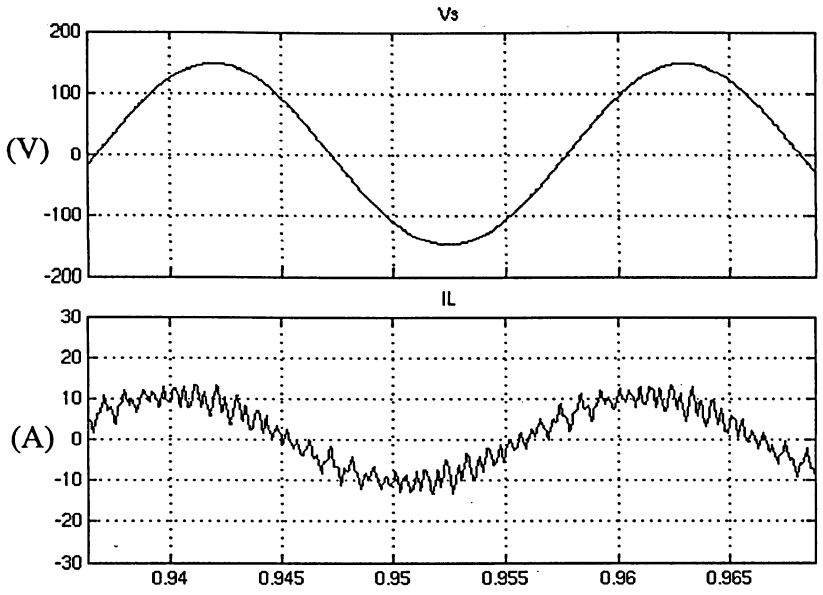

Figure 4-12: Simulation of half power, leading current

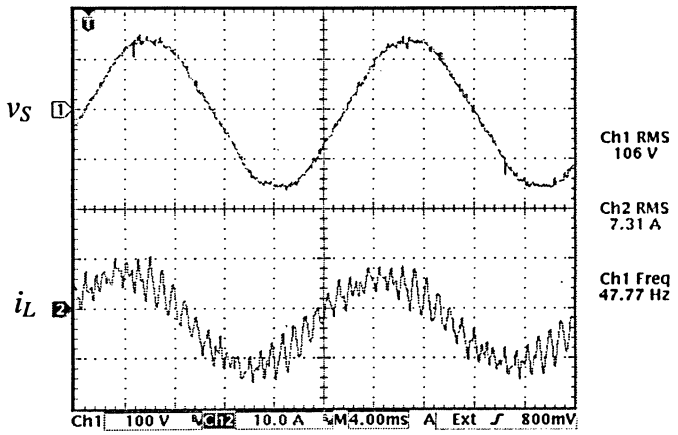

Figure 4-13: Experimental system operation at half power, leading current

In order to demonstrate operation as discussed in chapter 2 more conclusively, the FFTs for the steady-state half rated power operation are considered. This half power case was chosen to demonstrate the provision of reactive current to the machine since the reactive current provided by the capacitors is reduced due to lower frequency and lower source voltage. Figure 4-14 shows the FFTs overlaid on the currents at the node where the capacitor is connected.

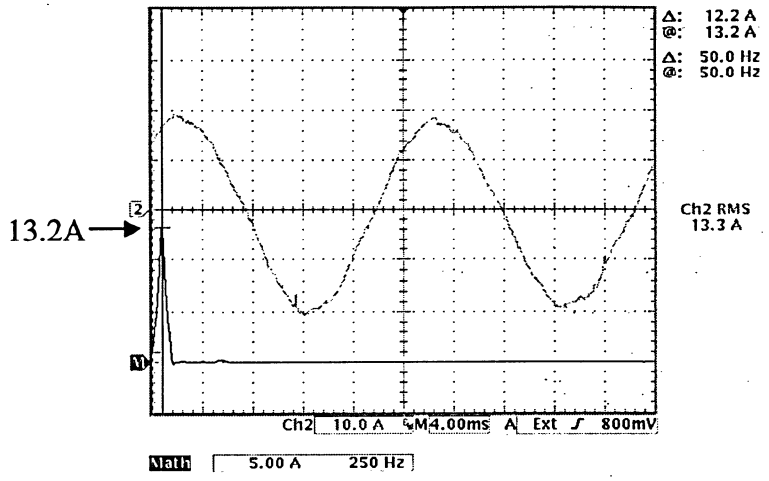

(a) Machine current, i_S

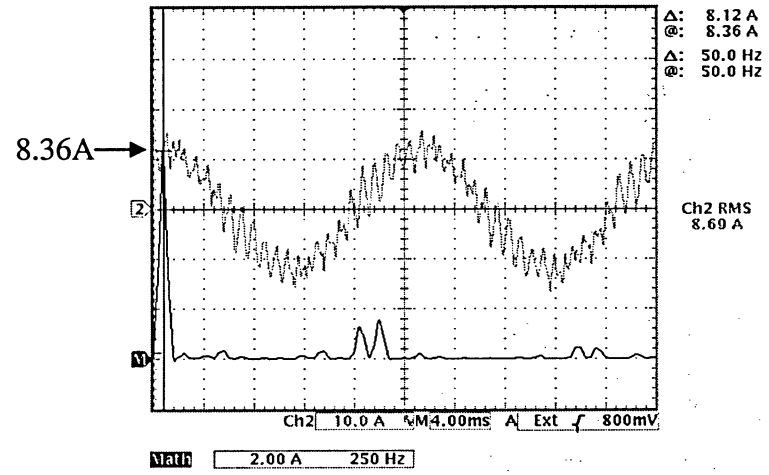

(b) Capacitor current, i_C

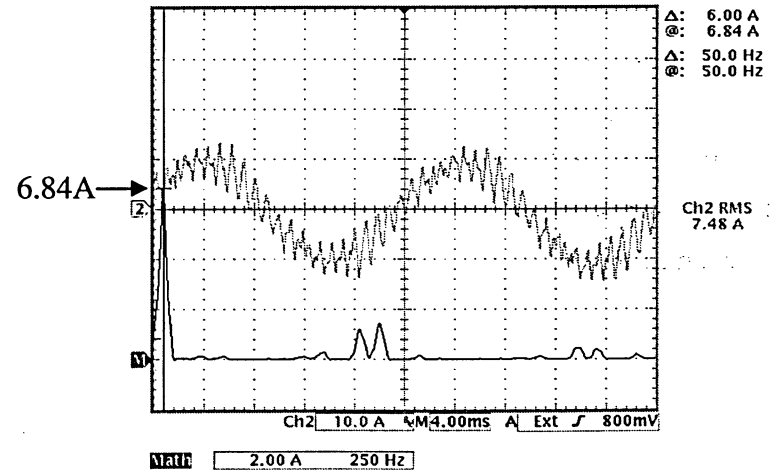

(c) Converter current, i_L

Figure 4-14: FFTs of current at half power, leading current operation

Recalling Figure 2-4 and placing the fundamental of the respective measured currents on the

phasor diagram provides Figure 4-15.

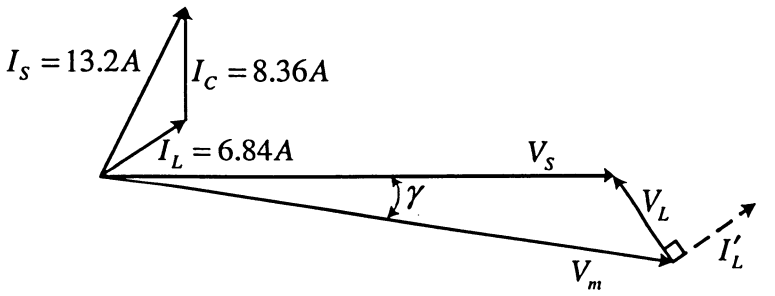

Figure 4-15: Resulting vector diagram of operation at half power, leading current

The magnitude of the rectifier input current ($\vec{I}_L$) demonstrates operation at half power is less than that in the full power case meaning that the converter does not require additional capacity to provide this current. The vector diagram clearly shows that the PWM rectifier input current ($\vec{I}_L$) leads the rectifier three-phase input terminal voltage ($\vec{V}_m$). Thus the reduction of the reactive current ($\vec{I}_C$) provided by the capacitance at lower frequency has been compensated for by the converter providing reactive current such that the machine is still provided the correct magnetization current. This verifies the correct operation of the control strategy described in chapter 2.

4.4 Conclusions

The wind driven SEIG fed PWM rectifier system has been experimentally verified in addition to the earlier successful simulations. The experimental results mimic the respective simulation results. Without connecting the excitation capacitors as presented, the rectifier must handle reactive power in addition to the real power. When they are used, the required rectifier power rating is minimized as it only needs to be sized for the real power. The experiments have considered an isolated system with a simple manually switched resistor bank as a load. This forced more focus on the control of the PWM rectifier resulting in the clarifications noted in the theory chapter. The proposed wind driven SEIG PWM rectifier energy conversion system control scheme and the system operation has been verified.

Chapter 5 – Conclusions

The research presented by this thesis developed a formula to optimize capacitor selection for variable frequency PWM rectifiers used for wind driven SEIG applications. Use of wound rotor induction machines is currently most prevalent, however they are expensive and require maintenance. The inexpensive, rugged, lightweight SEIG requires a more expensive converter and the research presented by this thesis has provided a method that can be used to minimize the cost of that converter. Simulations and experimental verification were successful. After discussing the contributions made by this research, possible future work is discussed.

5.1 Contributions

This section presents the contributions made by the work described by this thesis. The concept that underwent development to optimize capacitance for reactive power compensation is introduced, followed by a list of the specific contributions made to this field. These contributions can be incorporated into new designs and this particular design can also be retro-fit, along with an approved inverter, into existing installations that have converter issues. Reliability, efficiency, and power system stability concerns are among issues currently experienced by other designs.

The concept that underwent development uses a PWM rectifier to handle the power from a wind driven SEIG. This widely used simple squirrel-cage induction machine requires excitation current whether used as a motor or a generator. When used as a generator, establishing an initial terminal voltage upon start-up requires either an outside power source or excitation capacitors. Predominant wind driven induction generator schemes trade the simplicity of a squirrel-cage rotor and use a wound-rotor instead. Currently, the most typical doubly-fed design is to use a wound rotor induction machine where the converter only carries the rotor current while the stator is grid connected. The simple squirrel-cage induction machine can be used when an electronic converter is connected to its stator and used in the full power path. The fact that converters continue to drop in price means that their use will continue to become more widespread and more likely to be in the full power path. This project hastens that development by minimizing the required rating of the front-end converter required by optimizing the excitation capacitance.

Variable speed operation is required for peak power capture in wind driven applications. A

SEIG, the least expensive electrical machine, is used as a variable speed electrical generator. Using a Pulse Width Modulated (PWM) rectifier, it is possible to convert the output of the SEIG to provide a constant voltage power source for an off-the-shelf inverter approved for grid connection. The contributions made to the body of knowledge covering variable frequency PWM rectifiers for wind driven SEIGs are the following primary contribution and two subsequent corollaries discovered during the verification process.

Excitation capacitance calculation formula for wind driven SEIGs. A method of calculating a static capacitance value has been presented, which along with the variable frequency PWM rectifier maintains a wind driven Self-Excited Induction Generator's (SEIG) excitation. This approach allows the use of a converter sized for the rated real power while without the selected capacitance the converter will have to be at least 10% oversized (30% when considering smaller machines). This capacitor provides all of the reactive current for the rated power operation point. When operating at lower speed and thus lower frequency, the capacitor provides part of the excitation current while the converter provides the remainder. Since at lower speed the power is also reduced, even with this additional current demand, the converter current is lower than the real rated current. In addition, in the case of an isolated system, initial start-up excitation is not possible without excitation capacitors when the dc link is starting from a discharged state

In the process of the research, design and development following the theory of this concept, additional clarifications of PWM rectifier control were made:

Operation at extremely low rotational speed. One additional clarification is that, for an isolated SEIG system, operation at extremely low rotational speeds is not possible. This is due to the fact that these low rotational speeds correspond to low input voltages and the converter will be unable to operate at a low enough equivalent input impedance to provide the required magnetization current to the machine.

Direct coupled controller to be used. It was discovered that transients are more easily controlled when a direct coupled controller is used as opposed to a cross-coupled controller. In a functioning controller, V_d was linked to i_d and V_q was linked to i_q. The use of cross-coupled controller has previously been found to function for larger sampling time steps such as 10ms.

However, the test case included a significant resistive component in the line impedance and thus the test results are linked to a current that has an inherently different phase shift. At smaller sampling time steps such as 0.2 ms it is necessary to use a direct PI controller in order to achieve the most stable system. A direct PI controller was found to be stable with acceptable transient current response when used with a more modern sampling time step of 100μs.

The above contribution of a formula for the optimal selection of excitation capacitance and related secondary corollaries were successfully verified. Acceptable simulation results were obtained for a 1MW 690V 3-phase PWM rectifier. Further, a scaled proof of concept was built and used to experimentally verify this concept.

5.2 Future work

Wind power projects exist and continue to be developed at a growing rate. The novel developments described by this thesis can be applied to a wider range of wind power projects as well as other applications. Future work could expand the range of applications to industrial drives in order to provide dynamic reactive power compensation. Future work could also include machine specific modifications such that it could be installed even for topologies other than the induction generator for which it was specifically developed. Also, the excitation capacitance formula can be used to tie a SEIG to the grid with a current source back-to-back converter.

Appendix

Matlab m-file scripts

The scripts calculate the per-unit values, do the IEEE parameter machine test calculations, plot the excitation curve, and plot the capacitance curve. They are followed by a summary of the per unit calculation results in more typical equation format.

thesis_calculations.m

```
%Calculation script for plots and values in thesis (not a
function)
clear; % to ensure no stale data is used

%Let us first consider the 1MW turbine for which this
design is being
%developed:
cd thesis_scripts
oneMWturbine
cd ..

%get the screen size as a reference for the size of
captureable plots
scrsz = get(0,'ScreenSize');
%paint ctrl-e 470 350 if windows toolbar visible
%paint ctrl-e 470 360 if only unix toolbar visible

%For peak_power operation plot1 the model must be
opened first as per the
%note in the respective script file below
cd thesis_scripts
power_rpm
cd ..

%Let us consider the machines we have for experimental
verification
%and plot2 the magnetization curve
cd thesis_scripts
sevenpt5HPmachine
cd ..

%plot3 of power factor of induction machine
cd thesis_scripts
pf_rpm
cd ..

%optional plot of impact of capacitor choice on IL
cd thesis_scripts
capchoice
cd ..

%plot4 of capacitance required for excitation
cd thesis_scripts
capacitance_rpm
cd ..

%let us create a control parameter plot5:
cd thesis_scripts
mandgamma
cd ..

%let us plot6 Iq_command:
cd thesis_scripts
Iq_command
cd ..

%equivalent resistance plot7
cd thesis_scripts
equivimp
cd ..

%plot8 required converter rating:
cd thesis_scripts
VApu
cd ..

%Let us consider the source we have for experimental
verification
cd thesis_scripts
fiveHPmotor
cd ..

%plot9 of loaded pwm rectifier characteristic curves
cd thesis_scripts
loadedpwmrect
cd ..

%if plots are not needed:
close all

% no plots, just calculations from papers

%FROM 073.pdf
```

```
cd thesis_scripts
%pdf073
cd ..

%FROM 103.pdf
cd thesis_scripts
%pdf103
cd ..
```

oneMWturbine.m

```
%1MW turbine parameters:
A=2300; %m^2 of swept area
r=54.2/2; %m radius
Vacbase=690/sqrt(3);
omegabase=2*pi*60; % = 376.9911
Sreal=1e6;
Ireal=(Sreal/3)/Vacbase; % = 836.7395

Sbase=1.026e6;
Iacbase=Sbase/(Vacbase*3); % = 858.4947

Zbase=Vacbase/Iacbase; % = 0.4640
Lbase=Zbase/omegabase; % = 0.0012
Cbase=1/(omegabase*Zbase); % = 0.0057
%Lm per unit changes with machine size, rough figures
[kW Lm]
%[4 1.35
%7.5 1.7
%37 2
%75 2.2
%110 2.3
%160 2.4
%1000 4.5]
Lm=4.5*Lbase;
%Xc=Xm roughly to get ballpark figures
%1/(j*w*C)=j*w*L
%1/(j*w*L)=j*w*C
%C=1/(j^2*w^2*L)
C=1/(omegabase^2*Lm); % = 0.0013
Cpu=C/Cbase; % = 0.2222
Vc=Vacbase;
Ic=Vc*omegabase*C; % = 190.7766
Icomplex=sqrt(Ic^2+Ireal^2); % = 858.2125
%iterate Sb until Icomplex==Ib
[Iacbase Icomplex]; % = 858.4947  858.2125
SVA=Vacbase*Icomplex*3; % = 1.0257e+06

Vdcbase=3*sqrt(3)/pi * Vacbase*sqrt(2) *1.35 /1.0; % =
1.2580e+03
Idcbase=Sreal/Vdcbase; % = 794.9334
Rload=Vdcbase/Idcbase; % = 1.5825

%Using pu values from the experimental verification:
L=0.14*Lbase; % = 1.7232e-04
Cdc=11.9561*Cbase; % = 0.0683

Vfconst=Vacbase/omegabase; % = 1.0567

Imag=Ic; % = 190.7766 from above

%Capacitance that provides Imag
Imag/(Vacbase*omegabase); % = 0.0013
Imag/(Vacbase*omegabase)/Cbase; % = 0.2222pu

%From 2-26:
Cac=( Vacbase^2+2*omegabase*L*Vacbase*Imag-
sqrt(Vacbase^4-4*(Sreal/3*omegabase*L)^2)
)/(2*omegabase^2*L*Vacbase^2);
% = 0.0020
Cacpu=Cac/Cbase; % = 0.3578

%full power test speed x = 10 to 15 m/s (strong wind)
%From [62] it is clear that for a realistic
%turbine it is reasonable to expect efficiency of less than
50% of the betz
%limit:
%power=0.50*betzlimit*1/2*A*d*x^3
betzlimit=16/27; % = 0.5926
d=1.2; %density of air
x=( Sreal/(0.50*betzlimit*1/2*A*d) )^(1/3); % = 13.4730
%half power test speed y > 5 m/s (a wind speed with little
energy)
y=( Sreal/2 /(0.50*betzlimit*1/2*A*d) )^(1/3); % = 10.6935
%to determine optimal speed for turbine given a change of
in windspeed:
%Cp=power coefficient (depends on ratio of blade tip
velocity to wind velocity)
%blade tip velocity=r*omega_t
%lambda=r*omega_t/v %tip speed ratio
%omega_t proportional to windspeed as seen in
powervsrpm.mdl
%we declare 60Hz @ x
%we need the rotational speed for half power (y)
%full power 1MW=some_constant*60^3
some_constant=Sreal/(60^3); % = 4.6296
%half power 500kW=some_constant*rot_speed^3
rot_speed=((Sreal/2)/some_constant)^(1/3); % = 47.6220
Hz
rot_speed/60; % = 0.7937 which is 2^(-1/3)
```

power_rpm.m

```
%not a function
figure(1)
set(1,'Position',[-20 scrsz(4)/2-16 scrsz(3)/2
scrsz(4)/2],'Color','w')
%P=
%simulate(powervsrpm)
%need to open block to get wind turbine characteristic
curve
omega=[0:0.1:2*pi*60*1.2];
```

```
plot(omega./(2*pi*60),(omega./(2*pi*60)).^3,'--')
xlabel('\omega per unit')
ylabel('Per unit turbine output power')
```

sevenpt5HPmachine.m

```
%Let us consider the machines we have for experimental
verification
figure(2)
set(2,'Position',[-20 scrsz(4)/2-16 scrsz(3)/2
scrsz(4)/2],'Color','w')

Vacbase=230/sqrt(3);
omegabase=2*pi*60; % = 376.9911
Sreal=7.5*746; % = 5595W

Iacbase=21;
Sbase=3*Vacbase*Iacbase; % = 8.3658e+03

Zbase=Vacbase/Iacbase; % = 6.3234
Lbase=Zbase/omegabase; % = 0.0168
Cbase=1/(omegabase*Zbase); % = 4.1949e-04

Vdcbase=3*sqrt(3)/pi * Vacbase*sqrt(2) *1.35 /1.0; % =
419.3223
Idcbase=Sreal/Vdcbase; % = 13.3430
Rload=Vdcbase/Idcbase; % = 31.4265

L=5e-3;
Lpu=L/Lbase; % = 0.2981
Cdc=3*2300e-6/2; % = 0.0034
Cdcpu=Cdc/Cbase; % = 8.2243

Cacdelta=85e-6;
Cac=Cacdelta*3; % = 2.5500e-04
Cacpu=Cac/Cbase; % = 0.6079

%machine values

% no load test
PNL=106*3; % = 318
I1_NL=8.53;
Vph_NL=119;
R1=0.2;
Prot=PNL-3*R1*(I1_NL)^2; % = 274.3435
ZNL=Vph_NL/I1_NL; % = 13.9508
RNL=PNL/(3*(I1_NL^2)); % = 1.4568
XNL=(ZNL^2-RNL^2)^0.5; % = 13.8745
% blocked rotor test
Vph_BR=19.7;
I1_BR=19.7;
PBR=169*3; % = 507
ZBR=Vph_BR/I1_BR; % = 1
RBR=PBR/(3*(I1_BR^2)); % = 0.4355
XBR=(ZBR^2-RBR^2)^0.5; % = 0.9002
X2prime=XBR/2; % = 0.4501
X1approx=X2prime; % = 0.4501
Xm=XNL-X1approx; % = 13.4244
R2prime=RBR-R1; % = 0.2355
%per unit
R1pu=R1/Zbase; % = 0.0316
X2primepu=X2prime/Zbase; % = 0.0712
X1approxpu=X1approx/Zbase; % = 0.0712
Xmpu=Xm/Zbase; % = 2.1230
R2primepu=R2prime/Zbase; % = 0.0372
%To avoid oversaturation of the machine V/f=const*2*pi, in
which case the
%magnetizing current required by the machine is constant,
Vfconst=Vacbase/omegabase; % = 0.3522

%A rough calculation ignoring the effect of the other
branches in the IEEE
%equivalent circuit Van=Im*omega*Lm ->
Imrough=Vfconst / (Xm/omegabase); % = 9.8917
%it is also possible to estimate Cac from the nameplate
idle amps
CdirectfromIm=11/(Vacbase*omegabase); % = 2.1973e-04
CdirectfromImpu=CdirectfromIm/Cbase; % = 0.5238
%let us consider the magnitisztion current (reactive power)
required by the
%induction generator for excitation, at constant rated
frequency the
%following voltages are found for varying I at no load:
ImV= [0   0
1.3       20.73
1.81      40.8
2.58      60.18
3.35      80.6
4.11      100.4
4.89      120.6
5.74      140
6.68      160.4
7.21      180.9
8.2       200.5
9.96      220.3
11.1      230.8
11.9      236];
ImV2= [1.25   14.2 %start primary
1.28   17.1
%1.45   20.5
1.53   27.2
1.88   39.8
2.66   64.0
3.55   88.2
4.36   110
5.32   130
6.22   150
7.23   170
7.76   180
8.24   190
8.83   200
9.59   210
10.6   221
```

```
11.6   230
%11.7   232 %secondary
%12.6   240 %primary
%9.88   212 %rest secondary
%10.6   222
%11.7   232
12.0   234
12.6   238
%12.7   238
%12.8   239
%13.3   242
13.5   243
13.7   245%
14.3   248
14.6   248%
%15.1   251
%15.5   253
%16.0   255
%16.7   257
];
%plot(current,voltage)
%plot(ImV(:,1),ImV(:,2))
%plot(ImV(:,1),ImV(:,2),'b-',[11 11],[0 250],'b--',[0 12],[230
230],'b--')
%xlabel('Magnetization current (A)')
%ylabel('Voltage (V)')
%This works but curve to be drawn as an exponential best
fit instead:
%plot(ImV(:,1)/Iacbase,ImV(:,2)/sqrt(3)/Vacbase,'b-',...
%   [11 11]/Iacbase,[0 250]/sqrt(3)/Vacbase,'b--',[0
12]/Iacbase,[230 230]/sqrt(3)/Vacbase,'b--')
%xlabel('Magnetization current (per unit)')
%ylabel('Voltage (per unit)')
%axis([0 12/Iacbase 0 250/sqrt(3)/Vacbase])
%fit it to something like:
%plot([0:0.1:1],1-exp(-3).^[0:0.1:1])
xdata = ImV(:,1)/Iacbase;
ydata = ImV(:,2)/sqrt(3)/Vacbase;
[estimates, model] = fitcurvedemo(xdata,ydata);
[sse, FittedCurve] = model(estimates);
%plot(xdata, ydata, '*',[xdata;1], FittedCurve, 'r', ...
%plot(xdata, FittedCurve, 'r', xdata, ydata,
'*',ImV2(:,1)/Iacbase,ImV2(:,2)/sqrt(3)/Vacbase,'c+-',...
%   [11 11]/Iacbase,[0 1.1*230]/sqrt(3)/Vacbase,'b--',[0
0.7*21]/Iacbase,[230 230]/sqrt(3)/Vacbase,'b--')
plot(ImV2(:,1)/Iacbase,ImV2(:,2)/sqrt(3)/Vacbase,'b-',...
   [11.6 11.6]/Iacbase,[0 1.1*230]/sqrt(3)/Vacbase,'b--',[0
0.7*21]/Iacbase,[230 230]/sqrt(3)/Vacbase,'b--')
xlabel('Magnetization current (per unit)')
ylabel('Voltage (per unit)')
axis([0 0.7*21/Iacbase 0 1.1*230/sqrt(3)/Vacbase])
%This confirms the nameplate value of 11A required for
rated voltage at
%rated frequency with no load. Via experimentation at
57.37Hz it has been
%found that 15% additional is required to maintain rated
voltage under
%load connected via a 3-phase line inductance.
Imag=11; % *1.15 = 12.6500
%The three-phase line inductance draws the following
amount of reactive
%power:
%Iacbase*omegabase*L
```

pf_rpm.m

```
%script to plot excitation curve
figure(3)
set(3,'Position',[-20 scrsz(4)/2-16 scrsz(3)/2
scrsz(4)/2],'Color','w')
omega=[0:omegabase];
Vln=Vfconst*omega;
onephpower=(omega/omegabase).^3*Sreal/3;
Ireal=onephpower./Vln;
pf=Ireal./(sqrt(Ireal.^2+Imag^2));
plot(omega./omegabase, pf)
xlabel('\omega per unit')
ylabel('Power Factor')
axis([0 1 0 1])
```

capchoice.m

```
%not a function

%Let us calculate the equivalent per phase resistance of
the rectifier:
%Let Vm represent the voltage seem by the rectifier and:
%Let VL represent the voltage across the inductor

%the two roots will be Vm and VL where VL will be the
smaller quantity
Vm=sqrt((Vacbase^2 + sqrt(Vacbase^4-
4*(Sreal/3*omegabase*L)^2))/2);
% = 130.0083
VL=sqrt((Vacbase^2 - sqrt(Vacbase^4-
4*(Sreal/3*omegabase*L)^2))/2);
% = 27.0401
Req=Vm*omegabase*L/(VL); % = 9.0628
Req/Zbase; % = 1.4332 p.u.
IL=VL/(omegabase*L); % = 14.3452
gamma=asin(VL/Vacbase); % 0.2051
gamma*180/pi; % = 11.7493
ILreal=IL*cos(gamma); % = 14.0447
ILimag=-IL*sin(gamma); % = -2.9211
Crough=(Imrough+VL/(omegabase*L)*sin(gamma))/(omeg
abase*Vacbase);
% = 2.5595e-04

Vs=Vacbase;
Cac=( Vs^2+2*omegabase*L*Vs*Imag-sqrt(Vs^4-
4*(Sreal/3*omegabase*L)^2) )/(2*omegabase^2*L*Vs^2);
% = 2.7808e-04
Cac/Cbase; % = 0.6629 pu
```

```
ILplotcolour='b'; C=Cac
%ILplotcolour='r';C=Crough
%ILplotcolour='g';C=3e-4
%ILplotcolour='c';C=1e-4
%ILplotcolour='k';C=2.1972e-4
%ILplotcolour='y';C=2e-4
%ILplotcolour='m';C=2.4e-4
%L=Lbase*0.08;C=0
```

capacitance_rpm.m

```
%script to plot excitation curve
figure(4)
set(4,'Position',[-20 scrsz(4)/2-16 scrsz(3)/2
scrsz(4)/2],'Color','w')
Vcrated=Vacbase;
Vc_over_omega_constant=Vfconst;
Vc=Vc_over_omega_constant*omega;
Ic=Imag; % = 11
%Vc=1/(omega*C)*Ic
%Ic=Vc*(omega*C)
Cex=Ic./(Vc.*omega);
%plot(omega, Cex*1e6) %/muF
%AXIS([0 2*pi*60 0 1e3])
plot(omega/omegabase, Cex/Cbase)
xlabel('\omega per unit')
ylabel('Per unit capacitance required')
axis([0 1 0 1e-3/Cbase])
```

mandgamma.m

```
%not a function
figure(5)
set(5,'Position',[-20 scrsz(4)/2-16 scrsz(3)/2
scrsz(4)/2],'Color','w')
omega=[0:2*pi*60];
Vm=sqrt( ( omega*Vfconst.*(1-omega.^2*C*L) +
Imag*omega*L ).^2 ...
    + (omega.^3*Sreal*L/(omegabase^3*3*Vfconst)).^2 );
m=sqrt(3)/Vdcbase*Vm;
gamma=atan(
omega.^2*Sreal*L/(omegabase^3*3*Vfconst) ...
      ./( Vfconst*(1-omega.^2*C*L) + Imag*L ) );
%plot(omega,Vfconst*omega,'c') %goes with "hold"s
%hold
%plotyy(omega,Vm,omega,180/pi*gamma)
%plotyy(omega,m,omega,180/pi*gamma)
[AX,H1,H2]=plotyy(omega/omegabase,m,omega/omegaba
se,180/pi*gamma);
xlabel('\omega per unit')
set(get(AX(1),'Ylabel'),'String','modulation index')
set(get(AX(2),'Ylabel'),'String','\gamma in degrees')
set(H2,'LineStyle','--')
legend([H1 H2],'m','\gamma')
%hold
```

Iq_command.m

```
%script to plot excitation curve
figure(6)
set(6,'Position',[-20 scrsz(4)/2-16 scrsz(3)/2
scrsz(4)/2],'Color','w')
%test of equation 2-23
%( Vs^2+2omega*L*Vs*Imag-sqrt(Vs^4-4*(P*omega*L)^2)
)/(2*omega^2*L*Vs^2)
%test of equation 2-48
Iq_star=omega.^2*Sreal/(omegabase^3*Vfconst*3).*sin(ga
mma)+(Imag-omega.^2*C*Vfconst).*cos(gamma);
%plot(omega,omega.^2*Sreal/(omegabase^3*Vfconst*3).*s
in(gamma),...
%    omega,(Imag-omega.^2*C*Vfconst).*cos(gamma))
plot(omega/omegabase,Iq_star/Iacbase)
xlabel('\omega per unit')
ylabel('Iq* per unit')
```

equivimp.m

```
%not a function
figure(7)
set(7,'Position',[-20 scrsz(4)/2-16 scrsz(3)/2
scrsz(4)/2],'Color','w')
ILvector=(omega*Vfconst-
Vm.*cos(gamma)+j*Vm.*sin(gamma))./(j*omega*L);
%plot(ILvector)
IL=abs(ILvector);
%plot(omega,IL,ILplotcolour)
%plot(omega,Vm./IL)
plot(omega/omegabase,(Vm./IL)/Zbase)
xlabel('\omega per unit')
ylabel('per unit impedance')
```

VApu.m

```
%not a function
figure(8)
set(8,'Position',[-20 scrsz(4)/2-16 scrsz(3)/2
scrsz(4)/2],'Color','w')
%at rated power VA
S=3*sqrt( ( omega*Vfconst.*(1-omega.^2*C*L) +
Imag*omega*L ).^2 ...
    + (omega.^3*Sreal*L/(omegabase^3*3*Vfconst)).^2 )
.* ...
 sqrt( ( omega.^2*Sreal/(omegabase^3*Vfconst*3)).^2 ...
    + (Imag-omega.^2*C*Vfconst).^2 );
C=0; %test no cap case
So=3*sqrt( ( omega*Vfconst.*(1-omega.^2*C*L) +
Imag*omega*L ).^2 ...
    + (omega.^3*Sreal*L/(omegabase^3*3*Vfconst)).^2 )
.* ...
 sqrt( ( omega.^2*Sreal/(omegabase^3*Vfconst*3)).^2 ...
    + (Imag-omega.^2*C*Vfconst).^2 );
L=0; C=0; %test Bose case
```

```
Sb=3*sqrt( ( omega*Vfconst.*(1-omega.^2*C*L) +
Imag*omega*L ).^2 ...
    + (omega.^3*Sreal*L/(omegabase^3*3*Vfconst)).^2 )
.* ...
 sqrt( ( omega.^2*Sreal/(omegabase^3*Vfconst*3)).^2 ...
    + (Imag-omega.^2*C*Vfconst).^2 );
plot(omega/omegabase,S/Sbase,'b-
',omega/omegabase,So/Sbase,'k:',omega/omegabase,Sb/
Sbase,'r--')
xlabel('\omega per unit')
ylabel('VA per unit')
legend('C optimised','C=0','C=0 &
L=0','location','NorthWest')
```

fiveHPmotor.m

```
%When operating at the rated power of 5595W the
machine's flux will
%rotate at the rated frequency of 60Hz. However when
testing the 5595W
%generator, only a 3730W source is coupled to it. Let us
consider the wind
%speed suitable to these testing facilities:
Psource=5*746; % = 3730W
x=( Psource/Sreal*1e6/(0.5*betzlimit*1/2*A*d) )^(1/3); % =
11.7698
%while half of that power is:
y=x/(2^(1/3)); % = 9.3417
%let us now consider the respective voltages and electrical
frequencies for
%operation at 3730W
rot_speed=((1e6*Psource/Sreal)/some_constant)^(1/3); %
= 52.4148
V=Vfconst*sqrt(3)*rot_speed*2*pi; % = 200.9235

%and for operation at (3730/2)W
rot_speed=((1e6/2*Psource/Sreal)/some_constant)^(1/3);
% = 41.6017
V=Vfconst*sqrt(3)*rot_speed*2*pi; % = 159.4734

%however since a key part of this project is to demonstrate
operation at
%unity power factor let us design the system as if the
induction machine is
%also a 5hp machine
%For the 7.5 HP base units the rated current Iacbase=21
but how about for
%its 5HP version, Imag is the same while Ireal changes.
notice
Ireal=Sreal/3/Vacbase; % = 14.0447
sqrt(Ireal^2+Imag^2); % = 17.8396
sqrt(Ireal^2+Imag^2)/Iacbase; % = 0.8495 to low to be the
efficiency as a motor
%let us calculate the 5HP variant's base units
Sreal=Psource;
Ireal=Sreal/3/Vacbase; % = 9.3631

Iacbase=sqrt(Ireal^2+Imag^2); % = 14.4453

Sbase=3*Vacbase*Iacbase; % = 5.7546e+03

Zbase=Vacbase/Iacbase; % = 9.1926
Lbase=Zbase/omegabase; % = 0.0244
Cbase=1/(omegabase*Zbase); % = 2.8856e-04

Vdcbase=3*sqrt(3)/pi * Vacbase*sqrt(2) *1.35 /1.0; % =
419.3223
Idcbase=Sreal/Vdcbase; % = 8.8953
Rload=Vdcbase/Idcbase; % = 47.1397

L=5e-3;
Lpu=L/Lbase; % = 0.2051
Cdc=3*2300e-6/2; % = 0.0034
Cdcpu=Cdc/Cbase; % = 11.9561

Vs=Vacbase;
Cac=( Vs^2+2*omegabase*L*Vs*Imag-sqrt(Vs^4-
4*(Sreal/3*omegabase*L)^2) )/(2*omegabase^2*L*Vs^2);
% = 2.4505e-04

Cacdelta=85e-6; % since 80uF only provides 80e-
06*3=2.4000e-04
Cac=Cacdelta*3; % = 2.5500e-04
Cacpu=Cac/Cbase; % = 0.8837

%iqstar for the 5hp and 2.5hp test
%60 Hz 376.9911 rad/s iqstar=0 Vll=230
%2.5HP case similar to the 500kW case
%47.6220 Hz 299.2179 rad/s iqstar=3.25 to 3.29
Vll=230*0.5^(1/3)=182.5511
```

loadedpwmrect.m

```
%not a function
figure(9)
set(9,'Position',[-20 scrsz(4)/2-16 scrsz(3)/2
scrsz(4)/2],'Color','w')
modVdc_math= [1   1122.178462
0.95      1181.240486
0.9       1246.864957
0.85      1320.209955
0.8       1402.723077
0.75      1496.237949
0.7       1603.112088
0.65      1726.428403
0.6       1870.297436
0.55      2040.324476
0.5       2244.356923
0.4       2805.446154
0.3       3740.594872];
%plot(modVdc_math(:,1),modVdc_math(:,2))

%full load
```

```
modVdc_05L= [0.8 1095
0.6      1240
0.4      1300
0.3      1230
0.2      995];

modVdc_10L= [1   660
0.9      670
0.85     670
0.8      680
0.75     665
0.7      660
0.6      640
0.5      590
0.3      425
0         0.1];

modVdc_15L= [1   442
0.9      429
0.75     400
0.6      355
0.4      260];

%10% load

modVdc_05L_07L= [0.8      1370     1340
0.6      1774     1750
0.4      2488     2267.5
0.2      3757     2950];

modVdc_10L_= [1  1060
0.95     1110
0.9      1155
0.85     1210
0.8      1290
0.75     1340
0.7      1420
0.65     1460
0.6      1575
0.55     1680
0.5      1750
0.4      1930
0.3      2095
0.2      2000
0.1      1400
0         0.095];

modVdc_101L= [1  1060
0.95     1100
0.9      1150
0.85     1200
0.8      1280
0.75     1330
0.7      1400
0.65     1440
0.6      1540
0.55     1630
0.5      1680];

plot(modVdc_math(:,1),modVdc_math(:,2)/1.2580e+03,'k-
',...

modVdc_05L_07L(:,1),modVdc_05L_07L(:,2)/1.2580e+03,'
b^:',...

modVdc_05L_07L(:,1),modVdc_05L_07L(:,3)/1.2580e+03,'
rv:',...

modVdc_10L_(:,1),modVdc_10L_(:,2)/1.2580e+03,'mo:',...

modVdc_101L(:,1),modVdc_101L(:,2)/1.2580e+03,'m.:',...
   modVdc_05L(:,1),modVdc_05L(:,2)/1.2580e+03,'b^--',...
   modVdc_10L(:,1),modVdc_10L(:,2)/1.2580e+03,'ro--',...
   modVdc_15L(:,1),modVdc_15L(:,2)/1.2580e+03,'md--' )
xlabel('modulation index')
ylabel('Vdc (per unit)')
%legend('C optimised','C=0','C=0 &
L=0','location','NorthWest')
legend('Mathematical','L=0.05pu, 10% load','L=0.07pu,
10% load','L=0.10pu, 10% load','L=0.101pu, 10% load',...
   'L=0.05pu, full load','L=0.10pu, full load','L=0.15pu, full
load' )
```

pdf073.m

```
%FROM 073.pdf

%for 1pu test:
fs=57.37; %actual generated frequency in Hz
wr=1736; %actual rotor speed in rpm
%s=-0.0087
Rx=Zbase; %variable resistance of the the converter per
phase
Xc=1/(2*pi*fs*Cac); %variable capacitive reactance of the
exciting capacitor and the
    %converter per phase
%for 0.5pu test:
%fs=41.51; %actual generated frequency in Hz
%wr=1249; %actual rotor speed in rpm
%s=-0.0030
%Rx=??; %variable resistance of the the converter per
phase
%Xc=1/(2*pi*fs*Cac) +/- ?; %variable capacitive reactance
of the exciting capacitor and the
    %converter per phase

fsb=60; %rated frequency in Hz
a=fs/fsb;
wbs=60*60/2; %synchronous speed corresponding to rated
frequency in rpm
b=wr/wbs;
s=(a-b)/a;
```

```
%let
X1=X1approx;
Xmfrom073pdf=-(R2prime^2+(a-
b)^2*X2prime^2)*(Rx*Xc^2+(a^2*Rx^2+Xc^2)*R1) ...
 / (  a*(a-b)*R2prime*(Rx^2*Xc-(a^2*Rx^2+Xc^2)*X1) + ...
      (a-b)^2*X2prime*(Rx*Xc^2+(a^2*Rx^2+Xc^2)*R1)
); % = 79.4978
```

pdf103.m

```
%FROM 103.pdf

Rs=R1pu; % pu
Rr=R2primepu; % pu
Xlr=X2primepu; %pu
Xls=Xlr;
Xmsat=Xmfrom073pdf/Zbase; % = 5.6054 pu
Zb=Zbase; % Ohms
N=1800; % rpm
fb=60; % Hz
%load
R=Psource/Pbase; % pu
X=0.0; % pu
%speed
v=fs/fsb; % pu

%let A=a, B=b, and a=alpha
%let
Xsmax... % Xm
   = Xmsat;
%Appendix 8.1
T = Xls + Xm; % = Xlr + Xm
W = Xls + (Xls*Xm)/(Xls+Xm);
A1 = R*T*W + X*T*(Rs + Rr);
A2 = v*T*(R*W + Rs*X);
A3 = Rr*(X + T) + T*(Rs + R);
A4 = R*Rs*Rr;
A5 = v*T*(R + Rs);
B1 = X*T*W;
B2 = v*B1;
B3 = T*(X + W);
B4 = R*T*(Rs + Rr) + Rs*Rr*X;
B5 = v*B3;
B6 = v*R*Rs*T;
B7 = Rr*(R + Rs);

%Appendix 8.2
%Let
P=Xls+Xsmax; % =Xlr+Xsmax
Q=Xls+(Xsmax*Xlr)/(Xsmax+Xlr);
%P-Q=Xsmax-
(Xsmax*Xlr)/(Xsmax+Xlr)=Xsmax^2/(Xlr+Xsmax)>0
a4 = Rr*X^2*P*(P - Q) ...
+Rs*X^2*P^2+R*P^2*Q^2; % >0
a3 ...
= 2*v*Rs*P^2*X^2 + 2*v*R*P^2*Q^2 ...
+ v*Rr*X^2*P*(P - Q); % > 0
a2 ...
=v^2*Rs*P^2*X^2+v^2*R*P^2*Q^2+R*Rr^2*P^2+Rs*Rr^2*
X^2 ...
+ Rs*R^2*P^2 + R*Rs^2*P^2 ...
+ Rr*R^2*P*(P-Q) + 2*Rr*R*Rs*P*(P - Q); % > 0
a1 ...
=2*v*R^2*Rs*P^2+2*v*R*Rs^2*P^2+2*v*R*Rs*Rr*P*(P-Q)
...
+ v*Rr*R^2*P*(P-Q); % > 0
a0 ...
= R*Rs*(R + Rs)*(v^2*P^2 + Rr^2); % >= 0
%Equation 7
%a4*F^4-a3*F^3+a2*F^2-a1*F+a0=0;
%can plot as a4*F^4+a2*F^2+a0=a3*F^3a1*F
F=[-1.1:0.01:1.1];
plot(F,a4*F.^4+a2*F.^2+a0,F,a3*F.^3+a1*F)
axis([-1.1,1.1,-0.5,10]);grid;
F=roots([a4 -a3 a2 -a1 a0]);
index2=1;
for index=[1:size(F,1)]
   if (isreal(F(index)))
      Freal(index2)=F(index);
      index2=index2+1;
   end
end
F=Freal;
Xc= (A1*F.^3-A2*F.^2-A4*F) ...
   ./ (A3*F-A5);
C=1./(2*pi*max(F)*fb*Zb.*Xc);
Xc= (B1*F.^4-B2*F.^3-B4*F.^2+B6*F) ...
   ./ (B3*F.^2-B5*F-B7);
C=1./(2*pi*max(F)*fb*Zb.*Xc);
Cmin ... %=min{Ci,i<=4}]
   =min(C) % = 2.9996e-05
```

Per-Unit value summary

For the 1MW design case:

$$
\begin{aligned}
V_{ac-base} &= \frac{690}{\sqrt{3}}V \\
I_{ac-base} &= I_{rated} = 858A \\
S_{base} &= 3V_{ac-base}I_{ac-base} = 1.026MVA \\
\omega_{base} &= 2\pi 60 = 376.9911 rad/s \\
V_{dc-base} &= 1260V \\
I_{dc-base} &= \frac{\mathrm{Re}\{S_{base}\}}{V_{dc-base}} = 794A
\end{aligned}
\tag{1}
$$

Thus per unit impedance base values are:

$$
\begin{aligned}
Z_{base} &= \frac{V_{ac-base}}{I_{ac-base}} = 0.464\Omega \\
L_{base} &= \frac{Z_{base}}{\omega_{base}} = 1.2mH \\
C_{base} &= \frac{1}{\omega_{base}Z_{base}} = 5700\mu F
\end{aligned}
\tag{2}
$$

The line inductance used is:

$$L = 0.14L_{base} = 0.17mH \tag{3}$$

A one per unit dc load:

$$R_{load} = \frac{V_{dc-base}}{I_{dc-base}} = 1.58\Omega \tag{4}$$

dc capacitance using ac base value for a per unit representation:

$$C_{dc} = 12C_{base} = 68mF \tag{5}$$

For the experimental verification the per-unit base values used are:

$$\begin{aligned} V_{ac-base} &= \frac{230}{\sqrt{3}}V \\ I_{ac-base} &= 14.4A \\ S_{base} &= 3V_{ac-base}I_{ac-base} = 5755VA \\ \omega_{base} &= 2\pi 60 = 376.9911 rad/s \\ V_{dc-base} &= 420V \\ I_{dc-base} &= \frac{\mathrm{Re}\{S_{base}\}}{V_{dc-base}} = 8.881A \end{aligned} \tag{6}$$

Thus per unit impedance base values are:

$$\begin{aligned} Z_{base} &= \frac{V_{ac-base}}{I_{ac-base}} = 9.1926\Omega \\ L_{base} &= \frac{Z_{base}}{\omega_{base}} = 24.4mH \\ C_{base} &= \frac{1}{\omega_{base}Z_{base}} = 289\mu F \end{aligned} \tag{7}$$

The line inductance used is:

$$L_{p.u.} = \frac{5mH}{L_{base}} = 0.2051 p.u. \tag{8}$$

A one per unit dc load:

$$R_{load} = \frac{V_{dc-base}}{I_{dc-base}} = 47.14\Omega \tag{9}$$

dc capacitance using ac base value for a per unit representation:

$$C_{dc-p.u.} = \frac{3450uF}{C_{base}} = 12 p.u. \tag{10}$$

References

[1] D. Bergamini, *The Land and Wildlife of Australia.* New York: Time Inc., 1964.

[2] T. Cowan, "Alternative energy... the search continues," *The Toronto Star,* pp. D2-D3, Jul. 2004.

[3] F. Stokhuyzen, *The Dutch Windmill.* Netherlands: CAJ van Dishoek-Bussum-Holland, 1962.

[4] Danish Wind Industry Association, *Guided Tour on Wind Energy.* Copenhagen, Denmark: DWIA, 2003.

[5] BTM Consult ApS, *Wind Force 10 - A Blueprint to Achieve 10% of the World's Electricity from Wind by 2020.* European Wind Energy Association (EWEA): Greenpeace International, Forum for Energy and Development, 1999.

[6] Special Issue, "Global Market Overview," *Windpower Monthly,* vol. 20, pp. 35-72, March. 2004.

[7] Wikimedia Foundation Inc. Altamont pass. *(June 14),* Available: http://en.wikipedia.org/wiki/Altamont_Pass, *2006.*

[8] D. Bailey, "Getting down to details in Canada," *Windpower Monthly,* vol. 21, pp. 57-58, Mar. 2005.

[9] The Canadian Wind Energy Association. Canadian wind farms. *(June 16),* Available: http://canwea.ca/en/CanadianWindFarms.html, *2006.*

[10] The Canadian Wind Energy Association, "WindLink Issue #17," November 5. 2004.

[11] A. Betz, *Wind-Energie Und Ihre Ausnutzung Durch Windmuehlen.* Göttingen: Vandenhoeck et Ruprecht, 1926, Oekobuch reprint, Staufen 1994.

[12] A. N. Gorban, A. M. Gorlov and V. M. Silantyev, "Limits of the turbine efficiency for free fluid flow," *J. Energy Res. Technol.,* vol. 123, pp. 311, Dec. 2001.

[13] E. S. Abdin and W. Xu, "Control design and dynamic performance analysis of a wind turbine-induction generator unit," *IEEE Trans. Energy Convers.,* vol. 15, pp. 91-96, 2000.

[14] M. Karrari, W. Rosehart and O. P. Malik, "Comprehensive control strategy for a variable speed cage machine wind generation unit," *IEEE Trans. Energy Convers.,* vol. 20, pp. 415-423, 2005.

[15] W. E. Holley, "Wind turbine dynamics and control - issues and challenges," *Proc. American Contr. Conf.,* vol. 5, pp. 3794-3795, 2003.

[16] M. Orabi, M. Z. Youssef and P. K. Jain, "Investigation of self-excited induction generators

for wind turbine applications," *Canadian Conference on Electrical and Computer Engineering,* vol. 4, pp. 1853-1856, 2004.

[17] C. Abbey and G. Joos, "A doubly-fed induction machine and energy storage system for wind power generation," *Canadian Conference on Electrical and Computer Engineering,* vol. 2, pp. 1059-1062, 2004.

[18] M. G. Simões and F. A. Farret, *Renewable Energy Systems : Design and Analysis with Induction Generators.* Boca Raton, FL: CRC Press, 2004.

[19] Y. D. Song, B. Dhinakaran and X. Y. Bao, "Variable speed control of wind turbines using nonlinear and adaptive algorithms," *J. Wind Eng. Ind. Aerodyn.,* vol. 85, pp. 293-308, 4/24. 2000.

[20] C. J. A. Versteegh, "Design of the Zephyros Z72 wind turbine with emphasis on the direct drive PM generator," *NORPIE, NTNU Trondheim Norway,* Jun. 2004.

[21] S. Ruddell, *Improving Motor Efficiency.* Warrington, United Kingdom: ABB Automation Ltd, 2004.

[22] R. Bonert, "ECE315 Electro-mechanical Energy Conversion lecture notes," Mar. 2001.

[23] J. S. Hsu, "Direct control of air-gap flux in permanent-magnet machines," *IEEE Trans. Energy Convers.,* vol. 15, pp. 361-365, 2000.

[24] H. Polinder and M. J. Hoeijmakers, "Eddy-current losses in the segmented surface-mounted magnets of a PM machine," *IEE Proc. Electric Power Appl.,* vol. 146, pp. 261-266, 1999.

[25] E. de Vries, "Wind turbine technology trends - Review 2003," *Renewable Energy World,* vol. 6, Jul. 2003.

[26] American Wind Energy Association, "Wind Energy Delivery and Reliability," pp. March 30-31, 2005.

[27] R. J. Hamilton, "DC motor brush life," *IEEE Trans. Ind. Appl.,* vol. 36, pp. 1682-1687, 2000.

[28] F. Flinders, J. Zhang and W. Oghanna, "Investigation on excessive commutator and brush wears in DC traction machines," *IEEE Proc. Int. Conf. Power Electron. Drive Syst.,* vol. 1, pp. 200-205, 1999.

[29] J. Chen and R. Vook, "Characterization of sliding Al-Cu Electrical contacts," *IEEE Trans. Compon. , Hybrids, Manufact. Technol.,* vol. 9, pp. 17-22, 1986.

[30] T. D. Batzel, D. C. Swanson and J. F. Defenbaugh, "Predictive diagnostics for the main field winding and rotating rectifier assembly in the brushless synchronous generator," *IEEE Int. Symp. Diag. Electric Machines Power Electron. Drives,* pp. 349-354, 2003.

[31] F. Shibata and N. Naoe, "Characteristics of brushless and exciterless, self-excited synchronous generators," *IEEE Ind. Appl. Conf.,* pp. 293-300, 1990.

[32] N. Naoe, "Voltage compensation of permanent-magnet generator with capacitors," *IEEE Int. Conf. Electric Machines Drives,* pp. WB2/14.1-WB2/14.3, 1997.

[33] J. Rizk and M. Nagrial, "Design of permanent-magnet generators for wind turbines," *Proc. Int. Power Electron. Motion Contr. Conf.,* vol. 1, pp. 208-212, 2000.

[34] W. Wu, V. S. Ramsden, T. Crawford and G. Hill, "A low speed, high-torque, direct-drive permanent magnet generator for wind turbines," *IEEE Ind. Appl. Conf.,* vol. 1, pp. 147-154, 2000.

[35] V. Cingoski, M. Mikami, H. Yamashita and K. Inoue, "Computer simulation of a three-phase brushless self-excited synchronous generator," *IEEE Trans. Magn.,* vol. 35, pp. 1251-1254, 1999.

[36] M. R. Dubois, H. Polinder and J. A. Ferreira, "Comparison of generator topologies for direct-drive wind turbines," *Technische Universiteit Delft,* May. 2004.

[37] M. Ermis, H. B. Ertan, M. Demirekler, B. M. Saribatir, Y. Üçtug, M. E. Sezer and I. Çadirci, "Various induction generator schemes for wind-electricity generation," *Electr. Power Syst. Res.,* vol. 23, pp. 71-83, Jan. 1992.

[38] R. C. Bansal, "Three-phase self-excited induction generators: an overview," *IEEE Trans. Energy Convers.,* vol. 20, pp. 292-299, 2005.

[39] E. Levi and Y. W. Liao, "An experimental investigation of self-excitation in capacitor excited induction generators," *Electr. Power Syst. Res.,* vol. 53, pp. 59-65, Jan. 2000.

[40] R. Rabinovici, "Autonomous excitation of induction generators," *IEEE Trans. Magn.,* vol. 34, pp. 664-670, 1998.

[41] M. R. Dubois, "Review of electromechanical conversion in wind turbines," Technische Universiteit Delft, Nederlands, Tech. Rep. EPP00.R03, Apr, 2000.

[42] BTM Consult ApS, *International Wind Energy Development.* Denmark: 2005.

[43] Hydro-Québec and TransÉnergie Technologies, *SimPowerSystems User's Guide.* The MathWorks Inc, 2006.

[44] R. Brzezinski, "Transmission workshop: Wind energy delivery and reliability," vol. Toronto, Canada, Mar. 2005.

[45] M. Lilja and I. Rissanen, "Winwind takes a low speed approach to high reliability," *Modern Power Systems,* vol. 24, pp. 26, 2004.

[46] M. Lilja and I. Rissanen, "Multibrid Low Speed Synchronous Generator with Frequency Converter," *Nordic Wind Power Conference, Chalmers University of Technology,* March 1-2. 2004.

[47] R. Rocha and de Siqueira Martins Filho,L., "A discrete current control for PWM rectifier," *IEEE Proc. Int. Symp. Ind. Electron.,* vol. 2, pp. 681-686, 2005.

[48] S. Fukuda, "LQ control of sinusoidal current PWM rectifiers," *IEE Proc. Electric Power Appl.,* vol. 144, pp. 95-100, 1997.

[49] S. Mazumder, "DSP based implementation of a PWM AC/DC/AC converter using space vector modulation with primary emphasis on the analysis of the practical problems involved," *Proc. Applied Power Electron. Conf. Expo.,* vol. 1, pp. 306-312, 1997.

[50] C. A. Lynch, *Integration of Offshore Wind Farms into the Local Distribution Network.* BWEA Conference, UK Offshore Wind 2004: IPSA Power - Power Systems Consulting and Software, 2004.

[51] E. Torres and M. Garcia-Sanz, "Experimental results of the variable speed, direct drive multipole synchronous wind turbine TWT1650," *Wind Energy,* vol. 7, pp. 109, Apr. 2004.

[52] Asea Brown Boveri Ltd, *HVDC Light in Wind Farm Applications.* Zurich, Switzerland: ABB, 2004.

[53] D. B. Watson, J. Arrillaga and T. Densem, "Controllable d.c. power supply from wind-driven self-excited induction machines," *IEE Proc.,* vol. 126, pp. 1245-1248, Dec. 1979.

[54] R. Rocha, P. Resende and J. L. Silvino, "A robust control design for induction generator system," *IEEE Proc. Int. Symp. Ind. Electron.,* vol. 2, pp. 551-555, 1999.

[55] M. G. Simoes, B. K. Bose and R. J. Spiegel, "Design and performance evaluation of a fuzzy logic based variable speed wind generation system," *IEEE Ind. Appl. Conf.,* vol. 1, pp. 349-356, 1996.

[56] D. Seyoum, M. F. Rahman and C. Grantham, "Inverter supplied voltage control system for an isolated induction generator driven by a wind turbine," *IEEE Ind. Appl. Conf.,* vol. 1, pp. 568-575, 2003.

[57] Q. Yu, L. Norum, T. Undeland and S. Round, "Investigation of dynamic controllers for a unified power flow controller," *IEEE Proc. Int. Conf. Ind. Electron. Contr. Instrum.,* vol. 3, pp. 1764-1769, 1996.

[58] H. Weng, *Robust Control of Dual-PWM Three-Level Field-Oriented Induction Motor Drive System.* Ph. D. dissertation. Tsinghua University, Beijing, China: 2001.

[59] C. V. Nicolas, F. Blazquez, D. Ramirez, M. Lafoz and J. Iglesias, "Guidelines for the design and control of electrical generator systems for new grid connected wind turbine generators," *IEEE Ind. Electron. Soc. Conf.,* vol. 4, pp. 3317-3325, 2002.

[60] A. K. Al Jabri and A. I. Alolah, "Capacitance requirement for isolated self-excited induction generator," *IEE Proc. Electric Power Appl.,* vol. 137, pp. 154-159, 1990.

[61] K. E. Medri and B. Wu, "A Variable Frequency PWM Rectifier for Wind Driven Induction Generators," *IEEE Ind. Electron. Soc. Conf.,* pp. tbd, 2006.

[62] Anonymous "Wind Energy Literature Survey No. 2," *Wind Energy,* vol. 4, pp. 39, Jan. 2001.